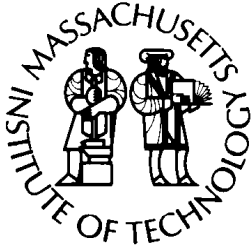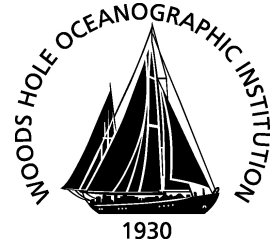# Massachusetts Institute of Technology
Woods Hole Oceanographic Institution

Joint Program in Oceanography/ Applied Ocean Science and Engineering

1930

DOCTORAL DISSERTATION

The Production and Fate of Nitrogen Species in Deep-sea Hydrothermal Environments

by

Chawalit Net Charoenpong

February 2019

The Production and Fate of Nitrogen Species in Deep-sea Hydrothermal Environments

by

Chawalit "Net" Charoenpong

M.S., University of Massachusetts Dartmouth, 2013
B.Sc., Chulalongkorn University, 2004

Submitted in partial fulfillment of the requirements for the degree of

Doctor of Philosophy

at the

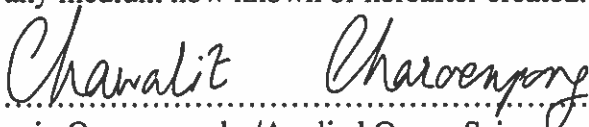MASSACHUSETTS INSTITUTE OF TECHNOLOGY
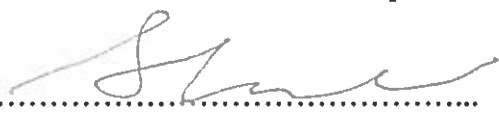
and the

WOODS HOLE OCEANOGRAPHIC INSTITUTION

February 2019

Signature of Author ....
Joint Program in Oceanography/Applied Ocean Science and Engineering
Massachusetts Institute of Technology and
Woods Hole Oceanographic Institution
December 21, 2018

Certified by ....
Scott D. Wankel
Associate Scientist
Woods Hole Oceanographic Institution
Thesis Supervisor

Accepted by ....
Shuhei Ono
Chair, Joint Committee for Chemical Oceanography
Massachusetts Institute of Technology
and Woods Hole Oceanographic Institution

THIS PAGE INTENTIONALLY LEFT BLANK

The production and fate of nitrogen species in deep-sea hydrothermal environments

by

Chawalit "Net" Charoenpong

Submitted to the Massachusetts Institute of Technology and the Woods Hole Oceanographic Institution on December 21, 2018, in partial fulfillment of the requirements for the degree of Doctor of Philosophy in Chemical Oceanography

Abstract

Nitrogen (N) species in hydrothermal vent fluids serve as both a nutrient and energy source for the chemosynthetic ecosystems surrounding deep-sea vents. While numerous pathways have been identified in which N-species can be produced and consumed in the context of submarine hydrothermal vent systems, their exact nature has been largely limited to interpretation of variations in concentrations. This thesis applies stable isotope approaches to further constrain the sources and fate of N-species in deep-sea vents across a variety of geological settings. First, I discuss isotope fractionation and reaction kinetics during abiotic reduction of nitrate (NO_3^-) to ammonium ($\Sigma NH_4^+ = NH_3 + NH_4^+$) under hydrothermal conditions. Results of lab experiments conducted at high temperatures and pressures revealed a wide degree of N isotope fractionation as affected by temperature, fluid/rock ratio, and pH—all of which exert control over reaction rates. Moreover, a clear pattern in terms of reaction products can be discerned with the reaction producing ΣNH_4^+ only at high pH, but both ΣNH_4^+ and N_2 at low pH. This challenges previous assumptions that NO_3^- is always quantitatively converted to NH_4^+ during submarine hydrothermal circulation. Next, I report measurements of ΣNH_4^+ concentrations and N isotopic composition ($\delta^{15}N_{NH4}$) from vent fluid samples, together with the largest compilation to date of these measurements made from other studies of deep-sea vent systems for comparison. The importance of different processes at sediment-influenced and unsedimented systems are discussed with a focus on how they ultimately yield observed vent $\delta^{15}N_{NH4}$ values. Notable findings include the role that phase separation might play under some conditions and a description of how an unsedimented site from Mid-Cayman Rise with unexpectedly high NH_4^+ may be uniquely influenced by N_2 reduction to ΣNH_4^+. Lastly, I explore ΣNH_4^+ dynamics in the context of low-temperature vent sites at 9°50'N East Pacific Rise to investigate dynamics of microbially-mediated N transformations. Through both measurements of natural samples, as well as isotopic characterization of N species from incubation experiments and model simulations thereof, an exceptionally high variability observed in $\delta^{15}N_{NH4}$ values emphasizes the complexity of these microbe-rich systems. In sum, this thesis highlights the role of microbial processes in low temperature systems, demonstrates a more mechanistic understanding of lesser-understood abiotic N reactions and improves the coverage of available data on deep-sea vent ΣNH_4^+ measurements.

Thesis supervisor: Dr. Scott D. Wankel
Title: Associate Scientist, Woods Hole Oceanographic Institution

THIS PAGE INTENTIONALLY LEFT BLANK

ACKNOWLEDGEMENTS

introduced me to the community, and was always available when I needed advice. I am fortunate to have had Kevin Sutherland and Jen Karolewski as my incredibly smart lab siblings. In addition to their friendships and scientific input, I have cherished the financial advice (from Kevin) and sweet treats (from Jen). Thanks for being such wonderful human beings and tolerating the mess, admittedly created by my hoarding habit! Sincere appreciation is also extended to Tyler Tamasi, summer student fellows and visitors of the Wankel Lab, and Colleen Hansel, Gabi Farfan, Kalina Grabb, Vero Oldham, Emily Estes, Julia Diaz, and Tong Zhang of the Hansel Lab.

Upper-class students, whom I often dubbed "the welcoming committee", included Alex Bergan, Greg Horning, Nick Hawco (also my mentor), Jordon Hemingway, Sophie Chu, Sarah Rosengard, Helen Feng, Kyrstin Fornace, and many others; they made me feel so at home in the JP community through potlucks, movie nights, home-brewing, gatherings and parties. My roommates have also been incredible friends, keeping me company outside of work. Special shout-outs go to Billy Thomas, Darron Kriegel, Kaitlin Haase, Shelby Ince, Scott Parkhill, Andrew Davidsohn, and Colton Craig.

Another group of people who contributed greatly to my having a whale of a good time here in Woods Hole is my Chemical Oceanography cohort. Thank you for your amazing support and friendships through these years. Gabi Farfan (my little academic twinnie) was a constant source of encouragement, dance partner, sommelier, and even a tent mate! Cris Shultz and Paul Lerner have been living in Woods Hole with me from the beginning. Remember those study groups for Marine Chemistry class? Cris, thanks for the wonderful cheese bread and for bringing Fulo into my life - starting my dog-sitting side jobs! Paul Lerner, thank you for lending your ears all these years, and the tremendous help when we taught the oceanography class at Mass Maritime Academy. Lauren Kipp, I don't think I have met anyone who is more competitive than you! Danielle Gruen and Tyler Rohr, I admire you both for knowing what you want in life and doggedly pursuing it. Of course, my circle of friends also includes Erin Black, Niya Grozeva, Jenny Panlilio, Jenny Wehof, Megan May, Camrin Braun, Seb Essink, Hannah Mark, and the many other two-legged or fury, four-legged, pawed friends I have come to know.

Many thanks to my former advisor, Mark Altabet (University of Massachusetts Dartmouth), with whom I first embarked on my journey in nitrogen biogeochemistry. Also, I thank my undergraduate chemical oceanography professor, Gullaya Wattayakorn (Chulalongkorn University), from whom I first learned about secondary nitrite maxima.

Finally, I owe my deepest gratitude to my family. They might not know that their weekly calls kept me in check through the many years of graduate schooling. Mom and Dad have always instilled the value of education, helping me attain the highest level of education. I also thank my younger brother, Chaiwat, who has been there with them while I have been on the other side of the globe.

I am certain that I missed naming a great number of people here in these two pages. I thank you all for being part of the journey through my grad school years!

To the teachers who molded my career path in oceanography…

**Suraphol Sudara
(1939-2003)**

**Kanjana Adulyanukosol
(1962-2015)**

**Pitiwong Tantichodok
(1953-2014)**

and a great friend who made me promise that I would come back to graduate school while he was gravely ill on his hospital bed,

**Pittayatorn "Todd" Tantavanich
(1982-2007)**

this thesis is dedicated to you.

THIS PAGE INTENTIONALLY LEFT BLANK

TABLE OF CONTENTS

LIST OF TABLES

THIS PAGE INTENTIONALLY LEFT BLANK

LIST OF FIGURES

THIS PAGE INTENTIONALLY LEFT BLANK

CHAPTER 1

GENERAL INTRODUCTION

The discovery of submarine hot springs, mineral deposits and rich biological communities on the Galápagos Rift in 1977 (Corliss et al., 1979) resulted in a paradigm shift in our conceptualization of the deep sea, previously regarded as a food-limited environment. Instead of relying on the delivery of organic matter originating from the sun-lit surface ocean, deep-sea hydrothermal vent ecosystems are supported by abundant chemical energy and microbial chemosynthesis. Deep-sea hydrothermal vents are found along the mid-ocean ridges, island-arc systems and seamounts and have been found in all ocean basins (Figure 1) covering a large range in depths as well as diverse geologic and volcanic/tectonic settings (Beaulieu et al., 2015).

During hydrothermal circulation in which seawater percolates downward through the porous oceanic crust, is heated, and buoyantly rises back to the ocean floor, circulating seawater reacts with rocks resulting in a net gain or loss of reactive chemical species (Figure 2), playing a central role in regulating the distribution of many elements in the ocean. However, while transformations of many elements during convective circulation of seawater through oceanic lithosphere is well established, those of nitrogen remains scarcely documented and poorly understood (Shock, 1992; Karl, 1995; Van Dover, 2000).

1.1. Nitrogen cycling in deep-sea hydrothermal vents

Nitrogen (N) is required by all forms of life on Earth as a key component of biochemical compounds including proteins and nucleic acids. While most of the world's ocean is replete in dissolved dinitrogen gas (N_2), this form is only accessible to very limited group of microbes (i.e., nitrogen fixing organisms or diazotrophs). Most other organisms rely on uptake other nitrogen forms including nitrate (NO_3^-), nitrite (NO_2^-), dissolved organic nitrogen (DON), and ammonium (NH_4^+). Oxic bottom seawater is typically rich in NO_3^- (tens of µM) with levels of NH_4^+ below detection. However, after water-rock interaction during hydrothermal circulation, high temperature venting fluids that resurface at the seafloor typically exhibit a much more reducing N speciation— undetectable NO_3^- yet replete in NH_4^+ (e.g., Butterfield et al., 2004; Bourbonnais et al., 2012b). These N transformations result in the N speciation in the vent fluids that is markedly different from that of the bottom seawater (Figure 3).

While the origin of NH_4^+ in vent fluids from sediment-covered vent systems (such as those at Guaymas Basin, Escabana Trough, and Okinawa Trough) have been attributed to low-temperature remineralization and thermal decomposition of organic matter (Von Damm et al., 1985; Campbell et al. 1988; Seewald et al., 1990; Seewald et al., 2003; Nunoura et al., 2010), the source of vent NH_4^+ at sediment-starved systems is still somewhat unclear. Several processes have been identified that may produce NH_4^+ in the subsurface. These include abiotic reduction of NO_3^- and N_2 to NH_4^+ in high-temperature reaction zones, as well as microbial reduction of NO_3^- to NH_4^+ in the low temperature recharge and discharge zones. These processes are illustrated in Figure 4.

Indeed within the hot, reducing reaction zones encountered during hydrothermal circulation, abiotic reactions prevail, as temperatures are too high for microbial life. However, in

low-temperature zones such as those associated with diffuse vents, microbes can thrive and actively metabolize bioavailable forms of N. In contrast to high-temperature vent fluids, these low-temperature, diffuse vents are formed from the mixing between hot fluid endmember and cold, ambient seawater resulting in low-temperature fluids that may contain both NH_4^+ and NO_3^- (e.g., Lilley et al., 1983; Johnson et al., 1988; Butterfield et al., 2004). Here as well as within the buoyant hydrothermal plume, elevated microbial activity is often reported and evidence for a range of microbially-mediated N transformations, both reductive and oxidative, has been found.

There are many different approaches to studying nitrogen cycling at deep-sea vents. For biological reactions, microbiological and molecular biology approaches including isolation and cultivation of representative microbes (e.g., Pérez-Rodríguez et al., 2010; Vetriani et al., 2004), as well as metagenomic and/or metatranscriptomic interrogation of the natural microbial community (e.g., Fortunato and Huber, 2016; Baker et al., 2013), or even extraction of information from relative abundances of biomarker molecules (e.g., Russ et al., 2013; Byrne et al., 2009). Alternatively, we can use geochemical approaches based on the changes in the concentrations of N species, incubations with N substrate either with isotopically labeled or unlabeled substrate (e.g., Bourbonnais et al., 2012a; McNichol et al., 2016; 2018), or by investigating natural abundance variations in the isotope ratios of different N pools (e.g., Bourbonnais et al., 2012b; Sylvan et al., 2017). Microbial N transformations at vents and how they have been studied were recently reviewed (Wankel et al., 2017).

Abiotic reactions, however, do not impart any signatures detectable by microbiological techniques and thus are only discernable using geochemical approaches (i.e., making inferences from changes in concentrations of chemical species of interests, incubations with or without

isotope labeling, or natural abundance stable isotope variations). Geochemical approaches, especially those leveraging stable isotope techniques, were used as the main tool in this thesis.

1.2. Thesis organization

As of now, every microbial N transformation that has been identified within the ocean has also been specifically shown to exist within deep-sea hydrothermal vent ecosystems (Wankel et al., 2017). While there have been many studies focusing on low-temperature, diffuse vents through examination of solute concentrations and molecular biological techniques, what remains lacking is the use of stable isotope geochemistry to help constrain how those microbial processes affect N speciation – especially the availability of NH_4^+ - a compound notable for its role as both a nutrient and energy source. Moreover, even fewer studies have been conducted addressing the dynamics of subsurface transformation at high temperatures and temperatures, which play a primary role in dictating the fundamental speciation of N in hydrothermal fluids long before reaching the biologically active seafloor.

Below, I outline some of the key questions in our understanding pertaining to N speciation at vents that I have addressed in this thesis primarily through the use of stable isotope geochemistry.

What are the reaction kinetics and isotope fractionation of abiotic NO_3^- reduction to NH_4^+? This question is addressed in **CHAPTER 2**, which describes the high temperature reduction of NO_3^- by the mixed-valence iron mineral, magnetite, as a model for this particular abiotic reaction. A variety of experimental conditions (i.e., temperatures, pH, and salinity) were explored to test their effects on reactions rates and patterns of isotope fractionation. While some aspects relevant to this question have been previously investigated (e.g., Brandes et al. 1998;

2008), these earlier studies did not examine changes in the isotopic compositions of substrate and product pools, instead only examining net changes in reaction and product concentrations. Here in Chapter 2, I followed the changes in both concentrations and isotopic compositions of both substrate and product pools over the course of lab simulated high-temperature, high-pressure reactions.

How can we discern sources of NH_4^+ and pertinent high-temperature reactions from the N isotopic composition of NH_4^+ ($\delta^{15}N_{NH4}$) in hydrothermal vent fluids? This study, as described in **CHAPTER 3**, provides new measurements of $\delta^{15}N_{NH4}$ and NH_4^+ concentrations on newly collected and archived samples along with previously reported measurements from other studies making this large compilation the first of its kind to assemble N speciation data from deep-sea vents all across the globe. In this chapter, I explain patterns found in NH_4^+ concentrations from vent fluids of both sediment-influenced and unsedimented systems, providing further interpretation based on $\delta^{15}N_{NH4}$ measurements to constrain potential sources of vent NH_4^+ and potential reactions occurring along the hydrothermal circulation giving rise to the $\delta^{15}N_{NH4}$ values observed in the discharged fluids.

What microbial processes are functioning at low-temperature, diffuse vents that may modify NH_4^+ concentrations and isotopic compositions? To address this question, I selected two low-temperature sites, *Crab Spa* and *Teddy Bear* at 9°50'N East Pacific Rise as model systems. **CHAPTER 4** details measurements from natural samples taken over several years as well as new isotopic measurements from previously performed incubation experiments conducted on fluids from *Crab Spa* (McNichol et al., 2016; 2018). In addition, I employed a simple kinetic isotope effect integrated Michaelis-Menten model, which incorporated three different N transformations (i.e., NO_3^- reduction to NO_2^-, NO_2^- reduction to N_2, and NO_2^-

reduction to NH_4^+). Results of this model, together with the results from natural and incubation samples suggest a complex interplay between a several microbial processes acting to exert control on measured NH_4^+ concentration and isotopic composition.

Finally, **CHAPTER 5** outlines the summary of each individual study in this thesis and the contribution in advancing the field. Moreover, several notes on potential research directions to further the results from this thesis are described.
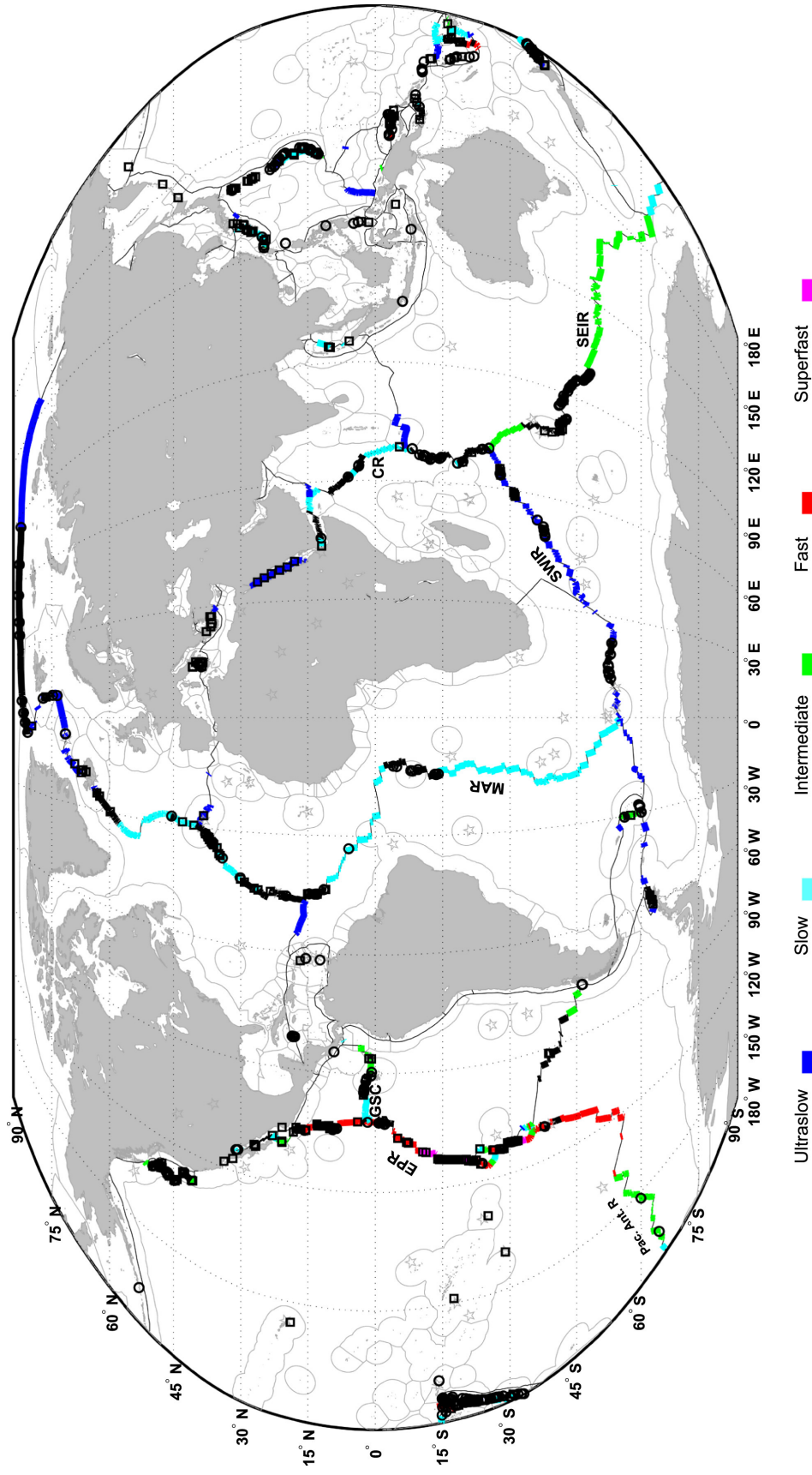
Figure 1. Global distribution of submarine hydrothermal vents (figure from Beaulieu et al, 2015). Colors denote spreading rate: ultraslow (<20 mm/yr), slow (20–55 mm/yr), intermediate (55–80 mm/yr), fast (80–140 mm/yr), or superfast (>140 mm/yr). Plate boundaries (thin black lines), exclusive economic zones (thin gray line), confirmed and inferred vent fields (black open markers: square=discovered prior to year 2000, circle=discovered during or after year 2000) are shown. Abbreviations: CR=Carlsberg Ridge; EPR=East Pacific Rise; GSC=Galápagos Spreading Center; MAR=Mid-Atlantic Ridge; Pac. Ant. R=Pacific Antarctic Ridge; SEIR=Southeast Indian Ridge; SWIR=Southwest Indian Ridge.
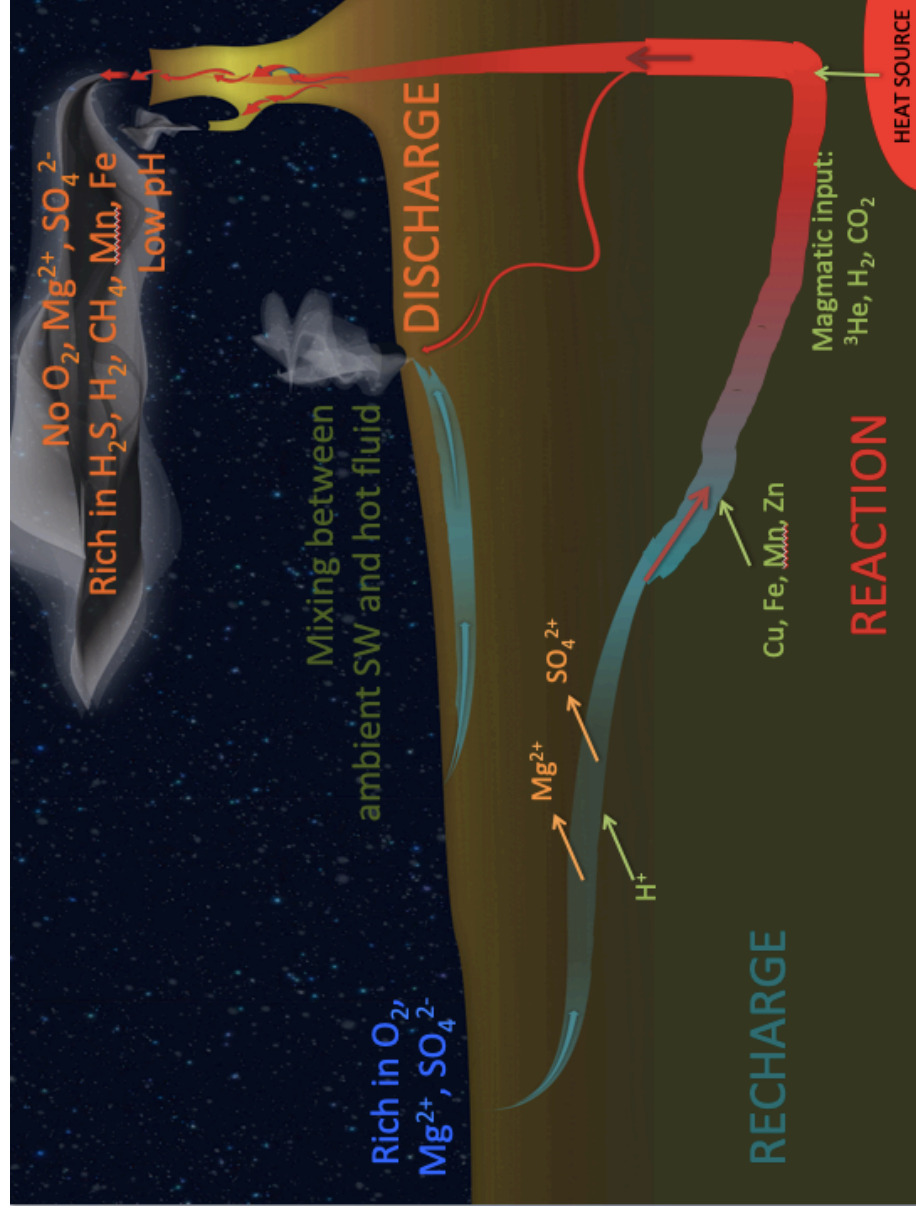
Figure 2. Typical hydrothermal circulation at mid-ocean ridges and chemical alteration therein. General hydrothermal circulations can be divided into three zones: (1) recharge zone, (2) reaction zone, and (3) discharge zone. As the bottom seawater percolates down through the crust in the recharge zone, O_2, Mg^{2+} and SO_4^{2-} are removed and H^+ is added. The combined effect of these reactions leads to a chemically modified fluid that is slightly acidic, anoxic, alkali-rich, and Mg-poor relative to seawater. Within the high-temperature reaction zone closer to the heat source, the acidity then leaches S and other metals from the rock, magmatic volatiles (including He, CO_2, CH_4, H_2) may be added, and other water-rock reactions occur When the temperatures and pressures exceed those of the boiling curve, separation of the fluid into a low-salinity, vapor-rich phase and a brine phase; this is termed phase separation. Finally, as the hot fluids buoyantly rise to the seafloor in the discharge zone, there may be some equilibration, with minor amounts of precipitation and/or dissolution of sulfide phases. The fluid may exit directly into the ocean through high-temperature, focused venting, or be modified in the subsurface if seawater is entrained in the vicinity of the vents resulting in the low-temperature, diffuse venting.
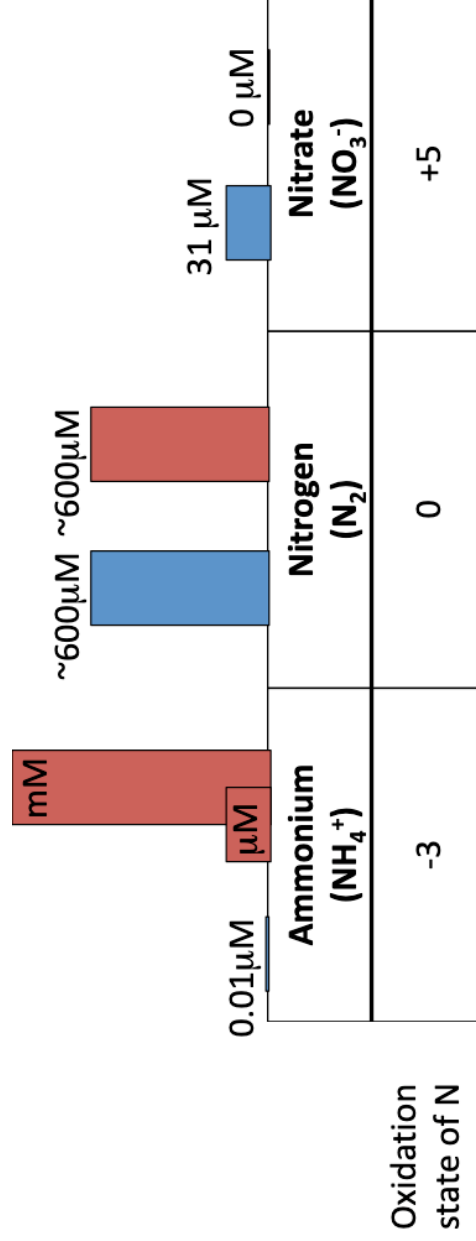
Figure 3. Typical N speciation in vent fluids (red bars on the right) vs bottom seawater (blue bars on the left). NH_4^+ in the bottom seawater averages 0.01 μM while in the vent fluids large range of concentrations can be found. Unsedimented systems typically exhibit μM-level concentrations and sedimented systems show much higher concentrations mostly > 1mM. N_2 is conventionally regarded as mostly inert chemically. Bottom seawater concentrations are in equilibrium with their atmospheric source. Few reports on the vent fluid N_2 show either similar concentration to the ambient seawater counterparts or N_2 enrichments (e.g., Charlou et al., 2002). NO_3^- in the deep ocean averages 31 μM (across all ocean basins) while it is virtually undetectable in high-temperature vent fluids.
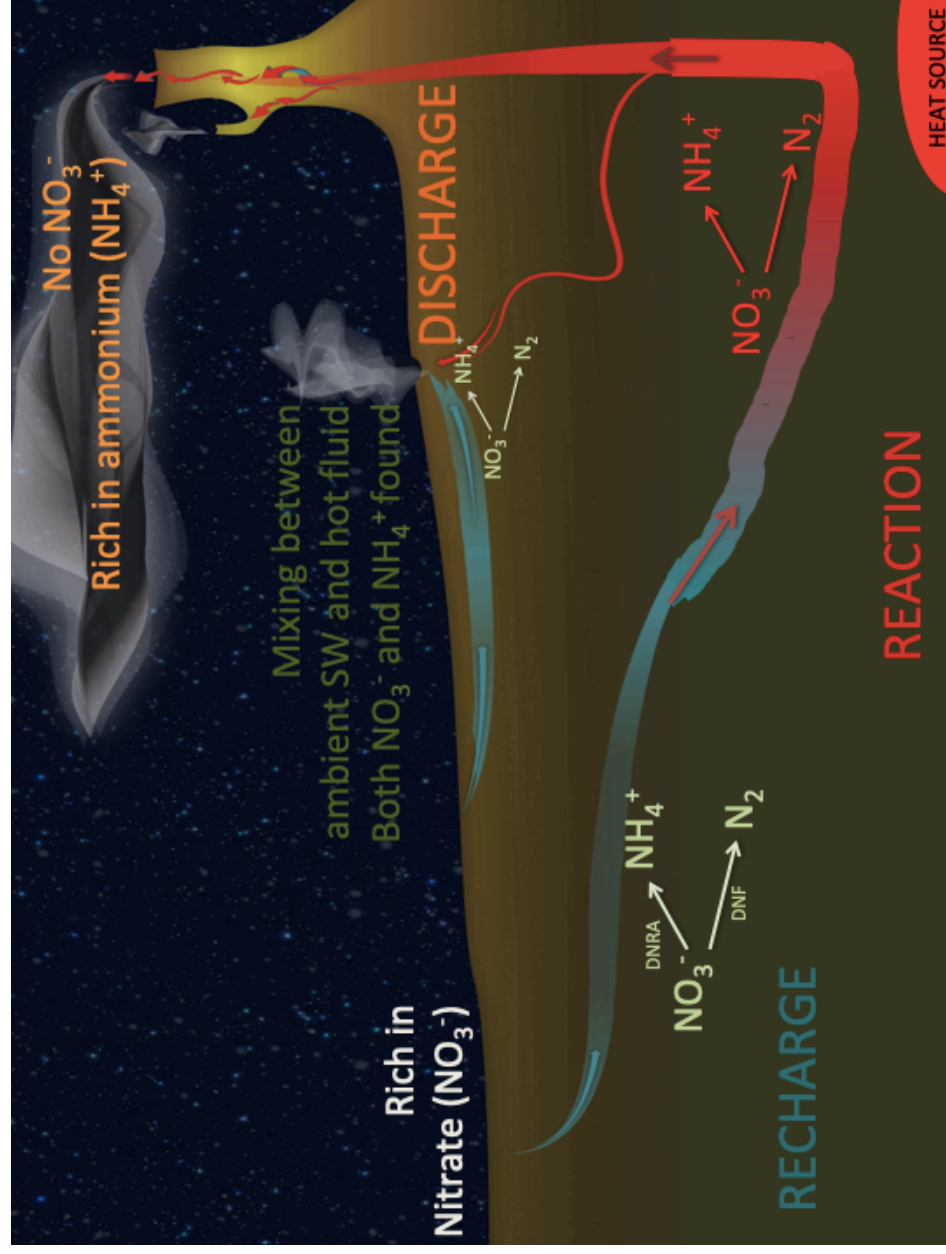
Figure 4. Nitrogen transformations at vents. As the seawater perculates downward, NO_3^- in the bottom seawater can be converted to NH_4^+ or N_2 through microbial reactions including denitrification (DNF) and dissimilatory nitrate reduction to ammonium (DNRA) and abiotic reactions. The former microbial processes prevail in the low-temperature zone while the latter abiotic counterparts dominates at higher temperatures. Organic matter when available can also be remineralized or pyrolyzed to NH_4^+. These products of NO_3^- reductions ultimately exit to the seafloor with the vent fluids. At low-temperature, diffuse vents, microbial communities can further metabolize these N species, thereby modifying the N species further.

REFERENCES

Baker BJ, Sheik CS, Taylor CA, Jain S, Bhasi A, Cavalcoli JD et al. (2013). Community transcriptomic assembly reveals microbes that contribute to deep-sea carbon and nitrogen cycling. *ISME J 7*: 1962–1973.

Beaulieu, S. E., Baker, E. T., & German, C. R. (2015). Where are the undiscovered hydrothermal vents on oceanic spreading ridges?. *Deep Sea Research Part II: Topical Studies in Oceanography*, *121*, 202-212.

Bourbonnais, A., Juniper, S. K., Butterfield, D. A., Devol, A. H., Kuypers, M. M. M., Lavik, G., ... & Lehmann, M. F. (2012a). Activity and abundance of denitrifying bacteria in the subsurface biosphere of diffuse hydrothermal vents of the Juan de Fuca Ridge. *Biogeosciences*, *9*, 4661-4678.

Bourbonnais, A., Lehmann, M. F., Butterfield, D. A., & Juniper, S. K. (2012b). Subseafloor nitrogen transformations in diffuse hydrothermal vent fluids of the Juan de Fuca Ridge evidenced by the isotopic composition of nitrate and ammonium. *Geochemistry, geophysics, geosystems*, *13*(2).

Brandes, J. A., Boctor, N. Z., Cody, G. D., Cooper, B. A., Hazen, R. M., & Yoder Jr, H. S. (1998). Abiotic nitrogen reduction on the early Earth. *Nature*, *395*(6700), 365.

Brandes, J. A., Hazen, R. M., & Yoder Jr, H. S. (2008). Inorganic nitrogen reduction and stability under simulated hydrothermal conditions. *Astrobiology*, *8*(6), 1113-1126.

Butterfield, D. A., Roe, K. K., Lilley, M. D., Huber, J. A., Baross, J. A., Embley, R. W., & Massoth, G. J. (2004). Mixing, reaction and microbial activity in the sub-seafloor revealed by temporal and spatial variation in diffuse flow vents at Axial Volcano. *The Subseafloor Biosphere at Mid-Ocean Ridges*, *144*, 269-289.

Byrne, N., Strous, M., Crepeau, V., Kartal, B., Birrien, J.-L., Schmid, M., Lesongeur, F., Schouten, S., Jaeschke, A., Jetten, M.S., Prieur, D. & Godfroy, A. (2009) Presence and activity of anaerobic ammonium-oxidizing bacteria at deep-sea hydrothermal vents. *ISME Journal* **3**, 117-123.

Campbell, A. C., Bowers, T. S., Measures, C. I., Falkner, K. K., Khadem, M., & Edmond, J. M. (1988). A time series of vent fluid compositions from 21° N, East Pacific Rise (1979, 1981, 1985), and the Guaymas Basin, Gulf of California (1982, 1985). *Journal of Geophysical Research: Solid Earth*, *93*(B5), 4537-4549.

Charlou, J. L., Donval, J. P., Fouquet, Y., Jean-Baptiste, P., & Holm, N. (2002). Geochemistry of high H2 and CH4 vent fluids issuing from ultramafic rocks at the Rainbow hydrothermal field (36 14′ N, MAR). *Chemical geology*, *191*(4), 345-359.

Corliss, J. B., Dymond, J., Gordon, L. I., Edmond, J. M., von Herzen, R. P., Ballard, R. D., ... & van Andel, T. H. (1979). Submarine thermal springs on the Galápagos rift. *Science*, *203*(4385), 1073-1083.

Fortunato, C.S., and Huber, J.A. (2016) Coupled RNA-SIP and metatranscriptomics of active chemolithoautotrophic communities at a deep-sea hydrothermal vent. *ISME J* **10**: 1925–1938.

Johnson, K. S., Childress, J. J., Hessler, R. R., Sakamoto-Arnold, C. M., & Beehler, C. L. (1988). Chemical and biological interactions in the Rose Garden hydrothermal vent field, Galapagos spreading center. *Deep Sea Research Part A. Oceanographic Research Papers*, *35*(10-11), 1723-1744.

Karl, D. M. (1995). Ecology of free-living, hydrothermal vent microbial community. In Karl, D. M. (Ed.), *The microbiology of deep-sea hydrothermal vents* (pp. 35-124). CRC Press.

Lilley, M. D., Baross, J. A., & Gordon, L. I. (1983). Reduced gases and bacteria in hydrothermal fluids: the Galapagos spreading center and 21 N East Pacific Rise. In *Hydrothermal processes at seafloor spreading centers* (pp. 411-449). Springer, Boston, MA.

McNichol, J., Stryhanyuk, H., Sylva, S. P., Thomas, F., Musat, N., Seewald, J. S., & Sievert, S. M. (2018). Primary productivity below the seafloor at deep-sea hot springs. *Proceedings of the National Academy of Sciences*, 201804351.

McNichol, J., Sylva, S. P., Thomas, F., Taylor, C. D., Sievert, S. M., & Seewald, J. S. (2016). Assessing microbial processes in deep-sea hydrothermal systems by incubation at in situ temperature and pressure. *Deep Sea Research Part I: Oceanographic Research Papers*, *115*, 221-232.

Nunoura, T., Oida, H., Nakaseama, M., Kosaka, A., Ohkubo, S. B., Kikuchi, T., ... & Hirayama, H. (2010). Archaeal diversity and distribution along thermal and geochemical gradients in hydrothermal sediments at the Yonaguni Knoll IV hydrothermal field in the Southern Okinawa Trough. *Applied and environmental microbiology*, *76*(4), 1198-1211.

Pérez-Rodríguez, I., Ricci, J., Voordeckers, J. W., Starovoytov, V., & Vetriani, C. (2010). Nautilia nitratireducens sp. nov., a thermophilic, anaerobic, chemosynthetic, nitrate-

ammonifying bacterium isolated from a deep-sea hydrothermal vent. *International journal of systematic and evolutionary microbiology*, *60*(5), 1182-1186.

Russ, L., Kartal, B., Op Den Camp, H. J., Sollai, M., Le Bruchec, J., Caprais, J. C., ... & Jetten, M. S. (2013). Presence and diversity of anammox bacteria in cold hydrocarbon-rich seeps and hydrothermal vent sediments of the Guaymas Basin. *Frontiers in microbiology*, *4*, 219.

Seewald, J. S., Seyfried Jr, W. E., & Thornton, E. C. (1990). Organic-rich sediment alteration: an experimental and theoretical study at elevated temperatures and pressures. *Applied Geochemistry*, *5*(1-2), 193-209.

Seewald, J., Cruse, A., & Saccocia, P. (2003). Aqueous volatiles in hydrothermal fluids from the Main Endeavour Field, northern Juan de Fuca Ridge: temporal variability following earthquake activity. *Earth and Planetary Science Letters*, *216*(4), 575-590.

Shock, E. L. (1992). Chemical environments of submarine hydrothermal systems. In Holm, N. G. (Ed.), *Origins of Life and Evolution of the Biosphere* (pp. 67-107). Springer, Netherlands.

Sylvan, J. B., Wankel, S. D., LaRowe, D. E., Charoenpong, C. N., Huber, J. A., Moyer, C. L., & Edwards, K. J. (2017). Evidence for microbial mediation of subseafloor nitrogen redox processes at Loihi Seamount, Hawaii. *Geochimica et Cosmochimica Acta*, *198*, 131-150.

Tivey, M. K. (2007). Generation of seafloor hydrothermal vent fluids and associated mineral deposits. *Oceanography*, *20*(1), 50-65.

Van Dover, C. (2000). Chemical and physical properties of vents fluids. In Van Dover, C. (Ed.), *The ecology of deep-sea hydrothermal vents* (pp. 76-98). Princeton University Press.

Vetriani, C., Speck, M. D., Ellor, S. V., Lutz, R. A., & Starovoytov, V. (2004). Thermovibrio ammonificans sp. nov., a thermophilic, chemolithotrophic, nitrate-ammonifying bacterium from deep-sea hydrothermal vents. *International journal of systematic and evolutionary microbiology*, *54*(1), 175-181.

Von Damm, K. V., Edmond, J. T., Measures, C. I., & Grant, B. (1985). Chemistry of submarine hydrothermal solutions at Guaymas Basin, Gulf of California. *Geochimica et Cosmochimica Acta*, *49*(11), 2221-2237.

Wankel, S. D., Bourbonnais, A., & Charoenpong, C. N. (2017). Microbial processes at submarine hydrothermal vents. In J. Kallmeyer (Ed.), *Life at Vents and Seeps* (pp. 179-222). de Gruyter, Berlin/Boston.

THIS PAGE INTENTIONALLY LEFT BLANK

CHAPTER 2

Reaction kinetics and isotopic fractionation during NO_3^- reduction to NH_4^+ under high-temperature and high-pressure conditions

2.1. ABSTRACT

While numerous studies have reported on the activity of biological nitrogen (N) metabolisms in hydrothermal vent ecosystems, the body of work on high temperature N transformations remains relatively scarce. While it has been generally assumed that bottom-seawater nitrate (NO_3^-) is quantitatively reduced to ammonium (NH_4^+), concentrations of NH_4^+ in vent fluids rarely reflect such quantitative conversion – suggesting the production and fate of NH_4^+ in these systems is controlled by a set of processes that is largely uncharacterized. Here, we simulated hydrothermal reaction conditions for evaluating both the reaction kinetics and N and O isotope fractionation occurring during reduction of nitrate (NO_3^-) to NH_4^+ in the presence of magnetite. Experiments were carried out at 350 bar and over temperatures ranging between 150°C and 280°C. Despite values for the N isotopic effect of nitrate reduction ($^{15}\varepsilon$) ranging widely from -68 to -5‰, the relationship between N and O isotope effects ($^{18}\varepsilon/^{15}\varepsilon$) was consistently ~0.64. In experiments where pH was unbuffered, the reaction quantitatively produced only NH_4^+. In contrast, experiments in which pH was maintained between 4 and 5 yielded N_2 as an additional product. The presence of N_2 as one of the reaction products suggests a role for abiotic high-temperature reduction of NO_3^- during hydrothermal circulation as a loss term for bioavailable N in the ocean.

2.2. INTRODUCTION

Hydrothermal vent systems are important features in all ocean basins. Water-rock interactions that occur under elevated temperatures as seawater percolates downward through ocean crust heavily modifies fluid chemistry as reflected in net gains or losses of a range of chemical species. Transformation of many elements during the convective circulation of seawater through the oceanic lithosphere is well established, yet nitrogen cycling in these environments remains poorly understood (Karl, 1995; Shock 1995; Van Dover, 2000). Aside from dissolved dinitrogen gas (N_2), total ammonium ($\Sigma NH_4 = NH_3 + NH_4^+$) can represent an abundant form of dissolved inorganic N in vent fluids (German and Von Damm, 2003). This source of reduced N allows proliferation of nitrifying bacterial communities that gain energy by oxidizing NH_3 (and NO_2^-) and elevated NH_3 oxidation activities have been reported in hydrothermal vent plumes (Lam et al., 2004; Lam et al., 2008), diffuse vent fluids (Bourbonnais et al., 2012; Sylvan et al., 2017), and on mineral deposits around the vent (Wang et al., 2007; Li et al., 2014).

In addition to serving as an energy source for chemolithoautotrophic productivity, NH_3/NH_4^+ also impacts the pH of venting fluids due to protonation of NH_3 to NH_4^+. Endmember vent fluids from sediment-hosted hydrothermal vents such as Guaymas Basin where ΣNH_4 is highly elevated relative to bottom seawater (i.e., in mmol/kg concentrations) exhibit higher pH than other unsedimented vent fluids such as the East Pacific Rise containing lower ΣNH_4 (i.e., in umol/kg concentrations). This NH_3/NH_4^+ mediated buffering system has been shown to maintain relatively higher pH required for precipitation of amorphous silica and sulfide minerals necessary for the growth of large vent structures such as those at the Endeavour Segment of the Juan de Fuca Ridge (Tivey et al., 1999).

Moreover, it has also been hypothesized that the origin and evolution of life may have occurred in submarine hydrothermal vent settings due to the presence of the key ingredients for life and the presence of strong physical and geochemical gradients (Baross and Hoffman, 1985; Corliss et al., 1981). Indeed, many studies have implicated the essential role of hydrothermally-produced, reduced N in the form of NH_3/NH_4^+ in the origin of life on Earth (Brandes et al., 1998; Summers and Chang, 1993) and elsewhere in our solar system (Capone et al., 2006; Krasnopolsky, 2006; Summers and Khare, 2007).

In contrast to bottom seawater where nitrate (NO_3^-) is found in abundance, endmember vent fluids are typically devoid of NO_3^- (Butterfield et al., 2004; Bourbonnais et al., 2012). Although the fate of NO_3^- as seawater transits the hydrothermal circulation regime remains unclear, the quantitative conversion of NO_3^- to ΣNH_4 has been widely accepted (e.g., Brandes et al., 1998). However, observed concentrations of ΣNH_4 from high-temperature venting fluids often do not match corresponding concentrations of bottom-water NO_3^- from off axis recharge zones. In this light, isotopes can offer useful constraints on the source of vent fluid ΣNH_4 and the nature of important reactions (whether biotic or abiotic). However, reliable interpretation of vent-derived ΣNH_4 is limited by a paucity of available information on reaction pathways, products, and isotope systematics of such reactions. Unfortunately, the only existing data to date are those provided by Brown and Drury (1967, 1969) for NO_3^- reduction by Fe^{2+} at temperatures below 110˚C as determined empirically and through first-principle calculations based on vibrational frequencies for the N-O bond of NO_3^-. A more quantitative treatment thus requires a more representative and robust characterization of such reactions under hydrothermal conditions, including extension of the temperature range and more robust constraint of reaction conditions.

Here we examined the kinetics and controls on N and O isotope effects during the reduction of NO_3^- reduction to NH_4^+ at elevated temperatures and pressures representative of submarine hydrothermal conditions. We demonstrated a clear pattern of reaction products with the reaction producing only NH_4^+ at elevated pH, but interestingly both NH_4^+ and N_2 at lower pH. In addition, by constraining the isotopic fractionation during this reaction, our results can be used to improve our interpretation of N isotope studies of NH_4^+ (and NO_3^-, where available in low temperature systems) in hydrothermal vent fluids.

2.3. MATERIALS AND METHODS

2.3.1. Setup of the experiments

All experiments were conducted at 350 bar over a temperature range of 150˚ to 280˚C inside a reaction-cell system consisting of a flexible gold bag (~60-mL volume), titanium closure piece, and titanium exit tube enclosed in a stainless steel pressure vessel, as described previously (Seyfried et al., 1987). Hydrostatic pressure within the vessel was regulated by pumping water into and out of the pressure vessel, while temperature was maintained by housing the reactor vessel inside a tubular furnace. Fluids and minerals were loaded into the gold bag, pressurized, and subsequently heated to prescribed temperatures. This flexible cell, closed system setup allowed fluid samples to be periodically withdrawn during the course of the reactions without impacting reaction conditions (e.g., pressure, temperature).

Contained within the flexible gold bag, the initial fluid composition was made by dissolving KNO_3 and KCl in deionized water and combining with the mineral mixture. In some experiments, pH was buffered by addition of sodium acetate/acetic acid buffer. H_2 fugacity was maintained by the presence of hematite-magnetite (HM) mineral mixture (high purity research

grade; Puratronic, Alfa Aesar). Before the reaction bag was loaded, the fluid and minerals were slurried and then purged with ultra-high purity Argon for at least 30 minutes to remove any N_2 and O_2 in solution before the cell was closed. Any headspace within the gold bag was purged with ultra-high purity Argon after capping. This step serves both to prevent oxidation of minerals by O_2 while the cell was heated to experimental temperatures as well as to maintain added NO_3^- as the sole source of N in the experimental system.

2.3.2. Fluid sampling

Fluid samples were taken using gas-tight syringes ($3 - 5$ mL each time point). For each time point, 4 syringes were used: (1) bleed syringe, (2) pH syringe, (3) anion syringe, and (4) cation syringe. After weighing the amount of fluid drawn into each sampling syringe, pH measurements were made by potentiometry using Fisher Scientific™ accumet™ AB15 Basic and BioBasic™ pH/mV/°C Meters equipped with an accumet™ liquid-filled, glass body combination pH Ag/AgCl Electrode (13-620-285). Fluid samples for pH measurement were kept gas-tight until measurements were made (typically within 5 minutes of sampling).

Samples used for ΣNH_4 concentrations and isotopic compositions were taken with attention toward avoiding N loss by NH_3 volatilization, a process known to be accompanied by large isotopic fractionation (e.g., Högberg, 1997). This sampling was achieved by rapid lowering of fluid pH during sample collection. Cation syringes for ammonium samples were pre-filled with known amounts of 100mM phosphoric acid to ensure pH of the collected solution was always below 4. This approach provided both accurate concentrations as well as high integrity N isotope composition of ΣNH_4 ($\delta^{15}N_{NH4}$). We also collected samples for gaseous N species in one of the experiments (Exp. 11), using a 5mL-serum vial capped with a butyl stopper and crimped

with an aluminum seal flushed with high-purity He gas. Sample fluid was taken with a gas-tight syringe and injected into the vial through a needle avoiding incorporation of any air (also verified by analytical absence of O_2).

2.3.3 Chemical analyses of the solute

Solute concentrations were measured by ion chromatography (IC) using a Dionex DX-500 IC System. Samples were gravimetrically diluted with DI water before concentration analyses for anions (NO_3^-, NO_2^-, CH_3COO^- and Cl^-) and cations (ΣNH_4, Na^+, and K^+). Anions were chromatographically separated using a Dionex IonPac AS15 column and carbonate removal cartridge (Dionex CRD200) run isocratically with eluent consisting of a 38mM NaOH flowing at 1.2 mL/min. Cations were chromatographically separated using Dionex IonPac CS12A column run isocratically with eluent made up of a 23mM H_2SO_4 flowing at 1.0 mL/min. Both anion and cation analyses were run in suppressed conductivity mode for increased sensitivity (suppressor current of 300 mA and 125 mA for anions and cations, respectively). Analytical uncertainty (2σ) was better than $\pm3\%$. While all N ions track the progress of the reduction reaction, K^+ and Cl^- serve as conservative tracers to ensure no leakage in the gold bag.

When Na^+ and Cl^- were high (e.g., seawater salinity such as in Exp. 11), measurement of NH_4^+ and NO_3^- by IC was inappropriate for a number of reasons. Firstly, both Na^+ and Cl^- are much more concentrated than NH_4^+ and NO_3^-. Secondly, for cation analyses, the large Na^+ peak often overlaps with NH_4^+ making it hard to obtain accurate NH_4^+ concentrations. Lastly, measuring low concentrations of NO_3^- can be challenging, as it requires less dilution leading to saturated Cl^- peak. Instead, NO_3^- was assessed using the reduction NO_3^- by hot, acidic vanadium producing NO, which was measured with chemiluminescent detection (Garside, 1982).

As for the ΣNH_4 measurement, we used flow injection analysis (FIA) as described in Hall and Aller (1992). Under flow, the sample was combined with a basic solution (10 mM NaOH with 150 mM sodium citrate) to raise pH and thereby convert all NH_4^+ to NH_3, which diffused through a Teflon membrane and into a dilute acid solution (20uM HCl) flowing on the opposite side of the membrane. Electrical conductivity of these dilute acid solutions carrying NH_4^+ was measured using Dionex conductivity detector (CDM-3) and calibrated against standard solutions of known concentrations. To ensure consistency between different techniques of measurements (IC vs chemiluminescence for NO_3^- and IC vs FIA for NH_4^+), all concentration standards used were all prepared from the same stock solutions.

2.3.4. Stable isotope analyses

All stable isotope analyses of N species (NO_3^-, NH_4^+ and total dissolved N) were carried out after conversion to N_2O prior to introduction into an IsoPrime100 (Elementar, Inc.) isotope ratio mass spectrometer (IRMS). Nitrate N and O isotopic composition ($\delta^{15}N_{NO3}$ and $\delta^{18}O_{NO3}$, respectively) were measured using the denitrifier method (Casciotti et al., 2002; Sigman et al., 2001), in which sample NO_3^- is quantitatively converted to N_2O using a lab-grown denitrifying bacterium, *Psuedomonas aureofaciens*, before being extracted and purified on a purge and trap system similar to that previously described in McIlvin and Casciotti (2011). To avoid potential interferences, NO_2^- was removed by sulfamic acid addition (Granger et al., 2009) prior to isotopic analysis of NO_3^-. Corrections for drift, size and fractionation of O isotopes during bacterial conversion were carried out as previously described (Casciotti et al., 2002; McIlvin and Casciotti, 2011) using NO_3^- standards USGS-32 ($\delta^{15}N = 180.0‰$), USGS-34 ($\delta^{15}N = -1.8‰$ and

$\delta^{18}O$ = -27.9‰) and USGS-35 ($\delta^{15}N$ = 4.5‰ and $\delta^{18}O$ = 57.5‰). Typical reproducibilities were

0.2‰ and 0.4‰ for $\delta^{15}N$ and $\delta^{18}O$, respectively.

Ammonium $\delta^{15}N$ ($\delta^{15}N_{NH4}$) analyses were carried out by hypobromite oxidation to NO_2^-

followed by azide reaction to produce N_2O as described previously (Zhang et al., 2007). Isotopic

composition of the NH_4^+ pool was normalized using international isotopic reference standards:

IAEA-N1 ($\delta^{15}N$ = +0.5‰), USGS-25 ($\delta^{15}N$ = -29.4‰) and USGS-26 ($\delta^{15}N$ = +52.9‰).

Repeated measurements of $\delta^{15}N_{NH4}$ had a typical precision of ±0.7‰.

Total dissolved N $\delta^{15}N$ ($\delta^{15}N_{TDN}$) analyses were carried out by persulfate oxidation where

all dissolved N is oxidized to NO_3^- using potassium persulfate at high pH inside an autoclave

(121°C) for 60 minutes, as previously described (Knapp et al. 2005), followed by conversion of

NO_3^- to N_2O via the denitrifier method as described above. Reported $\delta^{15}N_{TDN}$ values were

normalized to isotopic reference standards: USGS-40 ($\delta^{15}N$ = -4.52‰) and USGS-41a ($\delta^{15}N$ =

+47.55‰). The precision for this method was ±0.5‰.

2.3.4 Solid mineral analyses

Images of mineral mixtures used in this study were taken with a Hitachi TM3000

scanning electron microscope (SEM) operated under low vacuum. Minerals were further

characterized using X-ray diffraction (XRD). Powder X-ray diffraction was conducted on a

Rigaku D/MAX Rapid II micro X-ray diffractometer with a 2D imaging plate detector using Mo

Kα radiation (λ = 0.709300 Å). Samples were carefully aligned and run for 10 minutes with

omega fixed at 0 and phi rotating at 1 degree per second. Four analytical replicates were run for

each sample.

Powders were mounted on Kapton tips by MiTeGen by using a very thin layer of mineral oil on the tips. A subset of samples was also loaded into 0.8mm Kapton capillaries and compared to results from Kapton tips to assure that results did not vary due to sample mounting methods. XRD image files were background corrected (manual setting = 5) and integrated into intensity versus 2θ patterns from 3.0 to 45.0 2θ degrees and 81.6337 to 430.00 β using 2DP software. Full width at half maximum (FWHM) measurements were performed using PDXL 2 Rigaku software.

2.3.5. In situ pH calculations

The *in situ* pH (i.e., at reaction pressure and temperature) was calculated by speciating the measured fluid composition and pH at 25°C, and then re-speciating the fluid composition at the experimental conditions while conserving mass at in situ conditions, using the EQ3/6 software (Wolery, 1992) and a customized thermodynamic database prepared at 350 bars with SUPCRT92 (Johnson et al., 1992).

2.3.6. Equilibrium N isotope fractionation calculation

We calculate the equilibrium nitrogen isotope fractionation between dissolved NO_3^- and NH_3 based on first principle quantum mechanical calculations (Schauble, 2004). Molecular geometries were optimized and bond frequencies were calculated at the MP2/aug-cc-pVTZ level, with the solvent effects included using the polarizable continuum model (ICF-PCM). All calculations were conducted using the Gaussian09 program (Frisch et al. 2009) on the high performance cluster (Scylla) at the Woods Hole Oceanographic Institution.

2.4. RESULTS

In all experiments, nitrate consumption was observed and nitrate was reacted to completion or near completion except for cases where experiments were terminated early (because remaining solution in the vessel was low). In the absence of any pH buffering, reactions were accompanied by a marked increase in pH and the drawdown of NO_3^- exhibited quantitative conversion to ΣNH_4. In contrast, however, in experiments in which pH was buffered at ~4.5, this pH shift was greatly diminished and quantitative conversion of NO_3^- to ΣNH_4 was not observed, with yields typically around 40-60%.

As an example, at the start of Exp#5 (unbuffered pH; Figure 1) when the set temperature of 200°C was reached, $[NO_3^-]$ was 9.42 mmol/kg at pH~6.2. NO_3^- was consumed quickly in the beginning where $[NO_3^-]$ was high and the pH was low. Half of the initial NO_3^- disappeared within the first 32 hours. As $[NO_3^-]$ decreased and pH increased, the reaction became progressively slower. At the last time point (t = 407 hr), $[NO_3^-]$ was 0.04 mmol/kg and measured $[\Sigma NH_4]$ was ~100% of the initial $[NO_3^-]$.

In every experiment, the $\delta^{15}N$ and $\delta^{18}O$ of the remaining nitrate pool increased, consistent with normal kinetic isotope fractionation in a closed system or Rayleigh distillation model. In all cases, the degree of change in $\delta^{18}O$ was always smaller than that of the corresponding $\delta^{15}N$ (Table 1). Total dissolved N (TDN) generally accounted for >95% of the combined pools of NO_3^- and NH_4^+, indicating limited accumulation of any intermediate species. Nitrite was never detected and dissolved organic nitrogen was not thought to have formed as evidenced by the [TDN] fully accounting for the combined NO_3^- plus NH_4^+. At high pH, the final $\delta^{15}N_{TDN}$ values (comprised essentially entirely of NH_4^+) were comparable to the starting $\delta^{15}N_{NO3}$ (Figure 6), consistent with the closed-system Rayleigh distillation having a single product (Figure 7). In

addition, the $\delta^{15}N_{TDN}$ at each time point remained consistent over the course of the experiments. A notable exception to this was observed, however, in the pH-buffered experiments in which $\delta^{15}N_{TDN}$ values clearly deviated from the starting $\delta^{15}N_{NO3}$, indicating the production of an additional product not captured by the TDN analysis - likely gaseous N (i.e., either N_2 or N_2O). Although N_2O levels were below detection, accumulation of N_2 was noted and isotopic analysis of indicated $\delta^{15}N_{N2}$ of similar composition to the $\delta^{15}N_{NH4.}$

Scanning electron micrograph of the HM mineral matrix after the experiment reflected structural changes to mineral composition. The well-defined rhomboid crystals (~100 micron size) initially observed before the experiment appeared to disintegrate into much smaller grains (3-10 microns) (Fig 1). X-ray diffraction analyses (XRD) indicated net loss of magnetite and net gain of hematite at the end of the experiment (Fig 1), consistent with expected transformation resulting from oxidation of Fe(II) to Fe(III) when NO_3^- is reduced.

2.5. DISCUSSION

Below, we first discuss the presented reaction as predicted by thermodynamic equilibrium. At the high temperatures, high pressures, and reducing conditions manifested in our experiments, NH_4^+ and N_2 are thought to be the only two stable species of N, with the partitioning between these depending on a number of conditions as elaborated below. Building on this thermodynamically predicted framework, we then discuss experimental results including elements of reaction kinetics and isotope fractionation associated with abiotic reduction of NO_3^-. Finally, we end the discussion by placing these findings into the context of deep-sea hydrothermal vents.

2.5.1. Thermodynamic prediction

At thermodynamic equilibrium in a system of liquid water, inorganic N species (NO_3^-, NH_4^+, and N_2), and a hematite-magnetite (HM) mineral mixture, calculations indicate that NO_3^- is unstable over the temperature range examined in our study. Further, considering the reducing conditions of our experiments as buffered by hematite-magnetite (HM) minerals, thermodynamic calculations (Fig. 3) also predict that N_2 should be the more stable N phase relative to NH_4^+ at equilibrium.

In contrast to these thermodynamic predictions, our experimental results indicated quantitative NH_4^+ production regardless of reaction temperatures when pH was left unbuffered. This suggests that the pathway for production of N_2 is kinetically inhibited as inferred from the lack of N_2 as a product in all unbuffered experiments. Notably, speciation calculations in which N_2 formation was suppressed resulted in NH_3/NH_4^+ as the stable species in the system supporting observations from these unbuffered experiments. Indeed, only in the case where pH was maintained at ~4-5, was N_2 observed as a product in addition to NH_4^+. This suggests, perhaps, the removal of the kinetic barrier in the production of N_2 at lower pH. It is important to note that these thermodynamic predictions are based on assumptions that redox conditions within the system are set by the mineral mixture and that reactions in the system occur in the liquid phase (i.e., homogenous reactions). Deviation from these thermodynamic predictions could stem from the possibility that reduction of NO_3^- occurs on mineral surfaces in a heterogeneous reaction.

2.5.2. Reaction kinetics

Magnetite is a mixed valence Fe^{2+}/Fe^{3+} iron oxide mineral known to reduce NO_3^- to NH_4^+ under the high-temperature and high-pressure conditions (Brandes et al., 1998; Brandes et al.,

2008). Taking magnetite to be the sole reductant for the reaction as in Equation 1, the reaction can be written as:

$$8Fe_3O_4 + NO_3^- + H^+ + H_2O = 12Fe_2O_3 + NH_3 \qquad (1)$$
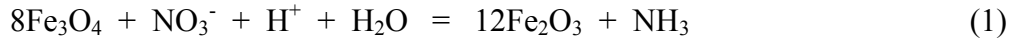
and the reaction rate can be expressed as:

$$Rate = -d[NO_3^-]/dt = -k[NO_3^-]^x[H^+]^y[Fe_3O_4]^z \qquad (2)$$

where k is the rate constant, [ ] denotes concentration for each species and the exponents x, y and z are the order of reaction for each individual species, which need to be determined experimentally. In this work, we did not conduct enough experiments to determine those terms. Instead we chose to express the reaction rate in terms of the reaction half-life ($t_{1/2}$; time taken to for substrate NO_3^- to reach half of its initial concentration), which were hence calculated for each experiment (Table 2).

Although never detected, whether the reduction of NO_3^- to NH_4^+ in this study occurred with NO_2^- as an intermediate is unknown. Most reactions involving both biological and abiotic NO_3^- reduction are thought to proceed through NO_2^- as an intermediate. For example, the biological NO_3^- reducing processes of denitrification and dissimilatory nitrate reduction to ammonium (DNRA) are known to proceed through NO_2^- as the first step before further reduction to N_2 or NH_4^+, respectively. Abiotic reduction of NO_3^- with H_2 (in the presence of a Rh or Rh-Cu catalyst on Al_2O_3 or TiO_2 support) to NH_4^+ and N_2 exhibited a buildup of NO_2^- as an intermediate, which subsequently disappeared at the end of the reaction (State et al., 2017). In contrast, another abiotic study using a Pd catalyst on a Fe_3O_4 support did not report any NO_2^- accumulation (Sun et al., 2012). In our study, we also did not observe any NO_2^- accumulation, suggesting, at a minimum, that reduction of any formed NO_2^- was not rate limiting. This agrees with another study on reaction of magnetite with NO_3^- and NO_2^- at lower temperatures (Dhakal

et al., 2013), which showed that the rate of NO_2^- reduction with magnetite was faster than NO_3^- reduction.

In experiments where an acetic acid/acetate buffer was used to maintain a low reaction pH (Exp#10 and Exp#11), yields of ammonium did not reflect quantitative conversion. To explain this, we consider two different scenarios: (1) a parallel NO_3^- reduction reaction producing N_2 in addition to the reaction producing NH_4^+, or (2) a reaction that subsequently converts NH_4^+ to N_2. With the mineral-buffered fugacity of H_2 being maintained by our experimental conditions, the system redox potential is very reducing – and NH_4^+ is the most reduced form of N. Thus, to explain the production of N_2, we postulate that an additional reduction reaction occurs through dissolved ferrous iron (Fe^{2+}). Aqueous Fe^{2+} has been shown to act as an effective reductant for NO_2^- (Summers and Chang, 1993; Summers and Lerner, 1998; Buchwald et al., 2016; Grabb et al., 2017). Similarly, Dhakal et al. (2013) showed that NO_2^- can be reduced faster by magnetite when Fe^{2+} was added. Therefore, Brandes et al. (2008) argued that Fe^{2+} should be similarly effective with NO_3^- at high temperature and high pressure. In an experimental alkaline system (Brown and Drury, 1967; Brown and Drury, 1969) at temperatures up to 100-110°C, quantitative NO_3^- reduction to ΣNH_4 has been shown to happen. Bearing in mind that our experimental conditions differ from those of Brown and Drury (1967; 1969), our low pH experiments may have promoted a different reaction mechanism altogether. If produced during reduction of NO_3^-, intermediate NO_2^- might react with Fe^{2+} to produce other products notably gaseous N (NO, N_2O and N_2) as shown by other studies conducted at low temperature (e.g., Buresh and Moraghan, 1974; Sorenson et al., 1981; Kampschreur et al., 2011; Buchwald et al., 2016).

The main source of aqueous Fe^{2+} in our experiment is most likely from magnetite. Although at room temperature magnetite is only shown to dissolve in very acidic conditions (Salmimies et al., 2011), increasing temperature has been shown to enhance its dissolution (Sidhu et al., 1981). In fact, in our low pH experiments, given the highly reducing conditions imposed by the presence of H_2, thermodynamic calculations indicate that some magnetite dissolution is expected, allowing for release of aqueous Fe^{2+}. Most of this magnetite derived Fe^{2+} should remain as a free cation as complexation with OH^- is only favored at high pH.

Rates of NO_3^- reduction varied as a function of different treatment conditions including temperatures, amount of magnetite and pH (Figures 4 and 5). With all other conditions held constant, rates of nitrate reduction were faster at higher temperature (compare Exp#3, #5, #6 and #7; Figure 4 top) and lower pH (compare Exp#9 to #10; Figure 5). Dhakal et al. (2013) attributed pH dependence during NO_3^- reduction by magnetite to surface complexation between the negatively charged anions (in this case, NO_3^-) and the positively charged sites within magnetite structures, which are more prevalent at low pH. It is also apparent that water/rock ratio plays a role in determining the reaction rate. Experiments containing more magnetite relative to the start solution volume (Exp#1 vs #9; Figure 4 bottom) had higher reaction rates when other parameters were held constant, consistent with NO_3^- reduction occurring mainly as a surface reaction. No high temperature-pressure study on NO_3^- reduction with magnetite (Brandes et al., 1998; Brandes et al., 2008) has looked at the effect of water/rock ratio to the rate of reaction. However, this trend agrees with the surface reaction described in Equation 4, as more available Fe^{2+} on magnetite surfaces in contact with the aqueous NO_3^- should increase reaction rate. No apparent influence was observed due to differences in ionic strength; comparison between Exp#10

(deionized water matrix) and Exp#11 (0.5M NaCl solution matrix) showed indistinguishable rates of NO_3^- reduction.

2.5.3. N and O Isotope fractionation

The N and O isotope effects (hereafter $^{15}\varepsilon$ and $^{18}\varepsilon$, respectively) for NO_3^- reduction are calculated using the method described in Mariotti et al. (1981). In all cases, $^{18}\varepsilon$ values were smaller than those of $^{15}\varepsilon$ (Table 2). As discussed above, higher temperature, lower pH and lower water/rock ratios all favor increases in NO_3^- reduction rates. Calculated $^{15}\varepsilon$ and $^{18}\varepsilon$ values also decrease as reaction rates increase. A notable exception to this trend was Exp#2 in which very large isotope effects were observed.

The degree to which the observed isotope effects reflect an equilibrium isotope fractionation is not easily determined. To our knowledge, no previous empirical studies have examined N isotope equilibrium between NO_3^- and NH_4^+. The calculated equilibrium N isotope effect between NO_3^- and NH_4^+ at elevated temperatures (Figure 8) ranges from 43.4‰ to 25.5‰ across the temperature range we investigated, with the preferential accumulation of ^{15}N in the NO_3^- pool. Although the elevated $\delta^{15}N$ of the NO_3^- pool and depleted $\delta^{15}N$ of the co-existing NH_4^+ pool are consistent in direction with the predicted equilibrium isotope distribution, the offset between $\delta^{15}N$ values of co-existing NO_3^- and NH_4^+ were almost always far below calculated equilibrium values suggesting that the observed isotope behavior is governed primarily by kinetic effects.

As for the potential influence of O isotope equilibrium between NO_3^- and H_2O, a study conducted at 80°C and pH 1.1 showed the reaction half-life for equilibration to be ~178 hours (Kaneko and Poulson, 2013). Extrapolation of these findings to our experimental conditions,

however, is not straightforward. On the one hand, higher reaction temperatures should enhance rates of isotope exchange. However, we suggest that isotopic exchange in our experiments was minimal given the elevated pH of our experiments. Given that the pKa for HNO_3/NO_3^- at 250°C and 350 bar is 0.81, we argue that in our experiments the exceptionally small fraction of HNO_3, the species promoting O exchange with H_2O (Böhlke et al., 2003; Kaneko and Poulson, 2013), precludes any influence of O isotope equilibration.

2.5.4 Dual isotope systematics

The combined use of two isotope systems in parallel has proven to be an effective tool for elucidating sources and transformations in biogeochemical reactions. In particular, where distinctive behavior of one isotope system differs from the other can be useful for discerning one reaction pathway from another as in the studies on reactions involving oxyanions (i.e., anions containing one or more O atoms) including sulfate reduction (e.g., Brunner et al., 2005; Antler et al., 2014) and perchlorate degradation (e.g., Sturchio et al., 2007; Hatzinger et al., 2009). In considering nitrogen cycling, dual N and O isotope systematics for both NO_3^- and NO_2^- involved in a range of mostly microbial transformations have been characterized (see Casciotti, 2016 for a comprehensive review). For instance, NO_2^- reduction by various pathways exhibits unique dual isotope fractionation patterns (often denoted by the ratio of O to N isotope effects, $^{18}\varepsilon/^{15}\varepsilon$). For example, the abiotic reduction of NO_2^- by green rust (a reactive, mixed-valence Fe oxide) proceeds with $^{18}\varepsilon/^{15}\varepsilon \sim 1$ (Grabb et al., 2017), while the microbially mediated reduction reaction exhibits markedly lower ratios with $^{18}\varepsilon/^{15}\varepsilon \sim 0.75$ for reduction by Fe-containing nitrite reductase *nirS* or $^{18}\varepsilon/^{15}\varepsilon \sim 0.1$ for reduction by Cu-containing nitrite reductase *nirK* (Martin and Casciotti, 2016).

The $^{18}\varepsilon/^{15}\varepsilon$ values from this current study on NO_3^- reduction consistently fall within the range of 0.6 to 0.8 (Table 2) with an average value of 0.64 (Figure 9). Nitrate reduction through biological processes occurs through two distinct pathways as manifest in dual N-O isotope systematics. During biological nitrate reduction by phytoplankton uptake (via assimilatory nitrate reductases), the values for $^{18}\varepsilon/^{15}\varepsilon$ cluster tightly around ~1 at the enzyme level (Karsh et al., 2012), at the organismal level as shown in cultured phytoplankton (Granger et al., 2004), and in the surface ocean (e.g., Casciotti et al., 2002; Fawcett et al., 2015; DiFiore et al., 2009; Trull et al. 2008; Peng et al., 2018). A similar ratio of ~1 is also found during respiratory nitrate reduction by denitrifying bacteria through membrane-bound nitrate reductase (NAR) (Granger et al., 2008). Notably, the reduction of NO_3^- via a periplasmic nitrate reductase (NAP) exhibits a significantly lower ratio of ~0.6 (Granger et al., 2008). From a first principles approach, Granger et al. (2004) calculated values of $^{15}\varepsilon$ and $^{18}\varepsilon$ resulting from the breaking of the N-O bond in NO_3^- to be 57‰ and 29‰, respectively, yielding a corresponding $^{18}\varepsilon/^{15}\varepsilon$ near 0.5. To the best of our knowledge, no dual N and O isotope fractionation for abiotic NO_3^- reduction has been previously described and our current study exhibits a $^{18}\varepsilon/^{15}\varepsilon$ value more similar to that previously shown in NO_3^- reduction by the periplasmic nitrate reductase enzyme (NAP; Figure 10).

2.5.5. Implications for submarine hydrothermal vents

Hydrothermal fluid venting occurs across a spectrum of high-temperature focused venting to lower-temperature diffuse flow venting. In terms of high-temperature venting such as that observed emanating from black smokers, circulating seawater from the recharge zone would have been exposed to the hot, reducing conditions of the reaction zone. The lack of nitrate and presence of ammonia in high temperature vent fluids, in contrast to the nitrate-rich and ammonia-depleted bottom seawater source for hydrothermal circulation, supports the first-order

observation that NO_3^- reduction occurs during subsurface circulation. A previous study (Brandes et al., 1998) postulated NO_3^- should be quantitatively reduced to NH_4^+. However, before bottom seawater enters the more deeply located high-temperature reaction zone, biological processes that might influence NO_3^- concentrations cannot be entirely excluded. In the absence of abundant dissolved oxygen, microbial processes such as denitrification and dissimilatory nitrate reduction to ammonia (DNRA) can convert NO_3^- to gaseous N (N_2 and N_2O) or NH_4^+, respectively. The extent to which these reactions are involved in the subsurface N cycling prior to exposure of seawater to temperatures above the limits of biological activity life ($\sim121°C$) remains poorly understood.

As bottom seawater enters the off-axis recharge zone, NO_3^- reduction to NH_4^+ should commence upon its contact with basaltic rocks at a sufficiently high temperature. In this study, the reaction half-life at the lowest temperature examined (150°C) was 40-150 hours, depending on the amount of magnetite and pH (Table 2). Considering water-rock ratios estimated by others are generally much lower than in our experiments (0.5-1 for mid-ocean ridge hydrothermal systems (Bowers, 1989; Berndt et al., 1988), NO_3^- reduction in subseafloor hydrothermal systems should proceed even more quickly. As shown in our study, however, NO_3^- reduction under more acidic pH may be expected to yield non-quantitative conversion to NH_4^+. Thus, the amount of NH_4^+ emitted in high temperature endmember fluids may be ultimately controlled by how long the subducting seawater remains in the 'quantitative-reduction' zone before entering a more acidic, Fe^{2+} rich reaction zone in which whatever NO_3^- is left may be completely and rapidly reduced to NH_4^+ and other gaseous N. Following this logic, if NO_3^- is not entirely consumed in the lower temperature recharge zone before entering a hot reaction zone, the resultant vent fluid should always have [NH_4^+] lower than input [$NO_3^- + DON$], and the relative

deficiency of N in these fluids may be an integrated indicator of larger scale residence times of fluids in low temperature reaction zones during recharge.

In typical mid-ocean ridge systems, recharge zones can be as far as 10 km away from ridge axes (Lowell and Rona, 1985; Lowell, 1991; Sleep 1991; Lowell et al., 1995); these areas are often thought to be unsedimented given their relatively young geologic age (Brandes et al., 2008). Thus, the only major non-N_2 species in bottom seawater expected to produce NH_4^+ are limited to NO_3^- and dissolved organic N (DON). If we assume that sediment-starved recharge zones host limited biological activity, we would expect $[NH_4^+]$ to be comparable to $[NO_3^-]$ plus [DON] provided quantitative conversion as previously suggested (Brandes et al., 1998). Nitrate concentrations in the deep sea generally vary between 16 and 44 µM depending on ocean basin and depth (Schlitzer, 2000; Gruber, 2008). While less is known about concentrations of DON in the deep sea, limited measurements suggest a more uniform 3 µM (Wong et al, 2002). Thus, for example, vent sites between 26° – 36°N along mid Atlantic ridge such as Rainbow, Lost City, Lucky Strike and TAG are recharged with bottom seawater having a $[NO_3^- + DON]$ of ~25uM. Interestingly, none of these sites exhibits endmember $[NH_4^+]$ of even half these levels (Reeves et al., 2014), calling in to question the suggested quantitative conversion – and perhaps reflecting extensive biological denitrification (N_2 production) in low temperature recharge zones.

The non-quantitative yield of NH_4^+ as found in the low-pH experiment in our current study is also a viable explanation for this concentration mismatch between bottom seawater $[NO_3^- + DON]$ and vent fluid $[NH_4^+]$. In fact, the pH values (at 25°C) of endmember fluids for most of the vents along the mid Atlantic ridge fall within the range of 3-4.5 (except for Lost City having a pH~10.5). Thus, our results would suggest that non-quantitative yield in these low-pH fluids is likely. As for Lost City vent fluids, the quantitative yield from our high-pH experiments

suggests that lower than expected $[NH_4^+]$ may result from other NH_4^+ consuming processes acting to consume $[NH_4^+]$ after it is produced. Indeed, a vastly different geochemical setup compared to typical mid-ocean ridges might be at work at Lost City considering the lower temperature venting, lack of Fe^{2+} and sulfide in the vent fluid and notably high pH (Kelley et al., 2005; Proskurowski et al., 2006).

Alternatively, hydrothermal circulation can follow low-temperature venting flow paths in which high-temperature hydrothermal fluids are thought to mix diffusely with seawater in the subsurface (e.g., Von Damm and Lilley, 2004). In these cases, incomplete NO_3^- reduction could be expected, due to reduced contact with the Fe^{2+}-bearing mineral phases resulting in a slower reaction and a shorter overall residence time of NO_3^-. Based on the work presented here, such incomplete consumption is expected to be accompanied by N and O fractionation leading to shifts in $\delta^{15}N_{NO3}$ and $\delta^{18}O_{NO3}$ relative to seawater NO_3^- exhibiting a $^{18}\varepsilon/^{15}\varepsilon = 0.6$.

Such a dual isotope fractionation trend during the abiotic NO_3^- reduction is identical with that biologically mediated by the periplasmic nitrate reductase enzyme (nap) found ubiquitously in epsilon-proteobacteria, a bacterial phylum known to proliferate in and around low-temperature deep-sea vents (e.g., Bourbonnais et al., 2012; Huber et al., 2010; Nakagawa et al., 2005; Lopez-Garcia et al., 2003). As such, isotopic patterns resulting from abiotic reduction may be indistinguishable from that of biological NO_3^- reduction in complex mixing environments in the shallow subsurface.

2.6. CONCLUSION AND FUTURE DIRECTIONS

We demonstrate here that under high temperature and high pressure NO_3^- is rapidly reduced in the presence of the redox-buffering mineral assemblage of magnetite-hematite. Further, our results indicate an important role for pH in determining reaction products. At high pH, the reaction product is solely NH_3 and conversion is quantitative, while at low pH, roughly half of the product was NH_4^+ with the remainder represented by gaseous N (likely N_2). This bifurcation in reaction pathways as regulated by the pH may, in part, explain the frequently observed discrepancy between concentrations of NH_4^+ in endmember vent fluids relative to the N content of recharge seawater into submarine hydrothermal vent systems. Furthermore, the similarity in the pattern of dual N and O isotope fractionation by reduction of NO_3^- by magnetite (as reported here) and by periplasmic nitrate reductase (NAP) make it difficult to discern biological from abiotic reduction through the interpretation of the isotopic composition of NO_3^- found in the low temperature vent fluids.

Our low pH experiments are perhaps most analogous to the conditions typified by the majority of submarine hydrothermal vent systems. The specific factors controlling the partitioning of reaction products of NO_3^- reduction between NH_4^+ and N_2, however, remain unclear with the limited perspective of our experiments. Furthermore, while our study examined magnetite as the reductant of NO_3^-, other iron-bearing sulfide minerals such as pyrite and pyrrhotite have also been shown to be effective in NO_3^- reduction (Brandes et al., 1998, 2008; Summers, 2005). Future work examining N isotope systematics using these mineral reductants should provide a more complete picture of NO_3^- reduction, as these iron sulfides are also ubiquitous within submarine hydrothermal vent systems.

Figure 1. Change in the solid phases in the experiments. (a) Starting mineral mix, (b) partially reacted minerals typical of all experiments in this study, (c) fully reacted minerals, (d) amounts of magnetite and hematite as calculated from XRD.
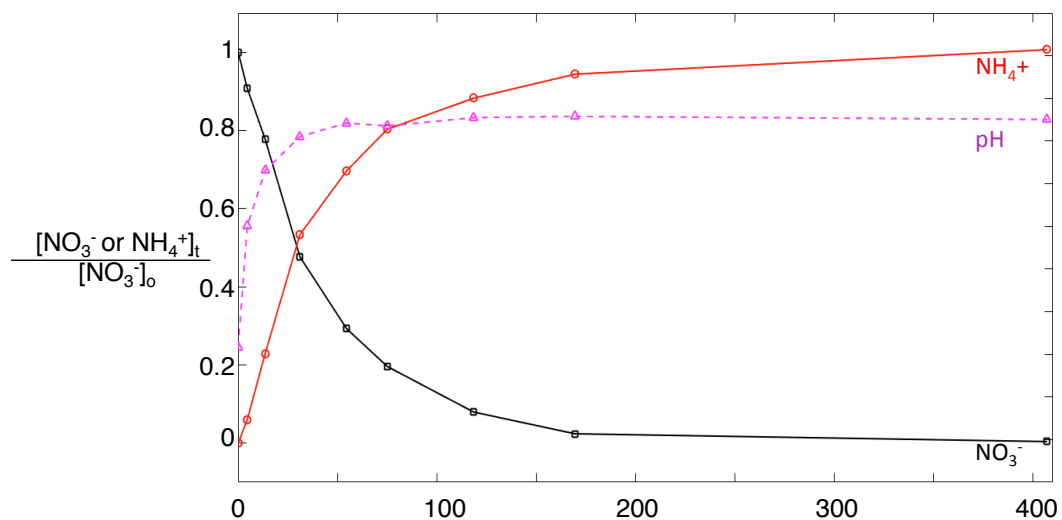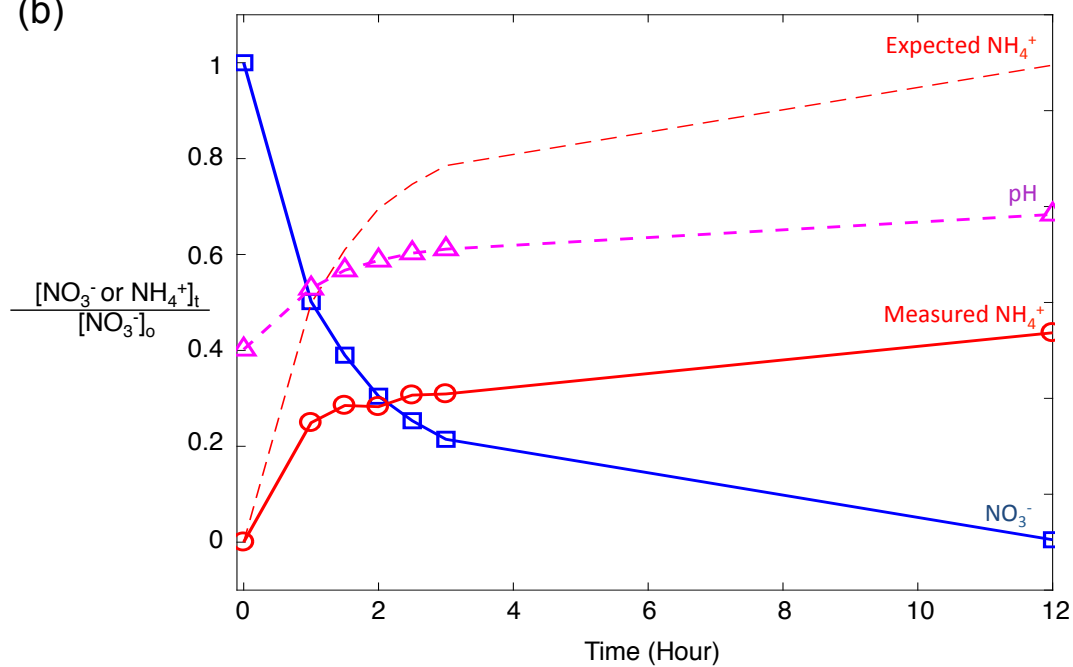
Figure 2. Concentration changes in selected experiments. (a) Exp#5 run at 200°C and unbuffered pH and (b) Exp#10 run at 250°C and buffered pH. Note the quantitative conversion of NO_3^- to NH_4^+ in the former case and non-quantitative conversion in the latter.

Figure 3. Nitrogen speciation at 350 bar and selected temperatures (150°C, 200°C, and 250°C). The plots on the left (a, c, and e) are generated with no species suppression while N_2, NO_2^-, and NO are suppressed in the plots on the right (b, d, and f). Crosses (for unbuffered experiments) and circles (for buffered experiments) represent the starting conditions and the arrows show the change to the final conditions. The representative experiments for 150°C (a and b) and 200°C (c and d) are Exp#3 and Exp#5, respectively. For 250°C (e and f), Exp#1 and Exp#10 are the unbuffered and buffered representative experiments respectively.
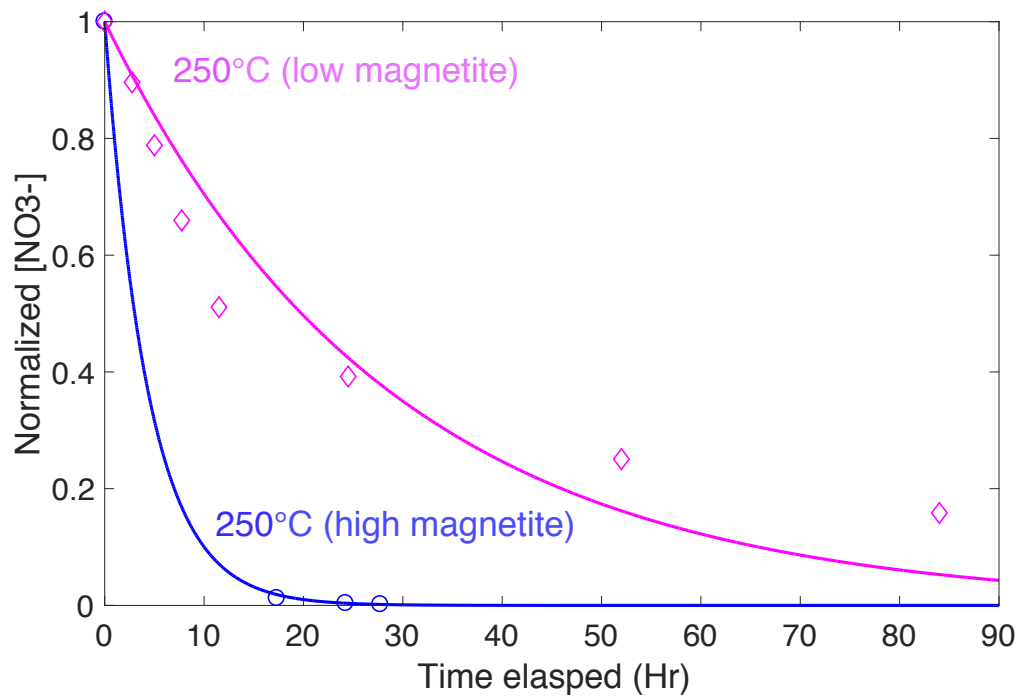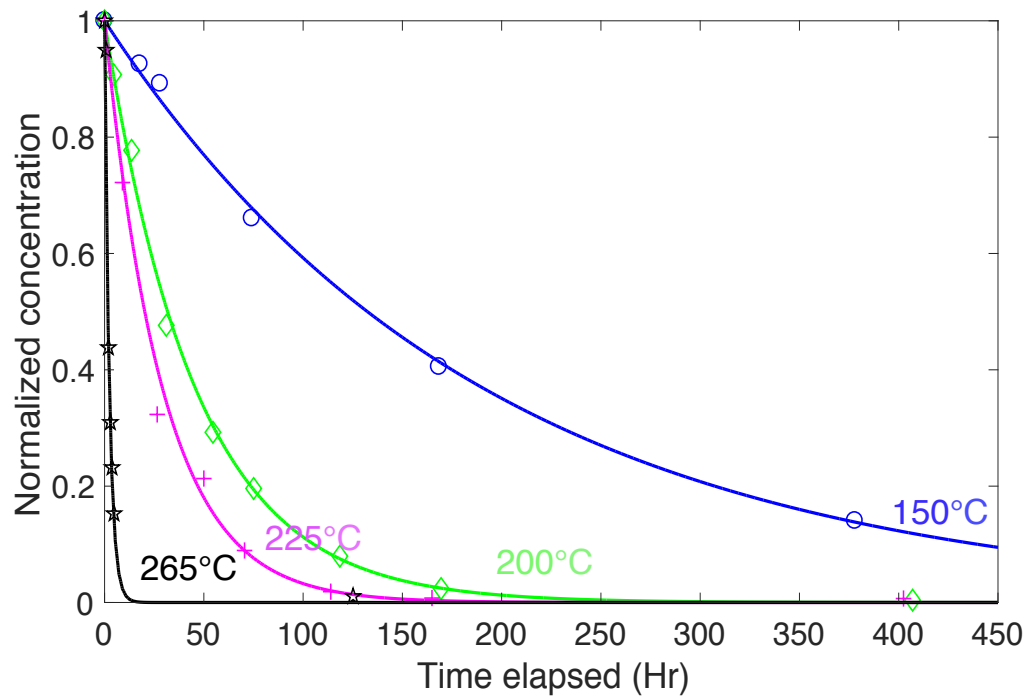
Figure 4. Reaction rates as affected by (top) temperature and (bottom) amount of solid magnetite. The lines indicate that modeled NO_3^- concentration change and the markers indicate the measured concentrations.
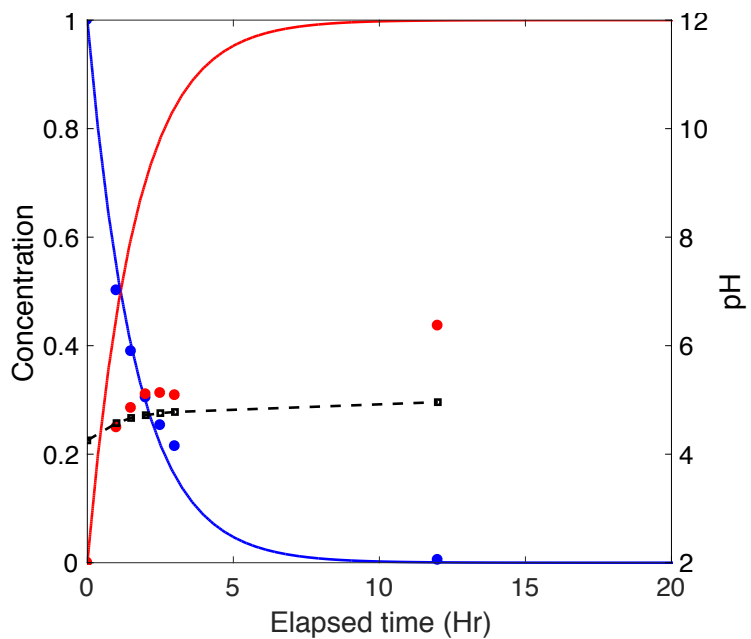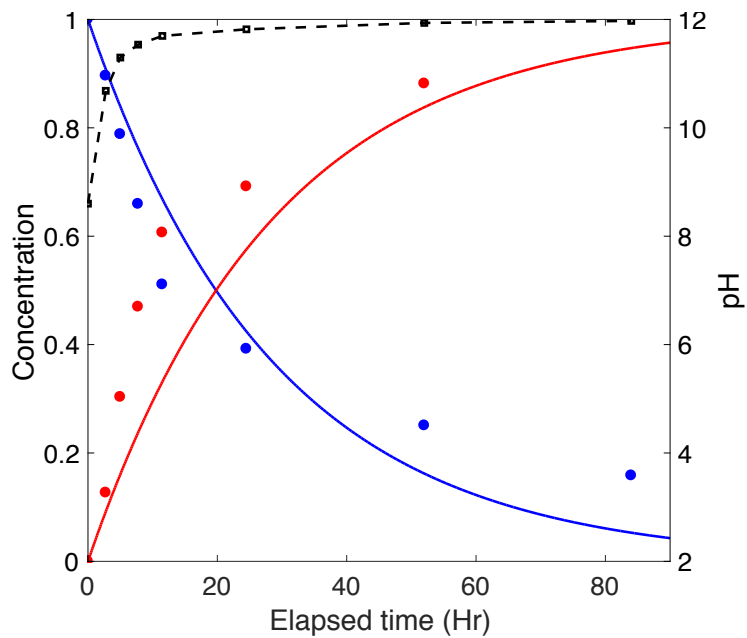
Figure 5. Reaction rates as affected by pH. Two experiments run at 250°C and similar initial conditions except for the presence/absence of pH buffer. The lines indicate that modeled concentration change and the markers indicate the measured concentrations (blue for NO_3^-, red for NH_4^+ and black for pH).
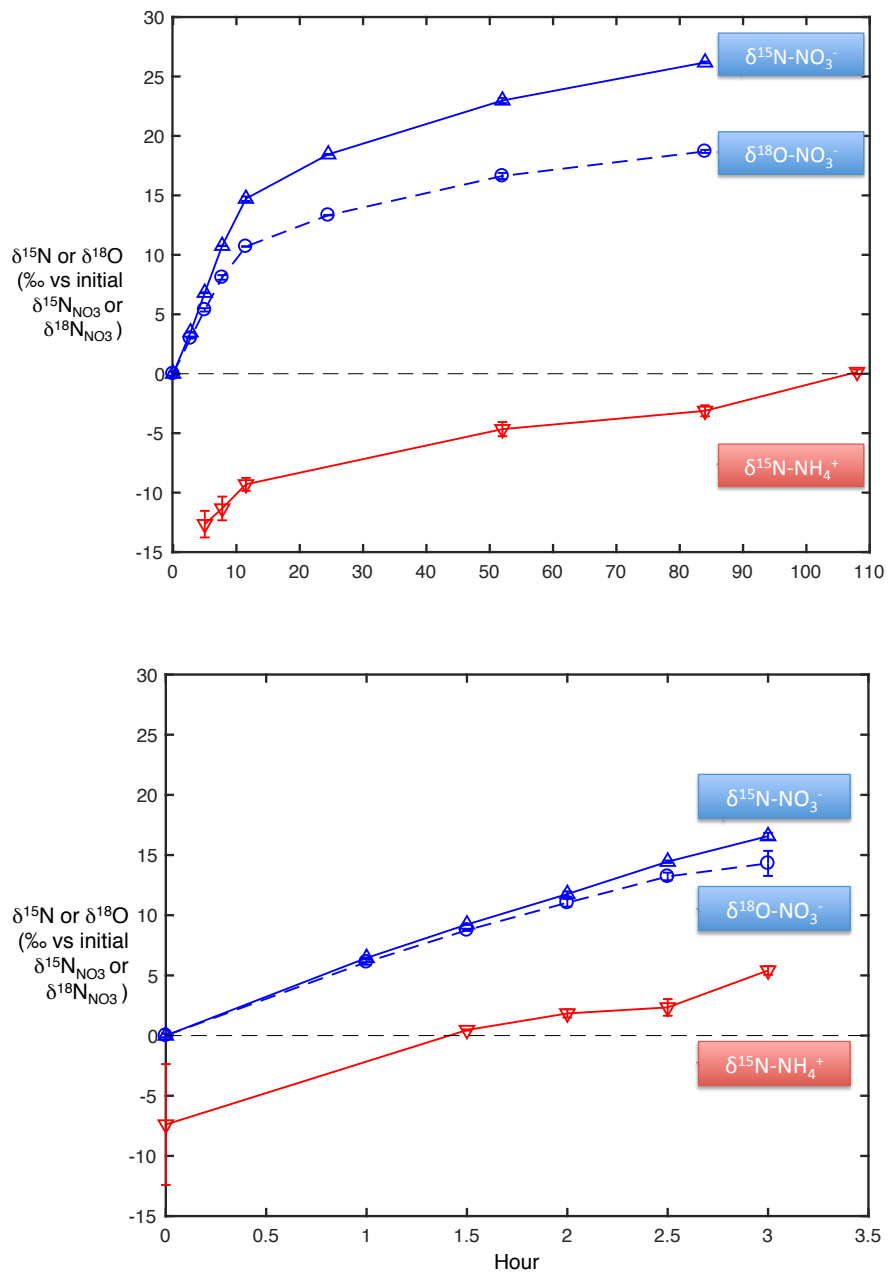
Figure 6. Changes in the $\delta^{15}N_{NO3}$ in selected experiments: (top) Experiment 9 with no pH buffer, and (bottom) experiment 10 with pH buffer.
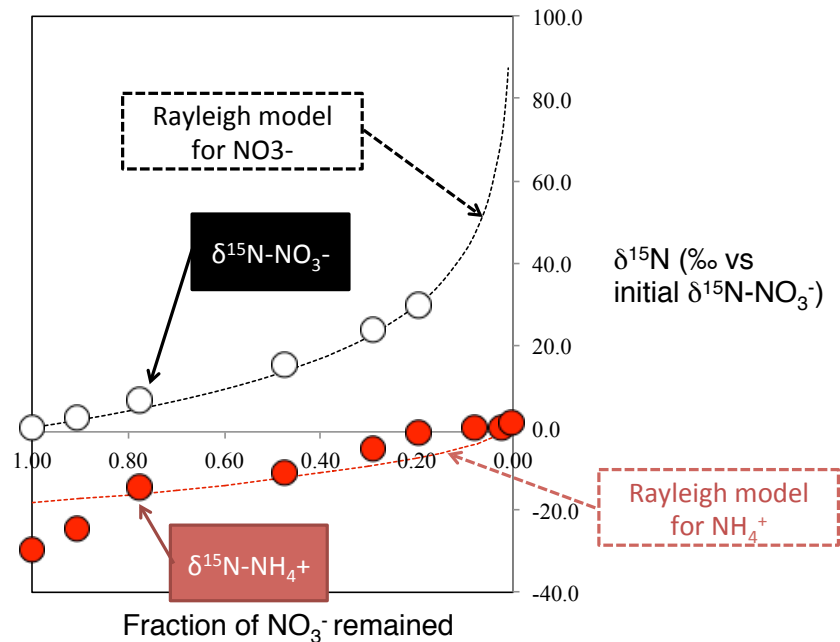
Figure 7. Closed-system Rayleigh plot. From Experiment X (250°C with no pH buffer), plotting the change in substrate $\delta^{15}N_{NO3}$ along the Rayleigh space (c) shows the product $\delta^{15}N_{NH4}$ falling nicely with the prediction.
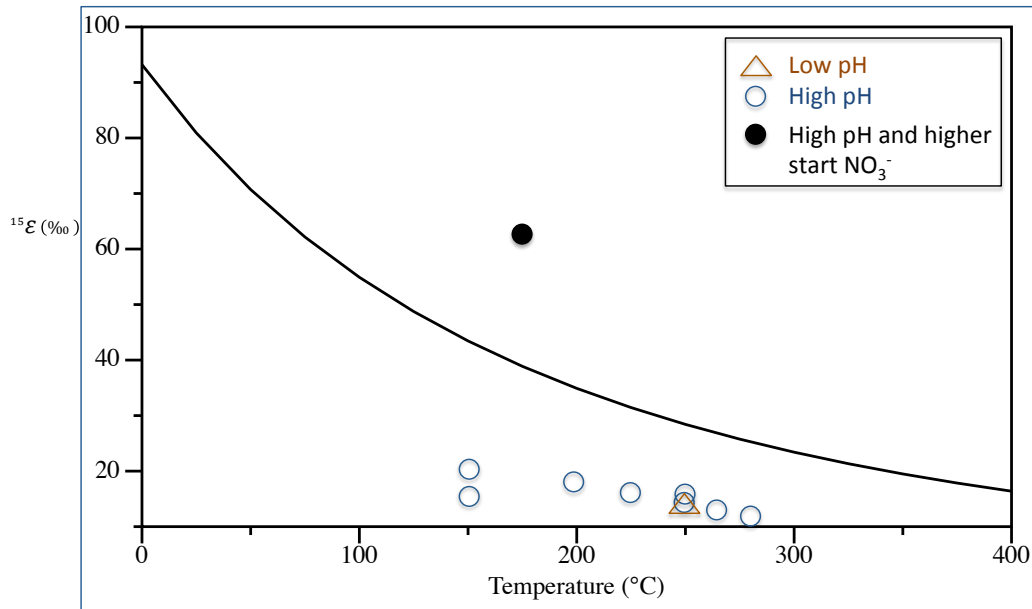
Figure 8. Predicted NH$_4^+$-NO$_3^-$ N equilibrium isotope effects. Actual values as calculated from our experiments are also shown on the plot.
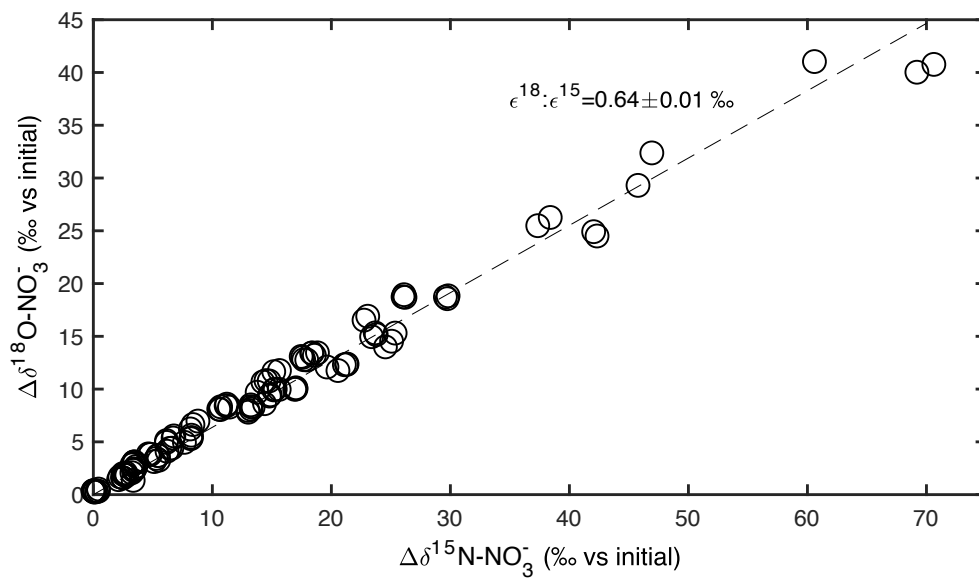
Figure 9. The $\delta^{18}O_{NO3}$ change plotted against the corresponding $\delta^{15}N_{NO3}$ change for this experiments in this study. The mean slope is 0.64 ± 0.01.
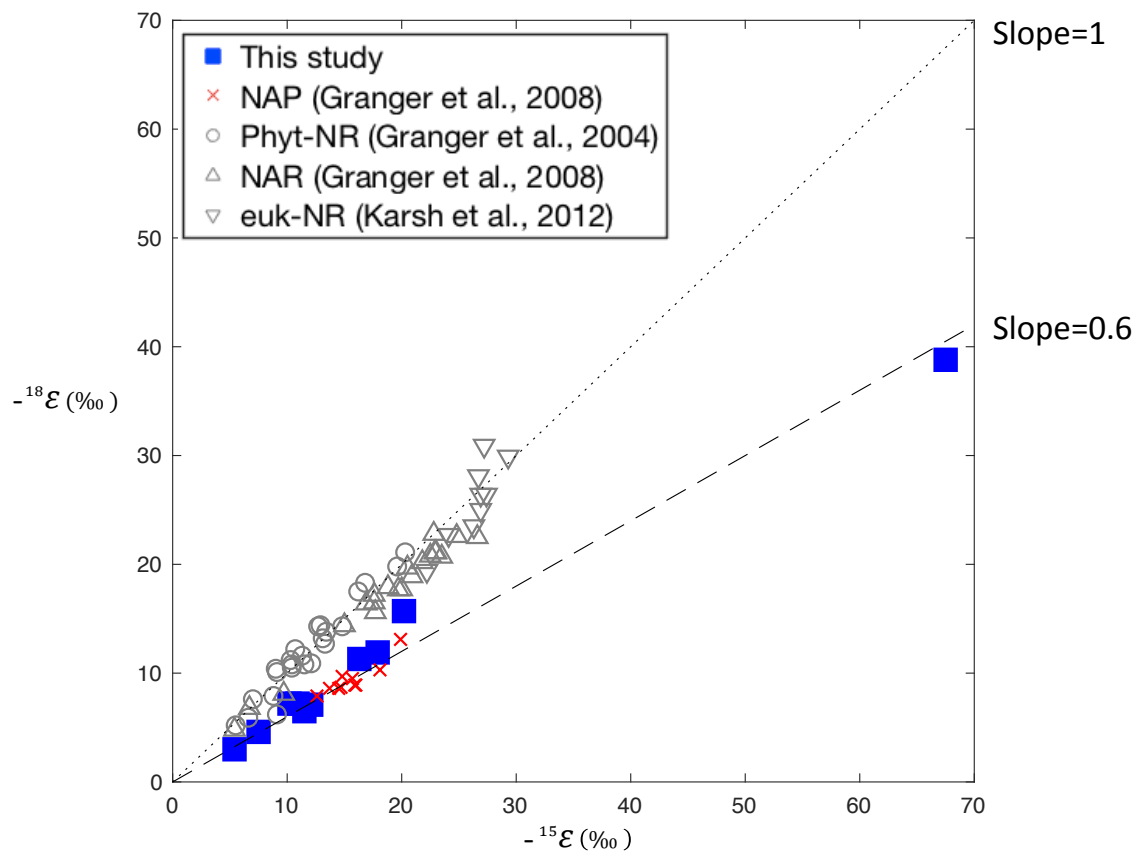
Figure 10. Comparison between the $^{18}\varepsilon/^{15}\varepsilon$ in this study and the other previously reported values from microbial NO_3^- reduction

Table 1. Fluid composition and isotopic composition during the experiments.

Sample	Time (h)	T (°C)	$pH_{25°C}$	$pH_{in\text{-}situ}$	Cl^- (m)	K^+ (m)	NO_3^- (m)	NH_4^+ (m)	$\delta^{15}N_{NO3}$	$\delta^{18}O_{NO3}$	$\delta^{15}N_{NH4}$	$\delta^{15}N_{TDN}$
Exp#1: 250°C												
Start heating	-2.5	20.2	6.43	-	6.054	14.978	9.080	0.000	47.94	24.95	-	-
0	0.0	249.8	-	-	-	-	-	-	-	-	-	-
1	17.3	251.4	11.58	8.64	5.614	13.845	0.112	8.402	94.36	55.70	-	-
2	24.3	249.3	11.57	8.63	5.626	14.083	0.033	8.793	108.61	65.89	-	-
3	27.8	251.3	11.65	8.71	5.558	14.037	0.016	8.894	117.76	70.62	-	-
4	42.3	251.4	11.62	8.68	5.713	14.222	0.000	9.000	120.31	73.56	-	-
Exp#2: 175°C												
0	0.0	175.0	7.50	4.67	23.186	67.345	42.968	2.162	20.54	19.09	-	-
1	23.3	176.4	11.76	9.14	23.233	66.005	39.309	8.682	26.27	27.08	-	-
2	58.0	175.7	12.10	9.48	22.866	65.086	28.172	4.348	46.44	38.91	-	-
3	99.3	173.7	12.37	9.75	23.241	68.969	22.424	14.572	68.53	51.70	-	-
4	167.3	176.0	12.53	9.91	23.357	68.207	13.682	20.684	96.26	67.38	-	-
5	241.5	175.9	12.68	10.06	23.280	67.423	7.063	32.411	-	-	-	-
6	310.5	176.4	12.72	-	-	-	-	-	-	-	-	-
7	385.3	176.3	12.72	10.10	23.202	64.845	0.981	35.360	-	-	-	-
8	480.0	176.3	12.67	10.18	23.124	70.877	0.000	41.715	-	-	-	-
Exp#3: 150°C												
Start heating	-2.0	28.8	6.84	-	5.186	11.005	10.396	0.000	48.83	25.00	-	-
0	0.0	150.0	8.50	5.92	5.348	11.167	10.193	0.056	48.81	25.29	-	50.15
1	17.8	152.4	9.26	6.56	5.246	11.065	9.721	0.362	51.08	26.77	-	50.19
2	28.0	149.5	10.56	8.17	5.405	11.224	9.355	0.546	51.84	27.11	-	49.30
3	74.3	152.4	11.15	8.77	5.397	11.216	7.360	2.233	56.66	30.36	-	51.14
4	168.5	152.7	11.30	8.92	5.734	11.554	2.909	6.072	63.11	34.04	-	52.40
5	378.0	152.7	10.13	7.41	5.559	11.378	1.519	8.775	73.43	39.52	-	53.55

Table 1. (cont.)

Sample	Time (h)	T (°C)	pH$_{25°C}$	pH$_{in\text{-}situ}$	Cl$^-$ (m)	K$^+$ (m)	NO$_3^-$ (m)	NH$_4^+$ (m)	δ^{15}N$_{NO3}$	δ^{18}O$_{NO3}$	δ^{15}N$_{NH4}$	δ^{15}N$_{TDN}$
Exp#4: 150°C												
Start heating	-2.0	25.0	8.17	-	4.854	10.618	6.548	0.635	54.00	28.45	-	-
0	0.0	150.0	9.51	6.82	5.378	10.568	6.246	0.625	59.44	31.81	-13.63	52.79
1	103.5	151.1	11.24	8.86	4.708	12.570	3.295	4.787	67.27	36.53	-	52.22
2	147.0	151.1	11.14	8.75	4.852	11.510	2.209	7.709	71.07	38.40	-	51.86
3	198.8	150.9	11.20	8.81	5.002	10.512	1.237	9.149	75.31	40.70	-	52.00
4	272.3	151.2	11.26	8.88	5.478	9.952	0.345	9.613	-	-	47.77	52.13
5	436.5	151.1	11.01	8.60	5.654	10.975	0.004	10.278	-	-	46.12	-
Exp#5: 200°C												
Start heating	-2.0	29.9	6.01	-	-	-	10.014	-	48.83	25.00	-	-
0	0.0	199.4	6.15	5.12	4.914	14.665	9.576	0.043	48.66	25.28	-	-
1	4.6	201.1	9.01	5.56	5.070	14.821	8.690	0.618	51.00	26.76	-	50.47
2	13.6	201.4	10.31	7.29	5.097	14.848	7.443	2.271	55.14	29.48	-	47.74
3	31.1	201.3	11.11	8.35	5.114	14.865	4.562	5.385	64.09	35.15	-	50.41
4	54.6	201.4	11.42	8.67	4.932	14.683	2.802	7.105	72.35	40.34	-	52.08
5	75.1	201.4	11.35	8.59	4.988	14.739	1.876	8.187	78.43	43.97	-	50.17
6	118.5	201.3	11.55	8.80	4.955	14.706	0.762	8.970	-	-	-	47.64
7	169.5	201.5	11.58	8.83	4.944	14.695	0.229	9.803	-	-	-	50.35
8	407.0	201.4	11.51	8.75	5.042	14.793	0.038	11.594	-	-	-	50.31
9	622.0	201.4	-	-	5.114	14.865	-	-	-	-	-	50.16
Exp#6: 225°C												
0	0.0	223.0	8.51	-	-	-	-	-	-	-	-	-
1	4.0	223.9	10.13	6.73	2.479	6.338	3.399	1.766	54.41	31.37	-	49.96
2	7.0	225.6	10.64	7.71	2.295	6.025	2.454	2.648	59.27	35.08	-	45.15
3	16.0	226.2	11.07	8.20	2.043	5.028	1.099	4.188	72.93	44.41	-	47.50
4	22.7	226.3	11.15	8.29	2.177	4.703	0.825	5.007	-	-	-	46.02
5	31.0	226.1	11.24	8.38	1.755	4.709	0.304	5.626	92.36	57.15	-	45.26
6	43.5	226.1	11.29	-	-	-	0.063	-	-	-	-	46.59
7	78.3	226.1	11.22	-	-	-	0.026	-	-	-	-	45.79
8	149.3	226.1	11.23	-	-	-	0.023	-	-	-	-	45.24

Table 1. (cont.)

Sample	Time (h)	T (°C)	pH$_{25°C}$	pH$_{in\text{-}situ}$	Cl⁻ (m)	K⁺ (m)	NO₃⁻ (m)	NH₄⁺ (m)	δ^{15}N$_{NO3}$	δ^{18}O$_{NO3}$	δ^{15}N$_{NH4}$	δ^{15}N$_{TDN}$
Exp#7: 265°C												
0	0.0	264.0	8.50	5.07	2.307	5.051	5.250	0.032	-	-	-	-
1	1.4	263.9	10.22	6.82	2.774	5.961	2.598	1.628	53.96	30.79	38.11	47.85
2	2.2	266.1	10.72	7.74	2.492	5.405	2.544	2.311	56.92	33.08	34.15	46.08
3	3.3	264.5	10.89	7.93	2.302	5.000	1.669	2.970	61.94	36.29	35.93	45.29
4	4.3	265.8	11.05	8.10	2.230	4.771	1.328	3.432	65.36	39.13	39.82	46.95
5	5.2	265.4	11.06	8.11	2.142	4.581	1.048	3.822	68.04	40.89	41.81	47.45
6	6.2	265.5	11.05	8.10	2.099	4.855	0.814	4.084	71.61	43.66	41.69	46.67
7	125.2	265.7	11.11	8.16	2.112	4.781	0.048	5.202	-	-	-	46.38
Exp#8: 280°C												
Start heating	-1.8	25.0	-	-	-	-	-	-	-	-	-	-
0	0.0	280.6	6.67	4.32	5.209	14.664	9.479	0.273	48.83	27.24	-	49.52
1	1.5	277.7	9.79	5.44	5.255	14.711	7.653	1.877	52.35	30.17	-	49.96
2	2.0	281.5	10.53	7.43	5.359	14.815	7.093	2.461	53.61	30.99	-	50.13
3	2.5	280.1	10.92	7.93	5.008	14.463	6.841	3.399	55.06	32.19	-	50.24
4	3.5	280.0	11.11	8.14	5.338	14.793	5.390	4.487	57.49	33.96	-	50.19
5	5.2	281.1	11.32	8.36	5.254	14.709	4.513	5.609	59.76	35.42	-	46.99
6	14.1	281.3	11.64	8.68	5.244	14.699	2.721	7.727	64.31	38.86	-	49.62
7	26.5	281.3	11.63	8.67	5.026	14.481	1.974	7.693	66.79	40.45	-	46.31
8	52.0	281.4	11.71	8.75	5.104	14.559	1.211	10.653	-	-	-	49.74
9	106.0	281.2	11.68	-	-	-	0.000	-	-	-	-	49.02
Exp#9: 250°C												
Start heating	-1.3	19.0	7.01	-	-	-	-	-	-	-	-	-
0	0.0	247.0	8.60	4.76	5.916	19.894	10.237	0.251	20.47	25.06	-	19.60
1	2.8	252.0	10.68	7.70	5.672	19.218	9.174	1.476	23.95	28.04	9.48	22.00
2	5.0	250.0	11.30	8.35	5.525	19.399	8.069	3.075	27.28	30.43	7.82	21.67
3	7.8	249.0	11.54	8.59	5.504	19.058	6.751	4.339	31.23	33.16	9.14	21.83
4	11.5	251.0	11.70	8.76	5.702	19.690	5.230	5.232	35.19	35.76	11.17	21.95
5	24.5	251.0	11.82	8.88	5.393	20.584	4.014	6.346	38.92	38.39	9.14	19.70
6	52.0	251.0	11.94	9.00	5.435	20.606	2.567	7.704	43.45	41.69	15.81	21.79
7	84.0	251.0	11.97	9.03	5.910	19.466	1.622	9.553	46.65	43.76	17.35	20.91
8	108.0	249.0	12.00	-	-	-	-	-	-	-	20.62	20.62

Table 1. (cont.)

Sample	Time (h)	T (°C)	pH$_{25°C}$	pH$_{in-situ}$	Cl⁻ (m)	K⁺ (m)	NO₃⁻ (m)	NH₄⁺ (m)	δ¹⁵N$_{NO3}$	δ¹⁸O$_{NO3}$	δ¹⁵N$_{NH4}$	δ¹⁵N$_{TDN}$
Exp#10: 250°C +Na-acetate (~15mmol/1kg H2O)												
Start heating	-1.5	75.0	-	-	6.506	16.724	10.104	-	-	-	-	-
0	0.0	247.0	4.26	4.54	6.320	16.538	9.333	0.920	20.43	25.52	13.04	19.76
1	1.0	250.0	4.57	4.37	6.326	16.544	4.683	3.246	26.88	31.63	-	25.31
2	1.5	250.0	4.67	4.42	6.312	16.530	3.640	3.581	29.66	34.28	20.89	26.68
3	2.0	250.0	4.72	4.47	5.847	16.064	2.841	3.557	32.19	36.56	22.27	27.43
4	2.5	250.0	4.76	4.48	6.396	16.613	2.364	3.783	34.88	38.74	22.77	29.69
5	3.0	250.0	4.78	4.50	6.247	16.465	2.003	3.805	37.00	39.83	25.84	29.49
6	12.0	251.0	4.96	4.54	5.372	15.589	0.047	4.996	-	-	-	
Exp#11: 250°C +Na-acetate (~15mmol/1kg H2O) +NaCl (~35g/1kg H2O)												
Before heating	20.0	-	-	-	-	-	11.310	0.000	48.45	24.90	-	18.48
Start heating	-2.3	130.0	4.15	-	-	-	-	-	-	-	-	-
0	0.0	249.0	4.20	4.21	-	-	4.830	4.660	118.85	78.93	-	19.67
1	0.5	251.0	4.27	4.22	-	-	3.357	5.434	74.74	44.10	-	24.11
2	1.0	250.7	4.29	4.21	-	-	3.302	5.845	66.55	38.36	-	14.93
3	1.8	250.4	4.33	4.21	-	-	2.417	6.513	64.31	36.53	-	23.82
4	2.5	249.9	4.34	4.20	-	-	2.305	6.685	54.03	35.22	-	18.78
5	5.0	249.7	4.42	4.24	-	-	1.113	7.286	59.96	32.48	-	11.10
6	14.0	250.0	4.49	4.25	-	-	0.251	8.149	57.77	31.04	-	0.84

Table 2. Summary of the experimental conditions with the calculated reactions kinetics and isotope fractionations

Experiment#	pH		Kinetics	Isotope fractionation					
	(at 25°C)		$t_{1/2}$	$^{15}\varepsilon$	R^2	$^{18}\varepsilon$	R^2	$\Delta\delta^{18}O:\Delta\delta^{15}N$	R^2
	Start	End	(hr)	(‰)		(‰)			
1: 250°C	6.43	11.62	3.0	10.9±0.2	0.9992	7.2±0.1	0.9974	0.66±0.01	0.999
2: 175°C	7.50	12.67	86.6	67.5±4.7	0.9982	38.8±2.8	0.9986	0.58±0.00	1
3: 150°C	8.50	10.13	138.6	20.2±1.4	0.9836	15.7±1.2	0.9678	0.77±0.04	0.995
4: 150°C	9.51	11.01	49.5	11.5±1.9	0.9383	6.5±1.0	0.9247	0.56±0.02	0.997
5: 200°C	6.15	11.51	31.5	17.9±0.6	0.9947	11.9±0.8	0.9924	0.67±0.03	1
6: 225°C	8.51	11.23	20.4	16.3±0.8	0.9987	11.3±0.6	0.9972	0.70±0.01	0.999
7: 265°C	8.50	11.11	1.7	8.4±0.5	0.9983	4.6±0.8	0.9895	0.59±0.06	0.996
8: 280°C	6.67	11.68	12.2	5.4±0.6	0.9716	3.0±0.6	0.9638	0.59±0.04	0.9980
9: 250°C	8.60	12.00	19.8	13.2±0.8	0.9491	7.7±0.6	0.9409	0.59±0.02	0.999
10: 250°C +acetate	4.26	4.96	1.1	10.2±0.2	0.9473	7.2±0.5	0.9524	0.71±0.04	0.993
11: 250°C +acetate +NaCl	4.20	4.49	1.3	11.9±0.3	0.9632	9.2±0.4	0.9534	0.77±0.05	0.999

Note: - Reaction half-lives ($t_{1/2}$) are in hour. They were calculated from the disappearance of NO_3^-.

- Isotope effects for N and O ($^{15}\varepsilon$ and $^{18}\varepsilon$) were calculated using closed-system Reyleigh fractionation model.

- The change in $\delta^{18}O_{NO3}$ and $\delta^{15}N_{NO3}$ ($\Delta\delta^{18}O$ and $\Delta\delta^{15}N$) at any time point was relative to the starting NO_3^- isotopic composition.

- The reported uncertainties for $^{15}\varepsilon$, $^{18}\varepsilon$ and $\Delta\delta^{18}O:\Delta\delta^{15}N$ values are 1 standard errors (± 1 S.E.) while the R^2 values are the coefficients of determination associated with linear regression models

REFERENCES

Antler, G., Turchyn, A. V., Herut, B., Davies, A., Rennie, V. C., & Sivan, O. (2014). Sulfur and oxygen isotope tracing of sulfate driven anaerobic methane oxidation in estuarine sediments. *Estuarine, Coastal and Shelf Science*, *142*, 4-11.

Baross, J.A. and Hoffman, S.E. (1985) Submarine hydrothermal vents and associated gradient environments as sites for the origin and evolution of life. *Origins of Life and Evolution of the Biosphere* 15, 327-345.

Berndt, M. E., Seyfried Jr, W. E., & Beck, J. W. (1988). Hydrothermal alteration processes at midocean ridges: experimental and theoretical constraints from Ca and Sr exchange reactions and Sr isotopic ratios. *Journal of Geophysical Research: Solid Earth*, *93*(B5), 4573-4583.

Böhlke, J. K., Mroczkowski, S. J., & Coplen, T. B. (2003). Oxygen isotopes in nitrate: New reference materials for 18O: 17O: 16O measurements and observations on nitrate‐water equilibration. *Rapid Communications in Mass Spectrometry*, *17*(16), 1835-1846.

Bourbonnais, A., Lehmann, M. F., Butterfield, D. A., & Juniper, S. K. (2012). Subseafloor nitrogen transformations in diffuse hydrothermal vent fluids of the Juan de Fuca Ridge evidenced by the isotopic composition of nitrate and ammonium. *Geochemistry, geophysics, geosystems*, *13*(2).

Bowers, T. S. (1989). Stable isotope signatures of water‐rock interaction in mid‐ocean ridge hydrothermal systems: Sulfur, oxygen, and hydrogen. *Journal of Geophysical Research: Solid Earth*, *94*(B5), 5775-5786.

Brandes, J. A., Boctor, N. Z., Cody, G. D., Cooper, B. A., Hazen, R. M., & Yoder Jr, H. S. (1998). Abiotic nitrogen reduction on the early Earth. *Nature*, *395*(6700), 365.

Brandes, J. A., Hazen, R. M., & Yoder Jr, H. S. (2008). Inorganic nitrogen reduction and stability under simulated hydrothermal conditions. *Astrobiology*, *8*(6), 1113-1126.

Brown, L. L., & Drury, J. S. (1967). Nitrogen‐isotope effects in the reduction of nitrate, nitrite, and hydroxylamine to ammonia. I. In sodium hydroxide solution with Fe (II). *The Journal of Chemical Physics*, *46*(7), 2833-2837.

Brown, L. L., & Drury, J. S. (1969). Nitrogen Isotope Effects in the Reduction of Nitrate, Nitrite, and Hydroxylamine to Ammonia. II. The MgO and CuSO4 Systems. *The Journal of Chemical Physics*, *51*(9), 3771-3775.

Brunner, B., Bernasconi, S. M., Kleikemper, J., & Schroth, M. H. (2005). A model for oxygen and sulfur isotope fractionation in sulfate during bacterial sulfate reduction processes. *Geochimica et Cosmochimica Acta*, *69*(20), 4773-4785.

Buchwald C., Grabb K. C., Hansel C. M. and Wankel S. D. (2016) Constraining the role of iron in environmental nitrogen transformations: dual stable isotope systematics of abiotic NO_2 reduction by Fe(II) and its production of N2O. Geochim. Cosmochim. Acta 186, 1–12.

Buresh R. J. and Moraghan J. T. (1976) Chemical reduction of nitrate by ferrous iron. J. Environ. Qual. 5, 320–325.

Butterfield, D. A., Roe, K. K., Lilley, M. D., Huber, J. A., Baross, J. A., Embley, R. W., & Massoth, G. J. (2004). Mixing, reaction and microbial activity in the sub-seafloor revealed by temporal and spatial variation in diffuse flow vents at Axial Volcano. *The Subseafloor Biosphere at Mid-Ocean Ridges*, *144*, 269-289.

Capone, D.G., Popa, R., Flood, B. and Nealson, K.H. (2006) Follow the nitrogen. Science 312, 708-709.

Casciotti, K. L. (2016). Nitrogen and oxygen isotopic studies of the marine nitrogen cycle. *Annual review of marine science*, *8*, 379-407.

Casciotti, K. L., Sigman, D. M., Hastings, M. G., Böhlke, J. K., & Hilkert, A. (2002). Measurement of the oxygen isotopic composition of nitrate in seawater and freshwater using the denitrifier method. *Analytical Chemistry*, *74*(19), 4905-4912.

Corliss, J. B., Baross, J. A., & Hoffman, S. E. (1981). An hypothesis concerning the relationships between submarine hot springs and the origin of life on earth. *Oceanologica Acta, Special issue*.

Dhakal, P., Matocha, C. J., Huggins, F. E., & Vandiviere, M. M. (2013). Nitrite reactivity with magnetite. *Environmental science & technology*, *47*(12), 6206-6213.

DiFiore, P. J., Sigman, D. M., & Dunbar, R. B. (2009). Upper ocean nitrogen fluxes in the Polar Antarctic Zone: Constraints from the nitrogen and oxygen isotopes of nitrate. *Geochemistry, Geophysics, Geosystems*, *10*(11).

Fawcett, S. E., Ward, B. B., Lomas, M. W., & Sigman, D. M. (2015). Vertical decoupling of nitrate assimilation and nitrification in the Sargasso Sea. *Deep Sea Research Part I: Oceanographic Research Papers*, *103*, 64-72.

Frisch, M. J., Trucks, G. W., Schlegel, H. B., Scuseria, G. E., Robb, M. A., Cheeseman, J. R., …, & Fox, D. J. (2010). *GAUSSIAN 09, Rev. A.02*, Gaussian Inc., Wallingford CT, 2009

Garside, C. (1982). A chemiluminescent technique for the determination of nanomolar concentrations of nitrate and nitrite in seawater. *Marine Chemistry*, *11*(2), 159-167.

German, C. R., & Von Damm, K. L. (2003). Hydrothermal processes. In *Treatise on Geochemistry: First Edition*. Elsevier Inc..

Grabb, K. C., Buchwald, C., Hansel, C. M., & Wankel, S. D. (2017). A dual nitrite isotopic investigation of chemodenitrification by mineral-associated Fe (II) and its production of nitrous oxide. *Geochimica et Cosmochimica Acta*, *196*, 388-402.

Granger, J., & Sigman, D. M. (2009). Removal of nitrite with sulfamic acid for nitrate N and O isotope analysis with the denitrifier method. *Rapid Communications in Mass Spectrometry*, *23*(23), 3753-3762.

Granger, J., Sigman, D. M., Lehmann, M. F., & Tortell, P. D. (2008). Nitrogen and oxygen isotope fractionation during dissimilatory nitrate reduction by denitrifying bacteria. *Limnology and Oceanography*, *53*(6), 2533-2545.

Granger, J., Sigman, D. M., Needoba, J. A., & Harrison, P. J. (2004). Coupled nitrogen and oxygen isotope fractionation of nitrate during assimilation by cultures of marine phytoplankton. *Limnology and Oceanography*, *49*(5), 1763-1773.

Hatzinger, P. B., Böhlke, J. K., Sturchio, N. C., Gu, B., Heraty, L. J., & Borden, R. C. (2009). Fractionation of stable isotopes in perchlorate and nitrate during in situ biodegradation in a sandy aquifer. *Environmental Chemistry*, *6*(1), 44-52.

Högberg, P. (1997). [15]N natural abundance in soil‑plant systems. *New Phytologist*, *137*(2), 179-203.

Huber, J. A., Cantin, H. V., Huse, S. M., Mark Welch, D. B., Sogin, M. L., & Butterfield, D. A. (2010). Isolated communities of Epsilonproteobacteria in hydrothermal vent fluids of the Mariana Arc seamounts. *FEMS microbiology ecology*, *73*(3), 538-549.

Johnson J. W., Oelkers E. H. and Helgeson H. C. (1992) SUPCRT92: A software package for calculating the standard molal thermodynamic properties of minerals, gases, aqueous species, and reactions from 1 to 5000 bar and 0 to 1000 _C. *Comput. Geosci.* 18, 899–947.

Kampschreur, M. J., Kleerebezem, R., de Vet, W. W., & van Loosdrecht, M. C. (2011). Reduced iron induced nitric oxide and nitrous oxide emission. *Water research*, *45*(18), 5945-5952.

Kaneko, M., & Poulson, S. R. (2013). The rate of oxygen isotope exchange between nitrate and water. *Geochimica et Cosmochimica Acta*, *118*, 148-156.

Karl, D. M. (1995). Ecology of free-living, hydrothermal vent microbial community. In Karl, D. M. (Ed.), *The microbiology of deep-sea hydrothermal vents* (pp. 35-124). CRC Press.

Karsh, K. L., Granger, J., Kritee, K., & Sigman, D. M. (2012). Eukaryotic assimilatory nitrate reductase fractionates N and O isotopes with a ratio near unity. *Environmental science & technology*, *46*(11), 5727-5735.

Kelley, D. S., Karson, J. A., Früh-Green, G. L., Yoerger, D. R., Shank, T. M., Butterfield, D. A., ... & Jakuba, M. (2005). A serpentinite-hosted ecosystem: the Lost City hydrothermal field. *Science*, *307*(5714), 1428-1434.

Knapp, A. N., Sigman, D. M., & Lipschultz, F. (2005). N isotopic composition of dissolved organic nitrogen and nitrate at the Bermuda Atlantic Time‑series Study site. *Global Biogeochemical Cycles*, *19*(1).

Krasnopolsky, V. A. (2006). Some problems related to the origin of methane on Mars. *Icarus*, *180*(2), 359-367.

Lam, P., Cowen, J. P., & Jones, R. D. (2004). Autotrophic ammonia oxidation in a deep-sea hydrothermal plume. *FEMS microbiology ecology*, *47*(2), 191-206.

Lam, P., Cowen, J. P., Popp, B. N., & Jones, R. D. (2008). Microbial ammonia oxidation and enhanced nitrogen cycling in the Endeavour hydrothermal plume. *Geochimica et Cosmochimica Acta*, *72*(9), 2268-2286.

Li, J., Sun, Y., Fang, J., Xie, W., Peng, X., Dong, L., ... & Zhou, H. (2014). Aerobic and anaerobic ammonia-oxidizing microorganisms in low-temperature hydrothermal Fe-Si-rich precipitates of the Southwestern Pacific Ocean. *Geomicrobiology Journal*, *31*(1), 42-52.

López‑García, P., Duperron, S., Philippot, P., Foriel, J., Susini, J., & Moreira, D. (2003). Bacterial diversity in hydrothermal sediment and epsilonproteobacterial dominance in experimental microcolonizers at the Mid‑Atlantic Ridge. *Environmental Microbiology*, *5*(10), 961-976.

Lowell, R. P. (1991). Modeling continental and submarine hydrothermal systems. *Reviews of Geophysics*, *29*(3), 457-476.

Lowell, R. P., & Rona, P. A. (1985). Hydrothermal models for the generation of massive sulfide ore deposits. *Journal of Geophysical Research: Solid Earth*, *90*(B10), 8769-8783.

Lowell, R. P., Rona, P. A., & Von Herzen, R. P. (1995). Seafloor hydrothermal systems. *Journal of Geophysical Research: Solid Earth*, *100*(B1), 327-352.

Mariotti, A., Germon, J. C., Hubert, P., Kaiser, P., Letolle, R., Tardieux, A., & Tardieux, P. (1981). Experimental determination of nitrogen kinetic isotope fractionation: some principles; illustration for the denitrification and nitrification processes. *Plant and soil*, *62*(3), 413-430.

Martin, T. S., & Casciotti, K. L. (2016). Nitrogen and oxygen isotopic fractionation during microbial nitrite reduction. *Limnology and Oceanography*, *61*(3), 1134-1143.

McIlvin, M. R., & Casciotti, K. L. (2011). Technical updates to the bacterial method for nitrate isotopic analyses. *Analytical Chemistry*, *83*(5), 1850-1856.

Nakagawa, S., Takai, K., Inagaki, F., Hirayama, H., Nunoura, T., Horikoshi, K., & Sako, Y. (2005). Distribution, phylogenetic diversity and physiological characteristics of epsilon‐Proteobacteria in a deep‐sea hydrothermal field. *Environmental Microbiology*, *7*(10), 1619-1632.

Peng, X., Fawcett, S. E., van Oostende, N., Wolf, M. J., Marconi, D., Sigman, D. M., & Ward, B. B. (2018). Nitrogen uptake and nitrification in the subarctic North Atlantic Ocean. *Limnology and Oceanography*, *63*(4), 1462-1487.

Proskurowski, G., Lilley, M. D., Kelley, D. S., & Olson, E. J. (2006). Low temperature volatile production at the Lost City Hydrothermal Field, evidence from a hydrogen stable isotope geothermometer. *Chemical Geology*, *229*(4), 331-343.

Reeves, E. P., McDermott, J. M., & Seewald, J. S. (2014). The origin of methanethiol in midocean ridge hydrothermal fluids. *Proceedings of the National Academy of Sciences*, 201400643.

Salmimies, R., Mannila, M., Juha, J., & Häkkinen, A. (2011). Acidic dissolution of magnetite: experimental study on the effects of acid concentration and temperature. *Clays and Clay Minerals*, *59*(2), 136-146.

Schauble E. A. (2004) Applying stable isotope fractionation theory to new systems. *Rev. Mineral. Geochem*. 55, 65–111.

Seyfried, W. E. Jr., Janecky, D. R., Berndt, M. E. 1987. Rocking autoclaves for hydrothermal experiments II : the flexible cell system. In Barnes, H. and Ulmer, O., *Experimental Hydrothermal Techniques*. New York : Wiley-Interscience.

Shock, E. L. (1992). Chemical environments of submarine hydrothermal systems. In Holm, N. G. (Ed.), *Origins of Life and Evolution of the Biosphere* (pp. 67-107). Springer, Netherlands.

Sidhu, P. S., Gilkes, R. J., Cornell, R. M., & Posner, A. M. (1981). Dissolution of iron oxides and oxyhydroxides in hydrochloric and perchloric acids. In *Clays Clay Miner*.

Sigman, D. M., Casciotti, K. L., Andreani, M., Barford, C., Galanter, M. B. J. K., & Böhlke, J. K. (2001). A bacterial method for the nitrogen isotopic analysis of nitrate in seawater and freshwater. *Analytical chemistry*, *73*(17), 4145-4153.

Sleep, N. H. (1991). Hydrothermal circulation, anhydrite precipitation, and thermal structure at ridge axes. *Journal of Geophysical Research: Solid Earth*, *96*(B2), 2375-2387.

Sorensen J. and Thorling L. (1991) Stimulation by lepidocrocite (!- FeOOH) of Fe(II)-dependent nitrite reduction. Geochim. Cosmochim. Acta 55, 1289–1294.

Sturchio, N. C., Böhlke, J. K., Beloso, A. D., Streger, S. H., Heraty, L. J., & Hatzinger, P. B. (2007). Oxygen and chlorine isotopic fractionation during perchlorate biodegradation: laboratory results and implications for forensics and natural attenuation studies. *Environmental science & technology*, *41*(8), 2796-2802.

Summers, D. P. (2005). Ammonia formation by the reduction of nitrite/nitrate by FeS: ammonia formation under acidic conditions. *Origins of Life and Evolution of Biospheres*, *35*(4), 299-312.

Summers, D. P., & Khare, B. (2007). Nitrogen fixation on early Mars and other terrestrial planets: experimental demonstration of abiotic fixation reactions to nitrite and nitrate. *Astrobiology*, *7*(2), 333-341.

Summers, D. P., & Lerner, N. (1998). Ammonia from iron (II) reduction of nitrite and the Strecker synthesis: do iron (II) and cyanide interfere with each other?. *Origins of Life and Evolution of the Biosphere*, *28*(1), 1-11.

Summers, D.P. and Chang, S. (1993) Prebiotic ammonia from reduction of nitrite by iron (II) on the early Earth. Nature 365, 630-633.

Sun, W.; Li, Q.; Gao, S.; Shang, J. K. Monometallic Pd/Fe_3O_4 catalyst for denitrification of water. *Appl. Catal. B: Environ*. 2012, 125, 1−9.

Sylvan, J. B., Wankel, S. D., LaRowe, D. E., Charoenpong, C. N., Huber, J. A., Moyer, C. L., & Edwards, K. J. (2017). Evidence for microbial mediation of subseafloor nitrogen redox processes at Loihi Seamount, Hawaii. *Geochimica et Cosmochimica Acta*, *198*, 131-150.

Tivey, M. K., Stakes, D. S., Cook, T. L., Hannington, M. D., & Petersen, S. (1999). A model for growth of steep‑sided vent structures on the Endeavour Segment of the Juan de Fuca Ridge: Results of a petrologic and geochemical study. *Journal of Geophysical Research: Solid Earth*, *104*(B10), 22859-22883.

Trull, T. W., Davies, D., & Casciotti, K. (2008). Insights into nutrient assimilation and export in naturally iron-fertilized waters of the Southern Ocean from nitrogen, carbon and oxygen isotopes. *Deep Sea Research Part II: Topical Studies in Oceanography*, *55*(5-7), 820-840.

Van Dover, C. (2000). Chemical and physical properties of vents fluids. In Van Dover, C. (Ed.), *The ecology of deep-sea hydrothermal vents* (pp. 76-98). Princeton University Press.

Wang, F., Zhou, H., Meng, J., Peng, X., Jiang, L., Sun, P., ... & Wu, L. (2009). GeoChip-based analysis of metabolic diversity of microbial communities at the Juan de Fuca Ridge hydrothermal vent. *Proceedings of the National Academy of Sciences*, *106*(12), 4840-4845.

Wolery T. J. (1992) EQ3/6, A Software Package for Geochemical Modeling of Aqueous Systems: Theoretical Manual, User's Guide, and Related Documentation (Version 7.0). Lawrence Livermore National Laboratory.

Zhang, L., Altabet, M. A., Wu, T., & Hadas, O. (2007). Sensitive measurement of NH_4^+ $^{15}N/^{14}N$ ($\delta^{15}NH4+$) at natural abundance levels in fresh and saltwaters. *Analytical Chemistry*, *79*(14), 5297-5303.

CHAPTER 3

Sources of ammonium in high-temperature submarine hydrothermal vent fluids: Insights from concentration and N isotopic composition measurements

3.1. ABSTRACT

Together with dissolved nitrogen gas (N_2), ammonium (NH_4^+) comprises a majority of nitrogen-containing ions/compounds in submarine hydrothermal vent fluids. While a dichotomy in NH_4^+ concentrations between sediment-covered and sediment-starved systems has long been recognized, many large variations, especially in the latter case, remain notably unexplained. To further constrain subsurface production and alteration of NH_4^+, we both analyzed and compiled $[NH_4^+]$ and N isotopic composition of NH_4^+ ($\delta^{15}N_{NH4}$) from a survey of submarine vent sites throughout the global ocean. In addition to previously recognized sources/processes including sedimentary organic matter, abiotic reduction of nitrate (NO_3^-) or N_2, interaction with secondary clay minerals, and possible biological processes, here we postulate and provide evidence for phase separation as an additional factor that may control NH_4^+ abundance at vents. Moreover, we discuss the contribution of biological processes happening in the recharge zone that may provide a first-order control on vent $[NH_4^+]$ and $\delta^{15}N_{NH4}$. This work highlights existing gaps in available data on $[NH_4^+]$ and N isotopic composition necessary to constrain exact pathways and detailed mechanisms of many possible subsurface processes involved in the production and release of NH_4^+ in hydrothermal vent fluids. Moving forward, we suggest best approaches in collecting and processing samples for $[NH_4^+]$ and $\delta^{15}N_{NH4}$ measurements.

3.2. INTRODUCTION

Since the first submarine hydrothermal system in the Galápagos Rift was discovered in 1977 (Corliss et al., 1979), great strides have been made in understanding how oceanic hydrothermal circulation impacts sources and sinks of different chemical species. These unique vent ecosystems host thriving microbial and metazoan communities within food webs supported by chemosynthesis. As with any forms of life on Earth, organisms inhabiting hydrothermal vents require nitrogen (N) to support metabolic functions, growth, and reproduction. While dissolved nitrogen gas (N_2) is found to be equally or more abundant in venting fluids than its typical bottom seawater counterpart (Charlou et al., 2002), this form is only available to highly specialized nitrogen-fixing microbes. On the other hand, ammonium (NH_4^+) is a form of inorganic nitrogen readily available as a nutrient to virtually all prokaryotes (Madigan et al., 2010). Large compilations of uptake measurements in marine and estuarine environments (Mulholland and Lomas, 2008) have demonstrated that NH_4^+ is the form of inorganic N that is assimilated most rapidly attributable to it being energetically efficient for cellular uptake (i.e., it is already reduced and thereby requiring little extra energy to assimilate). Furthermore, NH_4^+ is often the most or the second-most abundant N species in vent fluids, in stark contrast to the barely detectable levels of NH_4^+ found throughout most of the global ocean.

In addition to microbial uptake (i.e., assimilation), NH_4^+ can also be metabolized by microbes through dissimilatory processes, serving as substrates for processes such as nitrification and anammox. Indeed enhancement of nitrification has been reported in hydrothermal plumes (Lam et al., 2004, 2008; Baker et al., 2012; Dick and Tebo, 2010), within diffuse vent fluids (Bourbonnais et al., 2012b; Sylvan et al., 2017) and within vent structures (e.g., Baker et al., 2012). Similarly, the presence and activities of anammox bacteria at vents have also been

confirmed in numerous studies (Bourbonnais et al., 2012a, 2012b; Russ et al., 2013; Byrne et al., 2009).

Besides its significance to microbial communities as a nutrient and energy source, NH_4^+, when abundant, has also been noted for its capacity to buffer pH, promoting elevated pH and favoring precipitation of metal sulfides and the formation of massive sulfide structures as vent fluids cool down during their exit from the seafloor (Von Damm et al., 1985b; Tivey et al., 1999). The role of NH_4^+ in the formation of vent structures was demonstrated at the Endeavour Segment of the Juan de Fuca Ridge, where abundant fluid hosted NH_4^+ likely provided a mechanism for intense silicification and sulfide precipitation (Tivey et al., 1999).

Concentrations of NH_4^+ alone, however, provide only limited information on the processes that produce it. The nitrogen isotopic composition (hereafter referred to as $\delta^{15}N_{NH4}$) represents an additional constraint on source and any alteration of vent-derived NH_4^+ (Lilley et al., 1993; Bourbonnais et al., 2012b; Sylvan et al., 2017). Here, we present new results for NH_4^+ concentration and $\delta^{15}N_{NH4}$ values from a survey of fluids from several vent systems around the globe (Figure 1), as well as crustal fluids collected from an Integrated Ocean Drilling Program (IODP) borehole from sedimented young basaltic crust on the flank of the Juan de Fuca Ridge. We report these new data along with a summary of previously published measurements from other vent fields, in order to examine the range of processes giving rise to both NH_4^+ formation in high-temperature fluids as well as those that may play a role in its high temperature consumption before fluids reemerge at the seafloor.

3.3. GEOLOGIC SETTINGS AND SAMPLE COLLECTION

Samples used in this study were collected from deep-sea hydrothermal fields from around the globe and include the North and South Guaymas Basins, the East Pacific Rise, the Lau Basin, the Mid-Cayman Rise, and the Mid-Atlantic Ridge. With the exception of the north and south Guaymas Basins, all sites are unsedimented. The Guaymas Basin, situated in the Gulf of California, hosts two distinct spreading centers resulting in the formation of the northern and southern troughs (Longdale et al., 1980). Spreading along these axes is estimated at about 6 cm/yr (Von Damm et al., 1985b) and these systems are characteristically overlain by a thick layer (>500 m) of organic-rich sediments arising from high input of both terrestrial material and surface water primary production. Vent fluid samples from South Guaymas Basin (27°02'N and 111°24'W, ~2.0 km) were collected using 150 mL titanium isobaric gas-tight (IGT) samplers (Seewald et al., 2002) deployed by the HOV Alvin during R/V Atlantis cruise AT15-38 in October 2008. Samples from North Guaymas Basin (27°24'N and 111°23'W) both just outside of the spreading axis (~2.0 km) and several off-axis (1.7-1.9 km) sites (Soule et al., 2018) were collected using the same IGT samplers deployed by ROV Hercules during R/V Nautilus cruise NA090 in October 2017 (Seewald et al., 2018).

The East Pacific Rise (9°50'N and 104°17'W, ~2.5 km) is located on a sediment-starved, basalt-hosted, fast-spreading ridge (11 cm/yr full rate, Carbotte and Macdonald, 1994). Fluid chemistry from different focused and diffuse vents of 9°50' N EPR has been reported in several previous studies (e.g., Von Damm 2000; Reeves et al., 2014). Samples in this study were taken with 750mL titanium 'major samplers' (Von Damm et al., 1985a) deployed by HOV Alvin during the R/V Atlantis cruise AT37-12 in April-May 2017.

The Eastern Lau Spreading Center (ELSC, 20°49'S and 176°30'W, 1.8-2.1 km) is part of the southern portion of the Lau back-arc Basin located between the islands of Tonga and Fiji in the Southwest Pacific. Here at the ELSC spreading rates increase from 6.5 cm/yr toward the southern end (21°S) to 9.0 cm/yr at the northern end (18°S) (Taylor et al., 1996). Similarly there is also a transition in the host rocks from arc-like basaltic andesite, andesite, and rhyodacite in the south to tholeiitic back-arc basin basalt (BABB) in the north (Martinez and Taylor, 2002). The ELSC is hosted by tholeiitic basalts. Samples were collected from different vent sites spanning from the northern trough to the southern ridge of the ELSC using IGT samplers deployed by ROV Jason II during R/V Roger Revelle cruise RR1507 in April-May 2015. While some data on the chemistry of vent fluids from the ELSC collected on other cruises have been reported (Takai et al., 2008; Mottl et al., 2011; Evans et al., 2017), the full fluid chemistry for the samples used in this study is reported in Seewald (2017).

Samples from the Mid-Cayman Rise, an ultra-slow spreading ridge (1.5-1.7 cm/yr, Rosencrantz et al., 1988), were collected from the Piccard (18°33'N and 81°43'W, ~5.0 km) and Von Damm (18'23'N and 81'50'W, ~2.3 km) vent fields. The Piccard field is basalt-hosted and currently stands as the deepest known mid-ocean ridge system (Beaulieu et al., 2013). At the Von Damm field, unlike most basalt-hosted mid-ocean ridges, the basement is made up of meta-gabbro, dolerite dykes and serpentinized peridotites and the vent structures are comprised of talc (Hodgkinson et al., 2015). The full description and chemistry of fluids from various vent sites around Piccard and Von Damm have been reported previously (McDermott et al., 2018; McDermott, 2015; Reeves et al., 2014; and Hodgkinson et al., 2015). Samples used in this study were collected with IGT samplers deployed by HROV Nereus during R/V Falkor cruise FK008 in June 2013.

Samples representing the Mid-Atlantic Ridge were collected from the center of the rift valley at the Lucky Strike vent field (37°18'N and 32°17'W, ~1.7 km), located around a large seamount (~ 50 km^2) and influenced by the Azores hot spot (Langmuir et al., 1998). The area is characterized by slow-spreading center (21 mm/yr full rate, Dziak et al., 2004). The fluid samples of Lucky Strike were collected with IGT samplers deployed by ROV Jason II during R/V Roger Revelle cruise KNOX18RR in July-August 2008 and their chemical composition was previously reported (Pester et al., 2012; Reeves et al., 2014).

Crustal fluids from the Juan de Fuca ridge-flank were taken from boreholes U1362A and U1362B (47°45.662'N and 127°45.674'W, 2672 m) outfit with Circulation Obviation Retrofit Kits (CORK) allowing routine sampling of basement fluid (Becker and Davis, 2005). Borehole U1362A was drilled to 528 m below seafloor (mbsf), through 236 m of overlying sediment cover and 292 m of basaltic basement, while the borehole U1362B was drilled to 359 mbsf (242 m of which was the sediment cover). Further details on the boreholes can be found in the IODP Expedition 327 report (Shipboard Scientific Party, 2004). Site U1362 is located between Mama Bare and Baby Bare outcrops, southeast of the Endeavour Segment of the Juan de Fuca Ridge. Crustal fluids were sampled from CORKs in 2013 and 2014 with HOV Alvin according to procedures similar to those outlined in Lin et al. (2012).

3.4. METHODS

3.4.1. Ammonium concentrations

Concentrations of NH$_4^+$ were measured by flow injection analysis (FIA) as previously described (Hall & Aller, 1992) with minor modifications in the composition of carrier fluids (20 mM NaOH + 0.2 M Na-citrate and 50 μM HCl). This method relies on raising the pH of the

sample through mixing it with the basic carrier solution which will deprotonate dissolved NH_4^+ forming NH_3. The evolving NH_3 then diffuses across a Teflon exchange membrane to the other side containing an acidic carrier fluid that acts to re-protonate NH_3 to NH_4^+ before being carried into and quantified by a conductivity detector. High hydrogen sulfide (H_2S) content (typical of high-temperature vent fluids) can interfere during the measurement. Therefore, samples were purged with either high-purity argon or nitrogen gas prior to analysis. Alternatively, concentrations of NaOH in the carrier solution can be increased to titrate H_2S. However, experience shows that the former or the combination of the two approaches is preferable. Typical working concentration range is 0.5 to 50 μM and samples with higher NH_4^+ were diluted before injection.

3.4.2. Ammonium isotopic composition

The N isotopic composition of NH_4^+ was analyzed by passive diffusion of ammonia through Teflon membranes (Holmes et al., 1998; Sigman et al., 1997) coupled with persulfate digestion to NO_3^- (Knapp et al., 2005) followed by conversion to N_2O by the denitrifier method before being analyzed by isotope ratio mass spectrometry (IRMS). This diffusion/oxidation/ denitrifier protocol is similar to that described previously (Bourbonnais, et al., 2012b) with the following exceptions. We either diluted or pipetted all samples and isotope standards from the same ammonia diffusion step to obtain the same amount of NH_4^+ across each batch (typically 50 – 200 nmoles NH_4^+); whenever possible, we tried to add up to 200 nmoles NH_4^+ per vial to minimize the blank/sample ratio. This step ensures that the blank effect from the reagents used during the oxidation is minimized. The conversion of NH_4^+ to NO_3^- through persulfate digestion for isotope analysis has the advantage over the conventional oxidation using an elemental

analyzer (EA) that it requires at least two orders of magnitude less N per sample (i.e., ~10 nmoles N for persulfate vs ~1 μmole N).

The nitrogen isotopic composition of ammonium is expressed in delta notation, where

$$\delta^{15}N_{NH4} \text{ (‰ vs air)} = \left[\left(\frac{^{15}N:\,^{14}N_{sample}}{^{15}N:\,^{14}N_{air}}\right) - 1\right] \times 1000$$

Reported isotopic values are normalized to international isotope reference standards: IAEA-N1 (+0.4‰), USGS-25 (-30.41‰), and USGS-26 (+53.75‰). Reproducibility on repeated standards is typically better than 0.6‰.

3.4.3. Mg^{2+} and Cl^- measurements and endmember calculation

Concentrations of Mg^{2+} and Cl^- were measured by ion chromatography (IC) using a Dionex DX-500. Samples were gravimetrically diluted with DI water prior to being chromatographically separated using a Dionex IonPac AS15 column for Cl^- and Dionex IonPac CS12A column for Mg^{2+}. Both analyses were run in suppressed conductivity mode for increased sensitivity (suppressor current of 300 mA and 125 mA for Cl^- and Mg^{2+}, respectively). Analytical uncertainty (2S.D.) was better than ±3%.

Fluid samples taken either by IGT and major samplers often contain measureable amount of Mg^{2+} resulting from entrainment of surrounding seawater or mixing with seawater-containing dead space within the samplers. As field, experimental and theoretical studies have established that hydrothermal fluids have near-zero Mg^{2+} due to fluid-rock reactions at high temperature (Bischoff and Dickson, 1975; Mottl and Holland, 1978; Seyfried and Bischoff, 1981; Von Damm et al., 1985a), we calculated endmember concentrations for different chemical species through linear regressions of sample concentrations and bottom seawater concentrations to obtain extrapolated zero-Mg endmember fluid composition. Endmember crustal fluid calculation was

also carried out in the same manner as that for the vent fluids except that we did not extrapolate to zero Mg endmember. Instead, we used the lowest Mg concentration measured under optimal sampling conditions for a particular borehole.

3.5. RESULTS

Vent fluid samples analyzed in this study exhibit a range of Mg^{2+} concentrations. For those high-temperature fluids emanating from focused-venting orifices/chimneys where near-zero Mg^{2+} are expected we can attribute the presence of Mg^{2+} mainly to the dead space in the sampler used. Additionally, in some cases, ambient seawater is inadvertently entrained into the samplers during sampling. We therefore calculate the endmember NH_4+ concentrations and report them along with the measured values (Table 1) as the former may provide more meaningful numbers for interpretation and comparison. Endmember calculations, however, are not done on low-temperature samples primarily because they are likely subject to biological influence that might either increase or decrease the NH_4^+ concentrations.

At the sedimented Guaymas Basin, endmember NH_4^+ concentrations from high-temperature fluids at the Northern Trough (5.9-8.3 mM) are about half as high as those from the Southern Trough (11.8-16.0 mM). The $\delta^{15}N_{NH4}$ values for these high-temperature endmembers from North Guaymas (+8.6 ± 0.4‰) do not differ from those from South Guaymas (+8.7 ± 0.6‰).

Sediment-starved mid-ocean ridge vent fluids have notably lower concentrations of NH_4^+. High temperature fluids from 9°50'N EPR contain NH_4^+ in the range of 4.4-7.1 µM with slight variation between sites for both concentrations and isotopic composition. Most low-temperature, diffuse vents of 9°50'N EPR are isotopically different from their high-temperature

counterpart (samples especially from Crab Spa are discussed in greater detail in Chapter 4).

Lucky Strike exhibited endmember NH_4^+ concentrations of 3.8-4.3 µM with similar $\delta^{15}N_{NH4}$

values in the two vents studied. Interestingly, NH_4^+ concentrations at vents from the Mid-

Cayman Rise exhibited greater NH_4^+ in the vent fluids with 45.6 µM at Piccard and 18.6-23.0

µM at Von Damm. Similar to 9°50'N EPR, $\delta^{15}N_{NH4}$ values between vents at Von Damm and

Piccard seem to cluster around +5.3 ± 0.8‰. The lowest endmember NH_4^+ concentrations of all

those surveyed were observed at the East Lau Spreading Center with a combined average

concentration of 1.6 µM across all four surveyed vent fields. These low concentrations precluded

any successful $\delta^{15}N$ measurements due to insufficient sample volume.

The Juan de Fuca crustal fluids (Table 2) located proximal to the hydrothermal vent fields

provide a first-order look into the alteration of fluids in the low-temperature recharge zone. Here,

we observe low-Mg^{2+} crustal fluids that carry elevated NH_4^+ concentrations. Samples from the

two boreholes collected in two consecutive years are compositionally very consistent, both in

terms of $[NH_4^+]$ (overall 110 uM) and $\delta^{15}N_{NH4}$ values (+2.6 ± 0.2‰).

3.6. DISCUSSION

3.6.1 Sources and sinks for NH_4^+ at vents

The most striking feature from the perspective of NH_4^+ concentrations is the relationship

with the presence or absence of sediment cover. The first reports of NH_4^+ concentrations from

21°N East Pacific Rise (Von Damm et al., 1985a) and Guaymas Basin, Gulf of California (Von

Damm et al., 1985b) revealed a strong dichotomy between the unsedimented and the sediment-

hosted systems, respectively, in which concentrations can differ by three or more orders of

magnitude. Indeed, this trend persists through more measurements of NH_4^+ from different vents

around the globe years later (Table 3). Sediment-hosted systems, including Middle Valley on the northern Juan de Fuca Ridge, Escabana Trough on the Gorda Ridge, the Guaymas Basin in the Gulf of California, and the Okinawa Trough, all exhibit greatly elevated $[NH_4^+]$ values typically >1 mmol/kg (Figure 2). In contrast, in systems that are sediment starved, such as those along the Mid-Atlantic Ridge and the East Pacific Rise, maximum $[NH_4^+]$ are often well below 30 µM (Figure 4). Interestingly, there also exist some sediment-free systems that have been reported to exhibit anomalously elevated $[NH_4^+]$ interpreted as reflecting subsurface influence of sediment organic matter, notably along the Main Endeavour Segment of the Juan de Fuca Ridge (Lilley et al., 1993; Bourbonnais et al., 2012b) and at Loki's Castle along the Arctic Mid-Ocean Ridge (Baumberger et al., 2016).

While the high concentrations of NH_4^+ in sediment-hosted hydrothermal vents are largely attributable to the decomposition of sedimentary organic matter (Campbell et al., 1988; Nunoura et al., 2010; Seewald et al., 2003; Seewald et al., 1990; Von Damm et al., 1985b), the exact origin and processes that produce NH_4^+ in typical sediment-starved mid-ocean ridge settings remain unclear (Wankel et al., 2017; Brandes et al., 2008). Indeed bottom seawater entrained during hydrothermal recharge typically contains dissolved N_2 (~590 µM; Charlou et al., 2002), NO_3^- (20-50 µM; Garcia et al., 2014) and dissolved organic N (DON) (<3 µM; Wong et al., 2002) with typically undetectable levels of NH_4^+. Interestingly, some high temperature vent fluids from a number of vents along the Mid Atlantic Ridge have been reported to contain N_2 of similar concentration or more compared to the inflowing bottom seawater (Charlou et al., 2002). To the best of our knowledge, very little information has been reported on quantifying [DON] in high temperature vents. A recent study from 9°50'N EPR (Longnecker et al., 2018) reported the concentrations of total dissolved N in the sample from *Bio 9* in 2014. Using a back-of-envelope

calculation with the dissolved inorganic nitrogen concentrations (i.e., NO_3^- and NH_4^+) from our study, the DON concentration from *Bio 9* should be below 1 μM. Meanwhile the high temperature vent fluids are NO_3^- free based on the calculated end member compositions (Butterfield et al., 2004; Bourbonnais et al., 2012b).

In anoxic regions of recharge or discharge zones, where temperatures are still below the reported upper limit for life of 122°C (Takai et al., 2008), the subsurface microbial community can actively metabolize and assimilate N compounds. Where NO_3^- exists, some microbes can produce NH_4^+ through dissimilatory reduction of nitrate to ammonium (DNRA) (e.g., Sievert and Vetriani, 2012; Perez-Rodriguez et al., 2017; Slobodkina et al., 2017). In fact, anaerobic thermophiles have been isolated from the walls of vent chimneys on the East Pacific Rise having the ability to carry out DNRA at temperatures as high as 65°C (Perez-Rodriguez et al., 2010). In comparison, above temperatures of 122°C, all NH_4^+ production is considered solely attributable to non-biological processes.

A number of lab experiments at high temperature have demonstrated the feasibility of NO_3^- reduction with a range of reduced compounds often found in hydrothermal systems. Brown and Drury (1967) demonstrated that NO_3^- can be reduced by ferrous ion ($Fe^{2+}_{(aq)}$) to NH_4^+ with a quantitative product yield in a $NaOH/Ag_2SO_4$ solution (pH 13-14) at 110°C. Interestingly, a follow-up study (Brown and Drury, 1969) showed a contrasting result when conducted in a MgO buffered system (pH 8-9) at 110°C, wherein the reduction of nitrite (NO_2^-) resulted in production of NH_4^+ as well as additional gaseous products, N_2O and N_2. Although not indicated how NO_3^- reduction would behave under these conditions, we can assume similar non-quantitative production of NH_4^+ if NO_3^- reduction by Fe^{2+} proceeds through a NO_2^- intermediate (Brown and Drury, 1969). While we know that Fe^{2+} is widely abundant in many vent fluids, one might argue

against the relevance of the alkaline systems demonstrated by these earlier studies (Brown and Drury, 1967, 1969). Notably, however, although much rarer than their low pH counterparts, alkaline submarine vent fluids are found in serpentinite-hosted systems such as Lost City (pH up to 10.5: e.g., Klein et al., 2005; Seyfried et al., 2005; Reeves et al., 2014).

Aqueous Fe^{2+} is not the only available potential reducing agent for the reduction of NO_3^- to NH_4^+ under the environments relevant to submarine hydrothermal vents and indeed other reduced solid phases have also been shown to react with NO_3^-. Brandes et al. (1998) conducted a series of experiments spanning up to 24 hours under high pressures and high temperatures (>300°C) showing varying degree of NH_4^+ yield as a result of the reduction of NO_3^- with pyrite (FeS), magnetite (Fe_3O_4), native iron (Fe), and basalt. Furthermore, they expanded their findings to suggest that NO_3^- found in bottom seawater recharging submarine hydrothermal circulation should be quantitatively reduced to NH_4^+. However, Brandes et al. (2008) further investigated reduction of NO_3^- at elevated temperatures and pressures with magnetite and other solid phases including pyrrhotite ($Fe_{1-x}S$), millerite (NiS), chalcocite (Cu_2S) and chalcopyrite ($CuFeS_2$) for up to 19 hours and found that the amount of NH_4^+ produced did not always balance the disappearance of NO_3^- despite rapid reaction rates. A more recent study (Chapter 2) on the reduction of NO_3^- with magnetite under hydrothermal conditions also demonstrated that the disparity in the NH_4^+ yield is likely a consequence of pH, with quantitative reduction of NO_3^- to NH_4^+ achieved at high pH (>7) and conversely a non-quantitative conversion at lower pH (4-5).

Nitrite (NO_2^-), despite being generally undetectable in oxic bottom seawater, is produced as a biological denitrification intermediate during the entrainment of NO_3^- bearing seawater through the subsurface community inhabiting the anoxic region of the recharge zone. As earlier high-temperature, high-pressure lab experiments (Brandes et al., 1998; 2008) suggested, this

NO_2^- (just like NO_3^-) should also be reduced to NH_4^+. Along the same line of reasoning, DON is also expected to be deaminated releasing NH_4^+ at high temperature as suggested by several studies done on heat-induced deamination of amino acids (e.g., Lewis et al, 2016; Cleaves et al., 2018; Lepper et al., 2018).

The reduction of N_2 can also serve as a potential source of NH_4^+. It is widely understood that the breaking of the triple bond in di-atomic N_2 requires particularly high activation energy. However, lab studies in aqueous solutions demonstrate that this reaction is possible in the presence of transition metals (Bazhenova and Shilov 1995 and references therein). In addition, several studies have shown NH_4^+ production through the reaction of N_2 with iron sulfide (Dörr et al, 2003), hydrogen sulfide (Schoonen and Xu, 2001), and magnetite (Brandes et al, 1998). Based on the lack of N_2 deficit in the vent fluid from the Main Endeavour Field, Lilley et al. (1993) suggested that N_2 reduction is not occurring. However, no systematic attempt has been made to quantify how much N_2 reduction to NH_4^+ may occur elsewhere.

Another potential source of vent NH_4^+ is the through extraction of NH_4^+ from basalts as the hydrothermal fluid percolates through the crust (Lilley et al., 1993). Crustal rocks usually contain small amounts of NH_4^+ fixed in minerals (in ppm level; e.g., Vedder 1964; Busigny et al., 2003) as NH_4^+ ions may freely substitute for K^+ or Na^+-Ca^{2+} in many crystal lattices (e.g., Homma and Itihara, 1981). For example, altered basalts at a superfast spreading ridge at East Pacific Rise (ODP Site 1256) showed NH_4^+ in their secondary minerals notably K-bearing minerals including celadonite K-feldspar, and Na-feldspar (Busigny et al, 2005). Erzinger and Bach (1996) postulated that NH_4^+ would leach from basalts during nonoxidative high-temperature alteration.

NH_4^+ speciation plays an important role in determining how much NH_4^+ is readily exchangeable with the cations within the minerals that the NH_4^+-bearing fluids come in contact with. This is primarily controlled by the equilibrium between NH_4^+ and NH_3 at *in situ* conditions as it is only the charged species that is involved in ion exchange. Numerous studies have indicated enrichment of NH_4^+ in altered basalts compared to their unaltered counterparts (Busigny et al., 2005; Li et al., 2007; Bebout et al., 2018), making this another loss term for NH_4^+ in the vent fluids. For the rocks described in Busigny et al (2005), basalt alteration (and potential NH_4^+ incorporation into their mineral structure) is thought to occur at only 70°-100°C. This lower temperature range might constrain the locations (within hydrothermal circulation cells) for this NH_4^+ loss to be either in the recharge zone or within subsurface discharge zone beneath diffuse vents.

Fluids emanating from focused vents often exhibit temperatures far beyond the upper limit for life (122°C; Takai et al., 2008) and thus largely reflect abiotic processes. However, for low-temperature diffuse flow venting, temperatures are often well within the range of habitable conditions for microbial populations. Here, generation of NH_4^+ could stem from microbial processes such as DNRA and organic matter remineralization. Following its production, the consumption of NH_4^+ could also occur through assimilation or nitrification (i.e., oxidation of NH_4^+ to NO_2^- and then NO_3^-). Other microbial processes might also indirectly contribute to the production and consumption of NH_4^+ at diffuse vents (see Wankel et al., 2017 for more detail).

3.6.2. Impact of phase separation on NH_4^+

Another process that may alter NH_4^+ after its production is phase separation. Chemical constituents in circulating fluids can be fractionated during phase separation, thereby leading to

chemically distinct fluids: one with chlorinity greater than seawater (brine phase) and the other with chlorinity less than seawater (vapor phase). The chemical composition of vent fluids has long been attributed to water-rock reactions and phase separation, with the two processes intimately connected (German and Seyfried, 2014). The resultant discharge from hydrothermal circulation is thus inherently a combination of hydrothermal brines, chloride-poor vapor, and solutions that have not experienced any phase separation (e.g., Von Damm and Bischoff, 1987; Bischoff and Rosenbauer (1989) and can therefore exhibit large variations in chlorinity. Many dissolved gases (such as CO_2, CH_4, He, H_2, and H_2S) are typically reported to be enriched in the vapor phase (German and Seyfried, 2014) and NH_3 has been shown behave similarly. The dynamics of NH_3 mobilization into the vapor phase is not as straightforward as other dissolved gases, however, as its speciation is pH dependent.

Most MOR vent fluids have low pH (average pH ~3.3 as measured at 25°C; German and Seyfried, 2014), with actual *in situ* pH values being higher as a result of the change in the distribution and complexation of aqueous species at elevated temperatures and pressures (Ding and Seyfried, 2007; Ding et al., 2005). When pH is greater than the *in situ* pKa for NH_3-NH_4^+ equilibria, speciation is dominated by volatile NH_3 allowing it to readily partition into the vapor phase. Additionally, Seewald et al. (2003) noted the importance of considering whether phase separation occurred under subcritical vs supercritical conditions. The former occurs at temperatures below the critical point resulting in a vapor bubble with low-Cl and a liquid phase with unaltered chlorinity, whereas the latter occurs at temperatures above the critical point leading to a high-chlorinity brine. Two distinct conditions produce volatile enrichments that differ significantly (Seewald et al., 2003). For example, temporal variations in hydrothermal fluid NH_4^+ concentrations from the Main Endeavour Field during the evolving phase separation

regimes resulting from the 1999 seismic activity exhibited a significant decrease in NH_4^+ (Seewald et al., 2003). Another example illustrating the influence of phase separation over spatial scales comes from the Tiger Mound site in the Yonaguni Knoll hydrothermal field in the sedimented southern Okinawa Trough. Here, high temperature (310-328°C), circumneutral pH (6.7-6.8 at 25°C) fluids vent from 10-meter-tall sulfide structures located at relatively shallow depths of 1370-1385m. Phase separation is thought to be occurring just beneath the seafloor (Suzuki et al, 2008). End-member fluids collected from both the top and at base of the mound exhibited vastly different NH_4^+ concentrations. The endmember NH_4^+ concentration for the fluids collected at the top (low Cl^-) was 20.7mM while its counterpart for the fluids taken at the base (high Cl^-) was 8.6mM despite sharing the same fluid source and emanating from the same chimney structure (Suzuki et al, 2008). This doubling of NH_4^+ in the Cl-depleted fluids can be attributed to NH_3 enrichment in the vapor phase during phase separation.

3.6.3 NH_4^+ concentrations for unsedimented systems

While NH_4^+ in sediment-hosted systems can be largely attributed to sedimentary input (via remineralization and thermal alteration of organic matter), sources of NH_4^+ in unsedimented systems are essentially limited to the reduction of NO_3^- and/or N_2, or the deamination of DON. Assuming minimal contribution of NH_4^+ production by reduction of N_2 in most cases, given the very low yield shown in lab experiments (Brandes et al., 1998), here we consider only NO_3^- and DON as the potential sources for production of NH_4^+ in fluids emanating from unsedimented systems. Figure 2a shows the estimated total input of NO_3^- and DON into the recharge zone (e.g., contained in bottom seawater) along with the endmember NH_4^+ in the high-temperature vent fluids from the same areas. This analysis offers one general trend for almost all vent fields: high

temperature vent NH_4^+ concentrations are generally less than the molar input of NO_3^- plus DON. A closer inspection of these samples from different locations by normalizing the vent $[NH_4^+]$ to the bottom seawater input (i.e., NO_3^- plus DON) (Fig. 2c) makes Sea Cliff and Piccard stand out as the two systems where NH4+ is anomalously higher than expected.

3.6.4 N isotopic composition of NH_4^+ as constraint on processes in the subseafloor

Similar to many reactions in the nitrogen cycle, the reduction of NO_3^- during DNRA (Pérez-Rodríguez et al., 2017) or denitrification (e.g., Granger et al., 2008) imparts a kinetic isotope fractionation. If DNRA were the sole microbial reaction occurring and NO_3^- were then quantitatively converted to NH_4^+, the isotopic composition of both product NH_4^+ should be equal to the reactant NO_3^- (i.e., $\delta^{15}N_{NO3} = \delta^{15}N_{NH4}$). Incomplete conversion, on the other hand, would result in the accumulation of lower $\delta^{15}N$ in the product pool (i.e., $\delta^{15}N_{NO3} > \delta^{15}N_{NH4}$). However, the sole isotope effect of DNRA could be impacted when denitrification is operating in tandem as denitrification will also increase $\delta^{15}N_{NO3}$ in the remaining NO_3^- pool making the apparent $\delta^{15}N_{NH4}$ from DNRA greater than what is expected from just DNRA alone. These microbial alterations of the NO_3^- and NH_4^+ in the subducting fluid prior to its reaching higher-temperature zones where abiotic reactions dominate possibly represent important early modifications to the N species and isotopic composition during hydrothermal circulation.

A previous study at the Cobb Segment along the Juan de Fuca Ridge (Bourbonnais et al., 2012b) noted the mismatch between vent NH_4^+ and its total N input (bottom seawater NO_3^- and DON) when assuming quantitative reduction of NO_3^- to NH_4^+ and attributed this discrepancy to unaccounted sink terms for NH_4^+. Here, we propose an alternate explanation for this mismatch where a series of reactions both biotic and abiotic might occur in different temperature regimes

of the recharge and reaction zones within the subduction arm of the hydrothermal circulation cell (Fig. 3). For example, some NO_3^- may be denitrified to N_2 early in the recharge zone, which consequently reduces the source of NO_3^- for any further reduction of NO_3^- to NH_4^+ either through DNRA or abiotic processes while also increasing $\delta^{15}N_{NO3}$ of this pool. This remaining NO_3^- pool may be then partially converted to NH_4^+, with a composition that is isotopically lower than the source NO_3^- as the result of isotopic fractionation during DNRA. We adopt a value for $^{15}\varepsilon_{DNRA}$ of 7.6‰ as the average value of two representative thermophilic DNRA bacteria (*Caminibacter mediatlanticus* and *Thermovibrio ammonificans*) incubated at their optimal growth temperatures of 55° and 75°C, respectively (Pérez-Rodríguez et al., 2017). At high temperature, any remaining NO_3^- should be reduced during reaction with reduced minerals (Brandes et al., 1998; 2008; Chapter 2). Notably, lab experiments showed that this particular reaction may yield both NH_4^+ and N_2 as products with reactions conducted at 250°C in NaCl solution at pH 4-5 resulting in $\delta^{15}N_{NH4}$ values similar to that of the starting $\delta^{15}N_{NO3}$ once the reaction reached completion (Chapter 2).

With this example framework in mind, the deviation of vent $\delta^{15}N_{NH4}$ from bottom seawater $\delta^{15}N_{NO3}$ should be set by the degree of early biological processes (denitrification and DNRA) and the ratio of NO_3^- consumption between these two processes. An earlier study at Axial Volcano (Bourbonnais et al., 2012b) indeed indicated similarity between average vent $\delta^{15}N_{NH4}$ (6.7‰) and the counterpart bottom seawater $\delta^{15}N_{NO3}$ (6.4‰), with the large deficit in vent [NH_4^+] proposed to occur through the quantitative conversion of NO_3^- to NH_4^+ (with no isotope fractionation) and the loss of some NH_4^+ during ion exchange with secondary mineral phases (with negligible isotope fractionation). Here we argue that the loss of NH_4^+ can also be attributed to denitrification before the seawater percolates into the hot reaction zone. As

demonstrated in Fig. 3, denitrification and DNRA can work together providing additional

isotopic imprint on the vent $\delta^{15}N_{NH4}$ values (see also Chapter 4).

The compiled $\delta^{15}N_{NH4}$ from unsedimented vent fields varied greatly, both within the

same site and between sites (Fig. 2b). Here we compare the vent $\delta^{15}N_{NH4}$ values to the global

average deep-water $\delta^{15}N_{NO3}$ (dashed line in Fig. 2b). It should be noted that the bottom seawater

NO_3^- might have different $\delta^{15}N_{NO3}$ from this global average. However, it seems that values of

vent $\delta^{15}N_{NH4}$, while exhibiting some variation, do not deviate far from source seawater NO_3^-

$\delta^{15}N$ values. One additional process that could impact the $\delta^{15}N_{NH4}$ is phase separation. Fluid

endmembers containing more vapor phase should inherit lower $\delta^{15}N_{NH4}$ values from the NH_3 in

the initial fluid as NH_3 volatilization occurs with large isotope fractionation. Little is known

however about the fractionation factor of NH_3 volatilization under high temperature and high

pressure conditions such as those existing subsurface in the deep-sea hydrothermal vents.

3.6.5 Sedimentary influence on vent NH_4^+

The hallmark of the sediment-covered hydrothermal systems is the enrichment in the

concentrations of NH_4^+, CH_4, K, Rb, Cs, B, I and Tl, and high alkalinity and pH as reported from

Guaymas Basin in the Gulf of California (e.g., Von Damm et al, 1985b, Campbell et al., 1988;

Reeves et al., 2014), Escabana Trough on the Gorda Ridge (e.g., Campbell et al., 1994), Middle

Valley on the Juan de Fuca Ridge (e.g., Butterfield et al., 1994a; Cruse and Seewald, 2006), and

Okinawa Trough (e.g., Miyazaki et al., 2017a). Additionally, there exist other vent fields that are

not covered by sediments but that have been regarded as systems with sedimentary influence.

Among these are the Main Endeavour Segment on the Juan de Fuca Ridge (e.g., Lilley et al.,

1993; Butterfield et al., 1994b; Seewald et al., 2003; Bourbonnais et al., 2012a) and Loki's

Castle on the Arctic Mid-Ocean Ridge (e.g., Baumberger et al., 2016a, 2016b; Pedersen et al., 2010). The correspondence between the concentrations of NH_4^+ and CH_4 in the endmember fluids from sedimented systems provides evidence for such sedimentary influence (Fig. 5) as both are mostly derived from alteration of sedimentary organic matter.

While the endmember NH_4^+ concentrations from a number of vent fields may vary appreciably (Fig 4a), their $\delta^{15}N$ values (Fig 4b) cluster more closely compared to the unsedimented counterparts (Fig 2b). The $\delta^{15}N$ valuesof Guaymas Basin vent NH_4^+ (+8.6 ± 0.6 ‰) does not differ significantly from that of sinking organic matter in this area (+9.4 ‰, Altabet et al., 1999). However, all available $\delta^{15}N_{NH4}$ values from the Main Endeavour Segment on the Juan de Fuca Ridge are significantly lower than those from the Guaymas Basin. This is not unexpected considering that the input of NO_3^- fueling primary production in the Gulf of California waters overlying the Guaymas Basin has significantly higher $\delta^{15}N_{NO3}$ due to nearby water-column denitrification (max $\delta^{15}N_{NO3} \sim +12$ ‰; Altabet et al., 1999) compared to that of the northeast Pacific around Juan de Fuca Ridge ($\delta^{15}N_{NO3}$ = +6.4 ‰, Bourbonnais et al., 2012a). In fact, $\delta^{15}N$ values of organic matter taken from sediment traps in the vicinity of this region are indeed lower (+5.9 ‰; Kienast et al., 2002), albeit not as low as some $\delta^{15}N_{NH4}$ values reported from the Juan de Fuca Ridge vents (Table 3)

Vent fluids from the Main Endeavour Field have been repeatedly investigated over multiple years. The earliest study on the NH_4^+ and its $\delta^{15}N_{NH4}$ was from Lilley et al., 1993 reporting on the samples taken in 1988 with a mean $\delta^{15}N_{NH4}$ of +12.4 ‰ (representing an average of two samples with $\delta^{15}N_{NH4}$ = +14.8‰ and +9.9‰; Lilley pers comm, 2018). Later study on the samples taken between 2007 and 2009 showed significantly lower $\delta^{15}N_{NH4}$ values (+3.5 ± 0.4 ‰; Bourbonnais et al., 2012a). Here, our average $\delta^{15}N_{NH4}$ from the crustal fluid

nearby (+2.6 ± 0.2 ‰, 2013-2014) is much closer to the samples taken in these more recent

years. While we can observe seasonal variations in the $\delta^{15}N$ in the sediment traps (e.g., Altabet et

al., 1999) and variations in the longer time scale of sediment core records (e.g., Kienast et al.,

2002), the small variations in the $\delta^{15}N_{NH4}$ from the Main Endeavour Field as reported in

Bourbonnais and colleagues (2012a) might suggest that the difference between the numbers from

2007-2009 and 1988 are a consequence of the 1999 earthquake swarm (Johnson et al., 2000).

There are reports of changes in fluid chemistry after this event affecting especially the Cl^-

concentrations (i.e., proxy for phase separation) and volatile species (e.g., Lilley et al., 2003;

Seewald et al., 2003; Seyfried et al., 2003). In fact, the post-event decrease in the CH_4 and NH_4^+

concentrations have been postulated to result from the lower contribution of sedimentary input to

the Main Endeavour Field (Seewald et al., 2003).

The degree of sedimentary influence varies greatly in submarine hydrothermal vents.

The presence of sediment cover provides the first line of evidence for such influence; this is

telling in Guaymas Basin and Okinawa Trough where $[NH_4^+]$ in the endmember fluids can be

greater than 10mM. On the other end of the spectrum are those systems with no observable

sediment cover but clearly exhibiting sedimentary influence such as Loki's Castle and the Main

Endeavour Field. The latter has the endmember fluids can be ranging from 0.35mM to 1.15mM.

Some other unsedimented systems have $[NH_4^+]$ greater than its N input from bottom seawater by

more than twice as much. Is this a manifestation of very slight influence of sedimentary input

(one that is even smaller than at Main Endeavour)?

At Sea Cliff where the NH_4^+ is about 2 times of the bottom seawater NO_3^- plus DON,

there is some evidence for minor sedimentary influence: its proximity to the sedimented

Escabana Trough (~200km north of the sediment-covered Escabana vent field) and its

surrounding area estimated to have ~50m-thick sediment cover (interpolated result from Ryan et al., 2009). Here, the high pH of the vent fluid for a system lacking observable sediment (4.5 at 25°C and in situ pH of 5.7) has been previously attributed to calcite dissolution (Von Damm et al., 2006). While this notion can help account for the higher pH and alkalinity of the Sea Cliff vent fluids, the elevated NH_4^+ concentrations were left unexplained. Interestingly, the low chlorinity fluid at Sea Cliff indicated phase separation and the likely presence of a heat source (either magma or hot rocks) underneath the subsurface flow path (Von Damm et al., 2006). To this end, we posit that the combination of proximity to a sediment source (though undocumented), the high in situ pH, and phase separation suggesta that Sea Cliff fluids having a higher vapor phase endmember may lead to the higher than expected NH_4^+ concentrations. However, with little ancillary information, especially CH_4 and its isotopic composition, this remains difficult to confirm.

3.6.6. Potential for N_2 reduction to NH_4^+ at Piccard

The world deepest vent field to date, Piccard, is another location where vent NH_4^+ concentrations are notably elevated relative to N input from bottom seawater, despite no evidence of sedimentary influence. Compared to the nearby vent field at Von Damm, Piccard has ~2.5 times as much NH_4^+. Interestingly, pH values at 25°C of the Piccard fluids are near neutral. Concentrations and bulk isotopic composition of CH_4 (δD_{CH4} and $\delta^{13}C_{CH4}$) in Piccard fluids do not indicate any sedimentary influence (Wang et al., 2008; McDermott, 2015), indicating that sediment organic matter cannot explain the elevation in NH_4^+. In this case, we suggest that the reduction of N_2 to NH_4^+ may provide a novel explanation. Though this particular reaction is not considered to typically occur under conditions typified elsewhere, there are at least two lines of

support for its possible role at Piccard. First, Piccard is located at depths between 4957m and 4987m, with fluid formation proposed at temperatures above 500°C (McDermott et al., 2018). Such extreme conditions make this system more thermodynamically poised for N_2 reduction, which has been demonstrated through lab experiments to occur at very high temperatures (Brandes et al, 1998). Indeed, thermodynamic prediction shows (Figure 6) that at the high-temperature and pressure conditions existing at Piccard, N speciation should be dominated by NH_3 and not N_2. Second, Piccard vent fluids contain exceptionally high concentrations of H_2. High H_2 reflects the highly reducing condition of the fluids, which also favor the reduction of N_2. To this end we posit that N_2 reduction to NH_3 occurs in the vapor phase deep in the reaction zone, with the high pH favoring partitioning of NH_3 into the vapor phase, then released into the venting Piccard fluids.

3.6.7. Variation in the isotope ratios at low temperatures

Variations within each vent field are most conspicuous at low temperatures as shown when the $\delta^{15}N_{NH4}$ from a wide range of temperatures are plotted (Fig. 7). Larger variations in $\delta^{15}N_{NH4}$ values are far more apparent at lower temperature end (<120°C). These deviations from the mean high-temperature isotopic composition are attributed to biological activity, including both NH_4^+-producing processes (such as DNRA or remineralization) and NH_4^+-consuming processes (such as nitrification, NH_4^+ assimilation, and anammox) and remineralization/decomposition of biomass; most of which are known to exhibit isotope fractionation. Arguably, the range of $\delta^{15}N_{NH4}$ values in the low temperature fluids from the unsedimented systems is much greater than its sedimented counterparts because the large difference in NH_4^+ concentrations in the two types of systems. With the high, mM-level

concentrations of the sedimented systems, any relatively small change in $[NH_4^+]$ from biological activity is swamped, making detectable changes in $\delta^{15}N_{NH4}$ values difficult or impossible. In contrast, similar changes in $[NH_4^+]$ occurring in unsedimented systems produce a larger relative contribution to the concentration change and thus, the isotopic composition. In this respect, the range in $\delta^{15}N_{NH4}$ values from the 9°50'EPR fluids (lowest concentrations amongst the four chosen sites) is the largest (16.8‰) as compared to Axial Volcano (9.2‰), Main Endeavour (3.7‰), or Guaymas Basin (3.8‰). Besides a large range of $\delta^{15}N_{NH4}$ values previously reported from Juan de Fuca Ridge (Bourbonnais et al., 2012b), the unsedimented Loihi vent field also showed a similar trend (16.7‰ range of $\delta^{15}N_{NH4}$ values) indicating active NH_4^+ consumption and possibly some contribution from N_2 fixation (Sylvan et al., 2017).

3.7. CONCLUSION

Deep-sea hydrothermal vent fluids can be rich in NH_4^+, especially when compared to bottom seawater supplying N in recharge zones of hydrothermal circulation. Concentrations can be as high as mM levels commonly found in sediment-covered vent fields or at μM levels as found in typical unsedimented systems - albeit with some notable exceptions as detailed above. While the source of NH_4^+ in the sedimented systems almost entirely derives from the sedimentary origin as indicated by the congruence in vent fluids $\delta^{15}N_{NH4}$ to the source $\delta^{15}N_{sediment}$, the production of NH_4^+ in unsedimented systems can be attributed and influenced by many more processes. While previous studies (Brandes et al., 1998; Bourbonais et al., 2012b) favored the notion that all bottom seawater NO_3^- (and potentially DON) should be quantitatively converted to NH_4^+, our lab experiments (Chapter 2) suggested that this should not always be the case and that some NO_3^- may be reduced to both NH_4^+ and N_2. This could explain why most

unsedimented systems exhibit vent fluid $[NH_4^+]$ lower than that of the bottom seawater $[NO_3^-]$. Furthermore, we posit that biological activity occurring in low-temperature recharge zones might be important in controlling $[NO_3^-]$ and thus ultimately the $[NH_4^+]$ in venting fluids as well as setting their $\delta^{15}N_{NH4}$ values. This, of course, does not exclude the potential contribution from other processes that have been suggested to operate in the subsurface and may be intricately linked to the production and consumption of NH_4^+ in vents including ion exchange with secondary minerals and/or N_2 reduction.

ACKNOWLEDGEMENTS
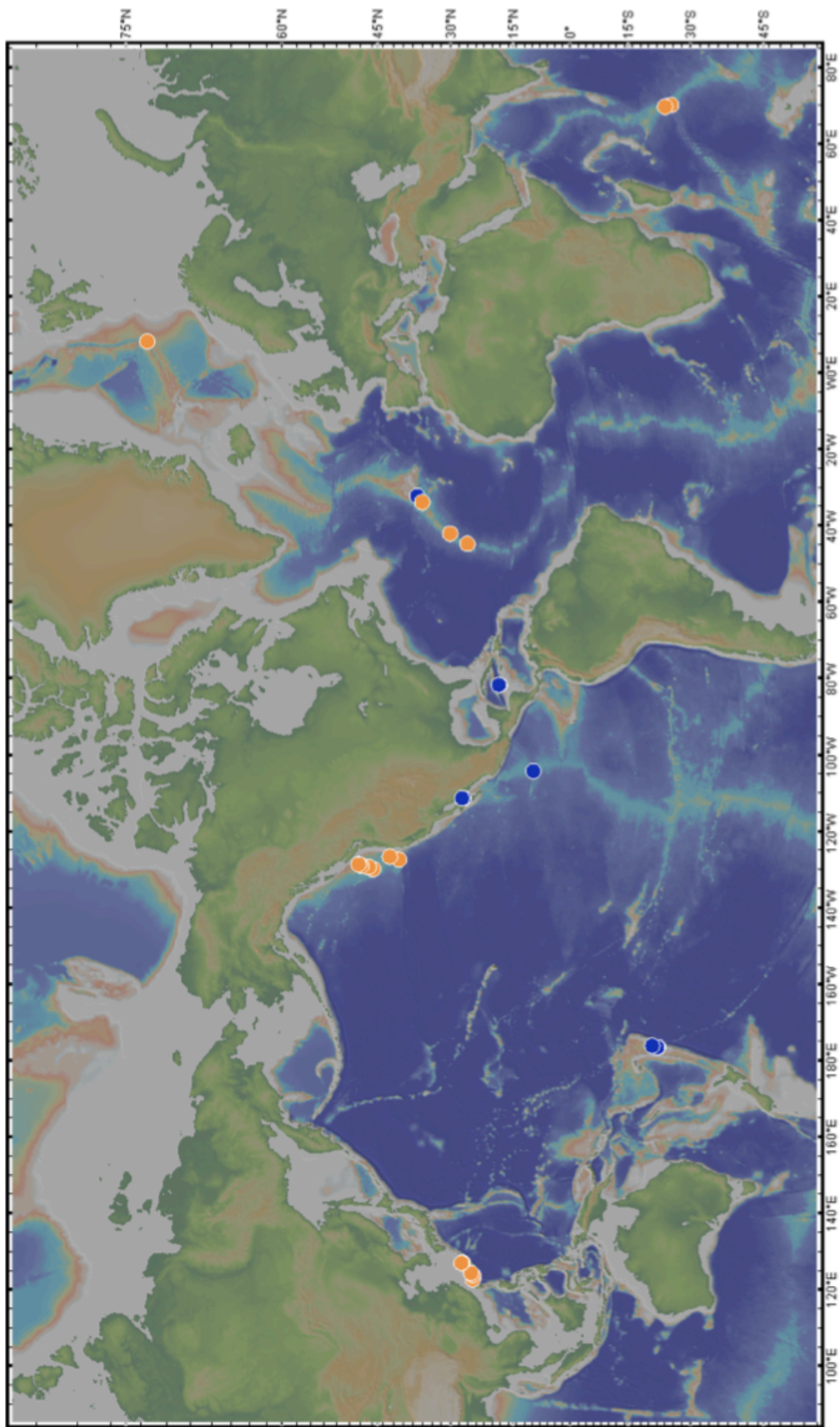
Figure 1. Map showing the locations of hydrothermal vent fields where fluid samples were taken. Samples analyzed in this study are shown in blue circles while those previously reported and compiled here are indicated in orange circles.

Table 1a. NH$_4^+$ (in mM), δ^{15}N$_{NH4}$, and other selected measurements for fluid samples taken from sedimented systems.

Vent field	Year	Vent site	Depth (m)	Sample	max T (°C)	pH at 25°C	[Mg^{2+}] (mm)	[Cl$^-$] (mm)	[NH$_4^+$] (mM)	δ^{15}N$_{NH4}$ (‰ vs air)
GUAYMAS BASIN										
Northern Trough		*BOTTOM SEAWATER*				~8	53.5	538	0	
	2017	*High temperature fluids*								
		Northern Trough Mound 1	1844	H1656-IGT7	331	4.77	3.3	625	5.5	8.30 (0.58, n=2)
		Endmember				*4.77*	*0.0*	*631*	*5.9*	
		Northern Trough Mound 2	1789	H1650-IGT4	309	5.24	22.1	590	4.7	8.40 (0.57, n=2)
		Northern Trough Mound 2	1789	H1650-IGT7	300	5.24	14.1	605	6.3	9.02 (0.90, n=2)
		Endmember				*5.24*	*0.0*	*628*	*8.3*	
		Low temperature fluids								
		Northern Trough Mound 1 (Low T)	1844	H1656-IGT6	64	5.52	46.9	504	1.4	6.34 (0.45, n=2)
		Ring Vent	1727	H1651-IGT2	78	6.63	27.9	559	10.6	10.05 (1.07, n=2)
		Ring Vent	1727	H1651-IGT6	78	6.60	14.4	565	15.6	10.10 (1.00, n=2)
		Ring Vent	1727	H1654-IGT2	79	6.53	23.7	560	8.1	9.43 (0.02, n=2)
		Ring Vent	1727	H1654-IGT7	80	6.57	14.1	562	10.9	9.33 (0.21, n=2)
Southern Trough	2008	*High temperature fluids*								
		Theme Park	2017	A4457-IGT5	232	5.73	37.9	543	4.1	
		Theme Park	2017	A4457-IGT6	215	6.61	53.1	540	0.1	
		Theme Park	2014	A4458-IGT1	249	5.78	3.5	598	12.3	8.71 (0.56, n=2)
		Theme Park	2016	A4458-IGT8	251	5.73	31.9	564	5.2	8.75 (0.40, n=4)
		Endmember				*<5.73*	*0.0*	*599*	*13.2*	
		Cathedral Hill	2011	A4459-IGT5	172	5.73	41.0	555	2.8	9.27 (0.18, n=4)
		Endmember				*<5.73*	*0.0*	*611*	*11.8*	
		Sulfide Spires	2015	A4461-IGT5	204	5.75	12.9	588	10.5	8.48 (0.25, n=2)
		Sulfide Spires	2015	A4461-IGT8	218	4.48	32.3	567	5.4	9.14 (0.33, n=4)
		Endmember				*<4.48*	*0.0*	*605*	*13.8*	
		Rebecca's Roost	1990	A4462-IGT1	299	6.14	3.1	597	14.6	9.48 (0.24, n=2)
		Rebecca's Roost	1990	A4462-IGT4	298	6.09	5.6	592	13.8	8.03 (0.24, n=2)
		Endmember				*6.09*	*0.0*	*600*	*15.5*	
		Toadstool	1995	A4462-IGT5	288	6.13	11.3	583	12.7	7.89 (0.09, n=2)
		Toadstool	1995	A4462-IGT6	278	6.09	2.4	595	15.2	7.53 (0.30, n=2)
		Endmember				*6.09*	*0.0*	*597*	*16.0*	

Table 1b. NH_4^+ (in μM), $\delta^{15}N_{NH4}$, and other selected measurements for fluid samples taken from unsedimented systems.

Vent field	Year	Vent site	Depth (m)	Sample	max T (°C)	pH at 25°C	$[Mg^{2+}]$ (mm)	$[Cl^-]$ (mm)	$[NH_4^+]$ (μM)	$\delta^{15}N_{NH4}$ (‰ vs air)
EAST PACIFIC RISE (EPR)										
9°50' N EPR										
BOTTOM SEAWATER					~8		53.5	538	0	0
	2017	*High temperature fluids*								
Tica (Alvinella Cupcake)			2511	A4895-Green1	190	5.39	35.5	443	3.8	
Tica (Alvinella Cupcake)			2511	A4895-Green1	190	5.39	36.0	443	2.4	
Tica (Alvinella Cupcake)			2511	A4898-Yellow1	196	4.56	23.0	341	2.3	
Tica (Alvinella Cupcake)			2511	A4898-Yellow2	196	4.75	27.0	394	3.2	6.91 (0.99, n=2)
Tica (Alvinella Mound)			2511	A4896-Black1	300	5.05	41.5	487	4.8	6.29 (n=1)
Tica (Alvinella Mound)			2511	A4896-Black1	300	5.05	41.8	491	2.2	
Tica (Alvinella Mound)			2511	A4896-Black2	300	5.91	42.5	492	2.1	
Tica (Alvinella Mound)			2511	A4896-Black2	300	5.91	51.3	549	1.9	
		Endmember				<4.56	0.0	236	7.1	
Biovent			2499	A4901-Red1	316	4.35	3.8	394	3.2	7.86 (0.12, n=2)
Biovent			2499	A4901-Black1	320	4.57	3.5	397	4.6	7.39 (0.60, n=5)
Biovent			2499	A4901-Black2	320	4.06	3.9	396	4.4	
		Endmember				4.06	0.0	385	4.4	
P-vent			2506	A4896-Red1	350	3.37	4.8	318	3.4	
P-vent			2506	A4896-Red2	350	3.70	4.2	324	4.9	
		Endmember				3.37	0.0	302	4.5	
Bio9			2503	A4898-Red1	364	3.59	5.8	256	5.3	7.93 (1.07, n=2)
Bio9			2503	A4898-Red2	364	3.63	6.0	266	5.8	8.80 (0.21, n=2)
Bio9			2503	A4895-Blue1	368	4.05	5.2	287	5.3	5.89 (1.63, n=2)
Bio9			2503	A4895-Blue1	368	4.05	5.2	285	3.8	5.48 (0.43, n=3)
Bio9			2503	A4895-Blue2	368	3.44	4.3	285	5.1	7.00 (0.25, n=2)
		Endmember				3.44	0.0	247	5.6	
		Low temperature fluids								
Teddy Bear			2514	A4898-Green1	13	6.10	51.0	544	6.6	13.86 (0.78, n=2)
Teddy Bear			2514	A4898-Green2	13	6.07	48.4	509	4.8	16.54 (0.8, n=2)
Teddy Bear			2514	A4903-Red2	12	5.75	51.1	541	2.9	
Crab Spa			2503	A4893-Green1	25	5.81	39.3	430	9.5	0.60 (0.02, n=2)
Crab Spa			2503	A4893-White2	25	5.81	36.3	393	9.6	-0.30 (0.27, n=2)
Crab Spa			2503	A4896-Yellow1	24	5.80	50.7	534	6.8	7.05 (n=1)
Crab Spa			2503	A4902-Yellow2	26	5.93	49.8	526	6.1	2.62 (0.71, n=6)
Tica Low T			2511	A4902-Red1	26	6.14	50.8	540	1.7	
Tica Low T			2511	A4902-Red2	26	5.75	42.0	491	1.3	
Tica Low T			2511	A4902-Black2	39	5.26	43.3	496	2.6	
M-vent			2500	A4898-Blue1	27	5.30	44.7	546	2.5	
M-vent			2500	A4898-Blue2	27	5.33	45.7	552	4.5	
Q-vent			2509	A4898-Black1	95	4.81	38.1	566	1.8	
Q-vent			2509	A4898-Black2	95	5.33	42.5	556	6.0	

Table 1b. (cont.)

Vent field	Year	Vent site	Depth (m)	Sample	max T (°C)	pH at 25°C	[Mg^{2+}] (mm)	[Cl$^-$] (mm)	[NH$_4^+$] (μM)	δ^{15}N$_{NH4}$ (‰ vs air)
		BOTTOM SEAWATER				~7.7	53.6	534	0	0
EAST LAU SPREADING CENTER										
ABE	2015	*High temperature fluids*								
		ABE (north), A13	2141	J2-815-IGT7	283	4.99	12.8	541	1.0	
		ABE (north), A13	2141	J2-815-IGT8	283	4.33	2.3	540	1.7	
		Endmember				*4.33*	*0.0*	*551*	*1.7*	
		ABE (north), A14	2139	J2-815-IGT1	288	5.14	16.8	538	1.2	
		ABE (north), A14	2139	J2-815-IGT3	300	4.00	1.9	539	1.3	
		Endmember				*4.00*	*0.0*	*550*	*1.5*	
		ABE (central), A15	2153	J2-815-IGT2	290	4.90	8.1	550	1.0	
		ABE (central), A15	2153	J2-815-IGT4	279	4.42	1.9	552	1.9	
		Endmember				*4.42*	*0.0*	*559*	*1.9*	
		ABE (central), A16	2141	J2-815-IGT6	263	4.54	1.7	553	1.4	
		Endmember				*4.54*	*0.0*	*556*	*1.4*	
Mariner	2015	*High temperature fluids*								
		Mariner (Toilet Bowl), MA13	1916	J2-816-IGT5	140	2.60	20.4	547	0.9	
		Mariner (Toilet Bowl), MA13	1913	J2-816-IGT6	78	2.57	18.1	548	1.3	
		Endmember				*<2.57*	*0.0*	*590*	*1.8*	
		Mariner, MA14	1909	J2-817-IGT5	318	2.38	2.6	578	0.9	
		Mariner, MA14	1909	J2-817-IGT6	319	2.33	2.8	578	1.2	
		Endmember				*2.33*	*0.0*	*584*	*1.2*	
		Mariner, MA15	1913	J2-817-IGT2	354	2.97	12.7	564	0.7	
		Endmember				*<2.97*	*0.0*	*593*	*0.9*	
		Mariner, MA16	1912	J2-817-IGT1	363	2.76	6.8	588	1.1	
		Endmember				*2.76*	*0.0*	*605*	*1.3*	
Vai Lili	2015	*High temperature fluids*								
		Vai Lili, VL4	1707	J2-817-IGT3	109	5.19	28.1	562	1.0	
		Vai Lili, VL4	1707	J2-817-IGT7	116	5.23	29.3	561	1.4	
		Endmember				*<5.19*	*0.0*	*665*	*2.5*	
Tui Malila	2015	*High temperature fluids*								
		Tui Malila, TM15	1898	J2-819-IGT2	269	4.96	22.0	600	1.1	
		Endmember				*<4.96*	*0.0*	*689*	*1.8*	
		Tui Malila, TM16	1893	J2-819-IGT7	242	4.21	6.7	609	1.5	
		Tui Malila, TM16	1893	J2-819-IGT3	251	3.91	5.5	620	1.2	
		Endmember				*3.91*	*0.0*	*633*	*1.5*	
		Tui Malila, TM18	1846	J2-819-IGT7B	296	4.60	10.4	620	1.5	
		Tui Malila, TM18	1846	J2-819-IGT2B	232	5.40	36.9	569	0.6	
		Endmember				*<4.60*	*0.0*	*670*	*1.8*	

Table 1b. (cont.)

Vent field	Year	Vent site	Depth (m)	Sample	max T (°C)	pH at 25°C	[Mg²⁺] (mm)	[Cl⁻] (mm)	[NH₄⁺] (µM)	$\delta^{15}N_{NH4}$ (‰ vs air)
MID-ATLANTIC RIDGE		*BOTTOM SEAWATER*				*~8*	*52.5*	*547*	*0*	
Lucky Strike	2008	*High temperature fluids*								
		Medea Vent	1648	J2-359-CGT-Y	270	3.81	3.8	553	5.6	7.49 (0.08, n=2)
		Endmember				*3.81*	*0.0*	*554*	*6.0*	
		2608 Spire, top	1719	J2-356-IGT4	324	4.25	1.9		4.8	7.69 (0.75, n=2)
		Endmember				*4.25*	*0.0*		*5.0*	
MID-CAYMAN RISE		*BOTTOM SEAWATER*				*~8*	*52.4*	*545*	*0*	
Piccard	2013									
		Beebe Vent 5	4495	N58-IGT7	398	5.09	43.0	499	10.2	5.58 (0.67, n=2)
		Beebe Vent 5	4495	N58-IGT8	398	3.18	1.5	358	44.0	4.71 (0.44, n=3)
		Endmember				*3.18*	*0.0*	*351*	*45.6*	
Von Damm	2013									
		East Summit	2293	N55-IGT4	215	6.50	39.9	571	7.2	4.13 (0.00, n=2)
		East Summit	2293	N56-IGT6	215	6.32	33.3	581	7.4	6.07 (0.46, n=4)
		Endmember				*<6.32*	*0.0*	*647*	*23.0*	
		Bartizan	~2400	N61-IGT4	147	6.04	24.6	601	11.3	6.32 (0.26, n=2)
		Bartizan	~2400	N61-IGT6	147	5.84	16.5	617	11.7	5.39 (0.04, n=2)
		Endmember				*<5.84*	*0.0*	*650*	*18.6*	
		Twin Peaks	2372	N60-IGT7	138	5.73	13.8	623	16.3	5.05 (0.06, n=2)
		Twin Peaks	2372	N60-IGT8	138	6.06	22.4	606	12.9	4.62 (0.24, n=2)
		Endmember				*<5.73*	*0.0*	*651*	*22.3*	

Table 2. Chemical compositions and N isotopic composition of basement fluids collected from CORK-1362A and CORK-1362B.

Year	Borehole	Sample Name	msb[a] (m)	T (°C)	pH at 25°C	[Mg²⁺] (mM)	[SO₄²⁻] (mM)	[K⁺] (mM)	[Cl⁻] (mM)	[TDN] (µM)	[NO₃] (µM)	[NH₄⁺] (µM)	δ¹⁵N$_{NH4}$ (‰ vs air)[d]
	Bottom seawater			2[b]	7.7[c]	53.7[c]	28.4[c]	10.2[c]	541[c]	44[c]	40.8[c]	>0.05[c]	
2013	U1362A	1362A#1	200	65	7.3	2.5	18.4	6.5	547	N.A.	0.1	N.A.	2.59 (0.01, n=2)
		1362A#2	200	65	7.3	2.5	18.1	6.4	542	N.A.	0.1	N.A.	2.44 (0.31, n=2)
		1362A#13	70	65	7.3	4.7	18.2	6.5	546	N.A.	0.3	N.A.	2.39 (0.21, n=2)
		1362A1#14	70	65	7.3	4.4	18.4	6.5	548	N.A.	0.4	N.A.	2.25 (0.30, n=2)
		Endmember			**7.3**	**1.9**	**18.0**	**6.4**	**546**		**0.0**		
	U1362B	1362B#2	40	65	7.3	2.5	18.2	6.4	548	N.A.	0.2	N.A.	2.27 (0.18, n=2)
		1362B#7	40	65	7.3	2.7	18.4	6.4	546	106	0.3	106	2.55 (0.21, n=2)
		1362B#8	40	65	7.3	2.5	18.2	6.3	546	N.A.	0.1	N.A	2.45 (0.31, n=2)
		Endmember			**7.3**	**1.9**	**18.1**	**6.3**	**547**	**111**	**0.0**	**111**	
2014	U1362A	1362A-MVBS 3	70	65	7.3	2.3	18.2	6.5	547	109	0.1	109	2.66 (0.03, n=2)
		1362A-MVBS 4	70	65	7.3	2.2	18.2	6.5	547	112	0.1	112	2.69 (0.08, n=2)
		1362A-MVBS 5	200	65	7.3	2.2	18.2	6.4	549	110	0.0	110	2.71 (0.08, n=2)
		1362A-MVBS 6	200	65	7.3	2.2	18.2	6.4	549	111	0.1	111	2.85 (0.31, n=2)
		1362A-LVBS 7	200	65	7.3	2.2	18.3	6.4	549	110	0.0	110	2.69 (0.01, n=2)
		Endmember			**7.3**	**1.9**	**18.2**	**6.4**	**548**	**115**	**0.0**	**115**	
	U1362B	1362B-MVBS-3	40	65	7.3	2.3	18.0	6.3	547	112	0.1	112	2.84 (0.09, n=2)
		1362B-MVBS-4	40	65	7.3	2.4	18.1	6.4	547	112	0.3	112	2.98 (0.11, n=2)
		1362B-MVBS-5	40	65	7.3	2.5	18.1	6.4	547	112	0.3	112	2.77 (0.06, n=2)
		1362B-MVBS-6	40	65	7.3	2.3	18.1	6.4	547	112	0.1	112	2.80 (n=1)
		1362B-LVBS-7	40	65	7.3	2.5	18.1	6.4	547	110	0.3	110	2.82 (0.04, n=2)
		Endmember			**7.3**	**1.9**	**18.0**	**6.3**	**547**	**117**	**0.0**	**117**	

Notes:

[a] meter below basement

[b] Average bottom seawater temperature around Main Endeavour Segment of Juan de Fuca Ridge collected in 2004-2009 (Bourbonnais et al., 2012)

[c] Average chemical composition for bottom seawater around the bore holes during 2008-2010 (Lin et al., 2012)

[d] Average δ¹⁵N$_{NH4}$ value (range, number of samples analyzed)

Table 3a. Endmember fluid concentrations and N isotopic composition of fluid samples from sedimented systems.

REGION/Vent field	Vent name	Depth (m)	Year	max T (°C)	pH at 25°C	[Cl] (mm)	[NH₄⁺] (mM)	δ¹⁵N_NH4 (‰ vs air)	[H₂] (mM)	[CH₄] (mM)	Reference
MID-OKINAWA TROUGH											
Sakai	pNoho	1600		331	5.40	678	7.60		0.35	3.2	Miyazaki et al., 2017a, 2017b
Izena Cauldron	CLAM	~1400	1989	>220	5.40		12.40				Sakai et al., 1990
	Hakurei			326	4.70	608	4.40		1.4	6.8	Miyazaki et al., 2017; Ishibashi et al., 2014
Iheya Ridge	JADE	~1400	1989	320	4.70		5.30				Sakai et al., 1990
	Aki	1101		316	4.45	594	1.97		0.03	0.4-0.9	Miyazaki et al., 2017;
S OKINAWA TROUGH											
Yokosuka	Hohenschwangau	2182		364	5.40	153	7.90		9.43	9.6	Miyazaki et al., 2017a
Daiyon Yonaguni	Lion	1385		328	5.70	614	14.70		0.8-5.5	1.2-13.5	Miyazaki et al., 2017a; Suzuki et al. 2008
Hatoma	C2			325	5.40	303	7.42		1.2	10	Miyazaki et al., 2017a; Toki et al., 2016
MIDDLE VALLEY, JUAN DE FUCA RIDGE											
Dead Dog	Site 858		1990	276	5.50	578	2.80				Butterfield et al., 1994
	H'Ken Hollow		2000	187		583	3.18		1.9	22.6	Cruse and Seewald, 2006
	Chowder Hill		2000	281		575	3.16		2.6	20.3	Cruse and Seewald, 2006
	Inspired Mounds		2000	261		546	2.87		2.3	21.6	Cruse and Seewald, 2006
	Puppy Dog		2000	202		586	2.99		2	18.5	Cruse and Seewald, 2006
ODP Mound	1035F		2000			448	1.26		2.1	2.99	Cruse and Seewald, 2006
	Shiner Bock		2000	272		434	2.34		8.2	7.07	Cruse and Seewald, 2006
	Spire		2000	263		432	2.27		2.2	6.71	Cruse and Seewald, 2006
	1035H		2000	267		449	2.10		6.1	5.85	Cruse and Seewald, 2006
ENDEAVOUR SEGMENT, JUAN DE FUCA RIDGE											
Sasquatch	Christmas Tree		2008	275	5.39		1.11	3.61			Bourbonnais et al., 2012a
	DK3/Flamingo		2008	277	4.79		1.15	3.83			Bourbonnais et al., 2012a
	Hobo (Marker C)		2008	285	4.77		1.12	4.76			Bourbonnais et al., 2012a
High Rise	Baltic		2009	333	4.15		0.89	4.72; 3.60			Bourbonnais et al., 2012a
	Boardwalk		2008	333	3.88		0.90	3.74			Bourbonnais et al., 2012a
	Boardwalk		2009	339	4.02		0.81	4.40			Bourbonnais et al., 2012a
	Fairy Castle		2009	314	4.46		0.67	4.51			Bourbonnais et al., 2012a
	Godzilla		2008	345	3.90		0.92	3.69			Bourbonnais et al., 2012a
	Godzilla		2009	349	4.15		1.09	3.42			Bourbonnais et al., 2012a
	Park Place		2008	331	4.11		0.79	4.08			Bourbonnais et al., 2012a
	Park Place		2009	332	3.98		1.06	4.53; 4.73; 4.54			Bourbonnais et al., 2012a
Main Endeavour	(combined)		1990?				0.64-0.95		0.16-0.42	1.8-3.4	Lilley et al. 1993; Lilley pers comm. 2018
	Bastille		1999	368		207	0.60		0.62	1.7	Seewald et al. 2003
	Bastille		2007	269	3.94		0.39	3.05			Bourbonnais et al., 2012a
	Bastille		2008	303	4.01		0.51	3.69			Bourbonnais et al., 2012a
	Bastille		2009	317	4.03		0.52	3.48			Bourbonnais et al., 2012a
	Cantilever		1999	375		390	0.65		0.7	1.7	Seewald et al. 2003
	Cathedral		2008	123	5.44		0.35	3.44			Bourbonnais et al., 2012a
	Crypto		1984-1988	351	4.50	479	0.51				Butterfield et al. 1994
	Crypto		2008	328	4.48		0.50	3.12			Bourbonnais et al., 2012a
	Dante		1988	370	4.40	457	0.58				Butterfield et al. 1994
	Dante		1999	350		419	0.53		0.52		Seewald et al. 2003; Ding et al. 2001
	Dante		2000	341		461	0.44		0.29	1.4	Seewald et al. 2003
	Dante		2007	332	4.40		0.46	3.29			Bourbonnais et al., 2012a
	Dante		2008	337	4.31		0.44	3.36			Bourbonnais et al., 2012a
	Dante		2009	336	4.47		0.51	3.47			Bourbonnais et al., 2012a
	Dudley		1988			349					Butterfield et al. 1994
	Dudley		2006	300	5.59			3.05			Bourbonnais et al., 2012a
	Dudley		2008	319	4.60		0.47	3.63			Bourbonnais et al., 2012a
	Grotto		2008	320	4.41		0.46	3.67			Bourbonnais et al., 2012a
	Grotto		2009	319	4.48		0.46	3.77			Bourbonnais et al., 2012a
	Grotto		1984-1988	357	4.20	425	0.63				Butterfield et al. 1994
	Hulk		1988	353	4.50	505	0.50				Butterfield et al. 1994
	Hulk		1999	347		426	0.50		0.33	1.6	Seewald et al. 2003
	Hulk		2000	120		477	0.45		0.23	1.5	Seewald et al. 2003
	Hulk		2007	324	4.51		0.49	2.96			Bourbonnais et al., 2012a
	Hulk		2008	324	4.43		0.49	3.74			Bourbonnais et al., 2012a
	Hulk		2009	299	4.18		0.47	3.13			Bourbonnais et al., 2012a
	LOBO		1984-1988	346	4.25	428	0.56				Butterfield et al. 1994
	LOBO		2000	342		452	0.43		0.29	1.4	Seewald et al. 2003
	LOBO		2008	320	4.56		0.44	3.40			Bourbonnais et al., 2012a
	LOBO		2009	165	5.53		0.49	3.61			Bourbonnais et al., 2012a
	North		1984-1988	356	4.50	477					Butterfield et al. 1994
	Peanut		1988	350		253	0.58				Butterfield et al. 1994
	Peanut		2000	382		347	0.43		0.47	1.3	Seewald et al. 2003
	Puffer		2008	252	4.09		0.35	4.39			Bourbonnais et al., 2012a

Table 3a. (cont.)

| REGION/Vent field	Vent name	Depth (m)	Year	max T (°C)	pH at 25°C	[Cl] (mm)	[NH₄⁺] (mM)	$\delta^{15}N_{NH4}$ (‰ vs air)	[H₂] (mM)	[CH₄] (mM)	Reference
ENDEAVOUR SEGMENT, JUAN DE FUCA RIDGE (CONT.)											
Main Endeavour	S&M		1988			334					Butterfield et al. 1994
(cont.)	S&M		2000	367		373	0.45		0.54	1.7	Seewald et al. 2003
	S&M		2006	281	5.31			3.96			Bourbonnais et al., 2012a
	S&M		2007	321	4.41		0.48	3.01			Bourbonnais et al., 2012a
	S&M		2008	322	4.41		0.53				Bourbonnais et al., 2012a
	S&M		2008	210	4.99		0.46	3.86			Bourbonnais et al., 2012a
	Salut		2008	267	4.40		0.41	4.08			Bourbonnais et al., 2012a
	Sully		1999	379		310	0.67		0.96	1.7	Seewald et al. 2003
	Sully		2008	257	4.27		0.47	4.19			Bourbonnais et al., 2012a
	TP		1988	362		448					Butterfield et al. 1994
Mothra	Cauldron		2008	291	4.71		0.43	3.05			Bourbonnais et al., 2012a
	Crab Basin		2008	244	4.65		0.41	3.24			Bourbonnais et al., 2012a
	Cuchalainn		2008	293	4.61		0.42	3.41			Bourbonnais et al., 2012a
	Hot Harold		2008	305	4.55		0.44	2.83			Bourbonnais et al., 2012a
	Stonehenge		2008	306	4.57		0.42	2.71			Bourbonnais et al., 2012a
ESCABANA TROUGH, GORDA RIDGE											
Escabana	(combined)		1988	108-217	5.40	668	5.60				Campbell et al. 1994
GUAYMAS BASIN											
Northern Trough	Mound 1	1844	2017	331	4.77	631	5.90	8.30	4.69	17.924	
	Mound 2	1789	2017	309	5.24	628	8.30	8.40; 9.02	3.21	14.938	
Southern Trough	Marker 1		1982		5.90	601	15.60				Von Damm et al., 1985b
	Marker 2		1982		5.90	589	15.30				Von Damm et al., 1985b
	Marker 3		1982		5.90	637	10.30				Von Damm et al., 1985b
	East Hill (Marker 4)		1982		5.90	599	12.90				Von Damm et al., 1985b
	East Hill (Marker 4)		1985		5.90	603	13.00				Campbell et al., 1988
	Marker 5		1982		5.90	599	14.50				Von Damm et al., 1985b
	Marker 6		1982		5.90	582	14.50				Von Damm et al., 1985b
	Marker 7		1982		5.90	606	15.20				Von Damm et al., 1985b
	Marker 9		1982		5.90	581	10.70				Von Damm et al., 1985b
	South Field		1985		5.90	580	15.30				Campbell et al., 1988
	Theme Park	2017	2008	251	<5.73	599	13.20	8.71; 8.75	0.54	44.7	Reeves et al., 2014; this study
	Cathedral Hill	2011	2008	172	<5.73	611	11.80	9.27	0.5	44.2	Reeves et al., 2014; this study
	Sulfide Spire	2015	2008	218	<4.48	605	13.80	8.48; 9.14	0.6	44.4	Reeves et al., 2014; this study
	Rebecca's Roost	1990	2008	298	6.09	600	15.50	9.48; 8.03	2.7	63.5	Reeves et al., 2014; this study
	Toadstool	1995	2008	288	6.09	597	16.00	7.89; 7.53	3.3	58.8	Reeves et al., 2014; this study
LOKI'S CASTLE											
	João		2010		5.56	519	5.63				Baumberger et al., 2016; Pedersen et al., 2010
	João		2009	>280	<6.56	471	5.10		4.6	12.6	Baumberger et al., 2016
	João		2008	306	5.52	502			4.8	13.7	Baumberger et al., 2016; Pedersen et al., 2010
	Menorah		2009	315	5.87	492	4.90		4.7	12.5	Baumberger et al., 2016
	Menorah		2008	310	5.52	500			5.0	13.3	Baumberger et al., 2016; Pedersen et al., 2010
	Camel		2010	305	5.62	589	6.13				Baumberger et al., 2016; Pedersen et al., 2010
	Camel		2009	315	5.77	478	5.76		4.8	13.5	Baumberger et al., 2016; Pedersen et al., 2010
	Camel		2008	317	5.5	496			4.9	15.1	Baumberger et al., 2016; Pedersen et al., 2010
	Sleepy		2009	312	5.9	475	4.52		5.5	15.6	Baumberger et al., 2016; Pedersen et al., 2010

Note: Endeavour Segment and Loki's Castle are not sediment covered but have been reported to reflect the influence of sediments.

Table 3b. Endmember fluid concentrations and N isotopic composition of samples from unsedimented systems.

REGION/Vent field	Vent site	Depth (m)	Year	max T (°C)	pH at 25°C	[Cl⁻] (mm)	[NH₄⁺] (μM)	δ¹⁵N_NH4 (‰ vs air)	[H₂] (mM)	[CH₄] (mM)	Reference
COBB SEGMENT, JUAN DE FUCA RIDGE											
Cobb	Hogwarts (Harry)		2007	205	4.38		47.5	4.21			Bourbonnais et al., 2012a
	Not Dead Yet		2007	167	<5.18		47.5	3.99; 4.17			Bourbonnais et al., 2012a
AXIAL VOLCANO, JUAN DE FUCA RIDGE											
'98 Lava Flow	Forum		2007	256	4.43		19.2	8.02			Bourbonnais et al., 2012a
ASHES	Hell		2004	176	3.74		16.7				Bourbonnais et al., 2012a
	Hell		2007	253	3.89		19.8	6.61			Bourbonnais et al., 2012a
	Hell		2008	282	3.77		14.9	7.31			Bourbonnais et al., 2012a
	Inferno		2006	264	3.65		17.9	5.74			Bourbonnais et al., 2012a
	Inferno		2007	313	3.33		16.2	7.35			Bourbonnais et al., 2012a
	Inferno		2008	318	3.60		14.2	7.85			Bourbonnais et al., 2012a
	Mushroom		2007	256			33.1	6.03			Bourbonnais et al., 2012a
	Phoenix		2007	284	3.53		19.5	5.40			Bourbonnais et al., 2012a
	Virgin Mount		2004	170	4.57		18.7				Bourbonnais et al., 2012a
	Virgin Mount		2006	247	4.56		15.6	5.07			Bourbonnais et al., 2012a
	Virgin Mount		2007	251	4.33		12.1	7.85			Bourbonnais et al., 2012a
	Virgin Mount		2008	232	4.56		15.7				Bourbonnais et al., 2012a
CASM	T&S		2007	305	3.88		27.7	6.79			Bourbonnais et al., 2012a
Coquile	Casper		2006	290	4.98		16.0				Bourbonnais et al., 2012a
	Casper		2007	301	3.94		14.6	7.47			Bourbonnais et al., 2012a
	Casper		2008	303	3.95		12.0				Bourbonnais et al., 2012a
	Vixen		2004	192	3.96		13.1				Bourbonnais et al., 2012a
	Vixen		2007	329	3.90		17.6	7.28			Bourbonnais et al., 2012a
	Vixen		2008	334	3.95		13.1				Bourbonnais et al., 2012a
International District	Castle		2007	237	4.27		14.5	6.78			Bourbonnais et al., 2012a
	El Guapo		2006	312	4.50		13.2				Bourbonnais et al., 2012a
	El Guapo		2007	319	3.71		15.5	6.67			Bourbonnais et al., 2012a
	El Guapo		2008	314	3.85		17.1	5.01			Bourbonnais et al., 2012a
	El Guapo		2009	289	3.54		13.0	7.49			Bourbonnais et al., 2012a
SEA CLIFF, GORDA RIDGE											
	Marker Y		2000	304	4.73	456	86.0				Von Damm et al., 2006
	Marker M		2000	305	<4.84	450	84.0				Von Damm et al., 2006
	Marker T		2000	305	4.59	456	94.0				Von Damm et al., 2006
	Marker Y		2002	>308	<4.50	462	88.0				Von Damm et al., 2006
	Marker M		2002	301	4.57	460	80.0				Von Damm et al., 2006
	Marker C		2002	302	4.54	462	83.0				Von Damm et al., 2006
	Makrer U		2002	303	4.55	458	77.0				Von Damm et al., 2006
	Marker L		2002	294	4.52	461	79.0				Von Damm et al., 2006
9°50' N EAST PACIFIC RISE											
	Tica	2511	2017	300	<4.56	236	7.1	6.91; 6.29			This study
	Biovent	2499	2017	320	4.06	385	4.4	7.86; 7.39			This study
	P-vent	2506	2017	350	3.37	302	4.5				This study
	Bio9	2503	2017	368	3.44	247	5.6	7.93; 8.80; 5.89; 5.48; 7.00			This study
MID-CAYMAN RISE											
Piccard	Beebe Vent 5		2013	398	3.18	351	45.6	4.71; 5.58			This study
Von Damm	East Summit		2013	215	<6.32	647	23.0	4.13; 6.07			This study
	Bartizan		2013	147	<5.84	650	18.6	5.39; 6.32			This study
	Twin Peaks		2013	138	<5.73	651	22.3	4.62; 5.05			This study
MID-ATLANTIC RIDGE											
Lucky Strike	Medea Vent		2008	270	3.18	554	6.0	7.49	0.063	0.89	This study; Reeves et al., 2014
	2608 Spire, top		2008	324	4.25		5.0	7.69			This study; Reeves et al., 2014
	Isabel		2008	292	3.81	487	6.2		0.034	0.86	Reeves et al., 2014
	US4		2008	299	3.89	414	9.3		0.053	0.74	Reeves et al., 2014
	Crystal		2008	308	4.43	538	16.0		0.041	0.82	Reeves et al., 2014
Rainbow	PP27		2008	350	3.35	758	2.7		12.3	2.01	Reeves et al., 2014
	Stylo 1		2008	367	3.31	765	2.3		16.1	2.10	Reeves et al., 2014
	CMSP&P		2008	365	3.36	766	2.2		15.9	2.05	Reeves et al., 2014
	Stylo 2 (X11)		2008	364	3.12	763	2.4		16.5	2.10	Reeves et al., 2014
Lost City	Poseidon Beehive		2008	94	10.20		3.5		10.4	1.08	Reeves et al., 2014
	Marker 6		2008	96	10.50		3.5		10.5	1.13	Reeves et al., 2014
TAG	Black Smoker Compl	3600	2008	363	3.28	547	4.6		0.1	0.14	Reeves et al., 2014
CENTRAL INDIAN RIDGE											
Edmond	Marker 2	3300	2001	273	<3.02	929	33.5		0.0222	0.415	Gallant and Von Damm, 2006
	Marker 10	3303	2001	293	<2.97	926	24.4		0.0391	0.395	Gallant and Von Damm, 2006
	Marker 12	3273	2001	370	3.13	933	30.6		0.249	0.381	Gallant and Von Damm, 2006
	Marker A	3281	2001	382	3.13	927	39.6		0.142	0.289	Gallant and Von Damm, 2006
Kairei	Marker 4	2422	2001	315	3.35	571	27.0		8.19	0.203	Gallant and Von Damm, 2006
	Marker 5	2448	2001	349	3.51	595	38.8		8.15	0.191	Gallant and Von Damm, 2006
	Marker 6	2452	2001	365	3.44	620	17.1		7.89	0.171	Gallant and Von Damm, 2006

Table 3b. (cont.)

| REGION/Vent field	Vent site	Depth (m)	Year	max T (°C)	pH at 25°C	[Cl] (mm)	[NH₄⁺] (μM)	δ¹⁵N_NH4 (‰ vs air)	[H₂] (mM)	[CH₄] (mM)	Reference
EAST LAU SPREADING CENTER											
ABE	ABE (north), A13	2141	2015	283	4.33	551	1.7				This study
	ABE (north), A14	2139	2015	300	4.00	550	1.5				This study
	ABE (central), A15	2153	2015	290	4.42	559	1.9				This study
	ABE (central), A16	2141	2015	263	4.54	556	1.4				This study
Mariner	Toilet Bowl, MA13	1916	2015	140	<2.57	590	1.8				This study
	Mariner, MA14	1909	2015	319	2.33	584	1.2				This study
	Mariner, MA15	1913	2015	354	<2.97	593	0.9				This study
	Mariner, MA16	1912	2015	363	2.76	605	1.3				This study
Vai Lilli	Vai Lili, VL4	1707	2015	116	<5.19	665	2.5				This study
Tui Malila	Tui Malila, TM15	1898	2015	269	<4.96	689	1.8				This study
	Tui Malila, TM16	1893	2015	251	3.91	633	1.5				This study
	Tui Malila, TM18	1846	2015	296	<4.60	670	1.8				This study
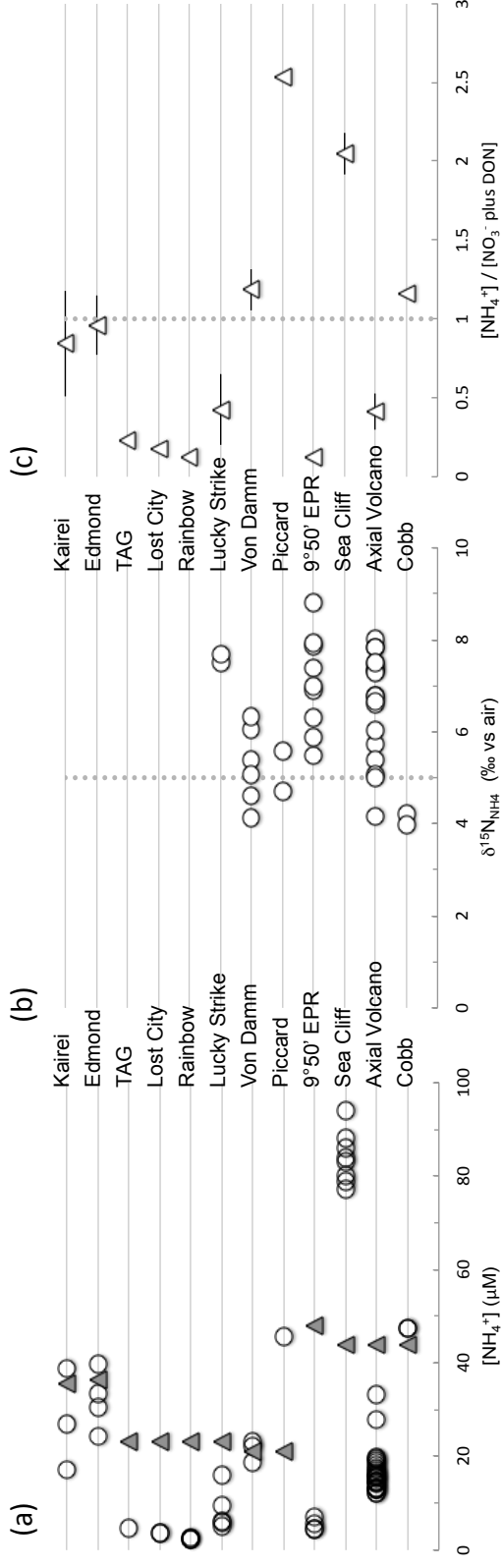
Figure 2. (a) Concentrations of vent NH_4^+ (open circles) and bottom seawater NO_3^- plus DON (filled triangles), (b) N isotopic composition of vent NH_4^+, and (c) ratios of $[NH_4^+]/[NO_3^-$ plus DON] in unsedimented systems. The dashed lines in (b) and (c) indicates the global average of the N isotopic composition of deep water NO_3^- and the ratio of 1 (i.e., vent NH4+ equal to the NO_3^- plus DON in the bottom seawater), respectively.
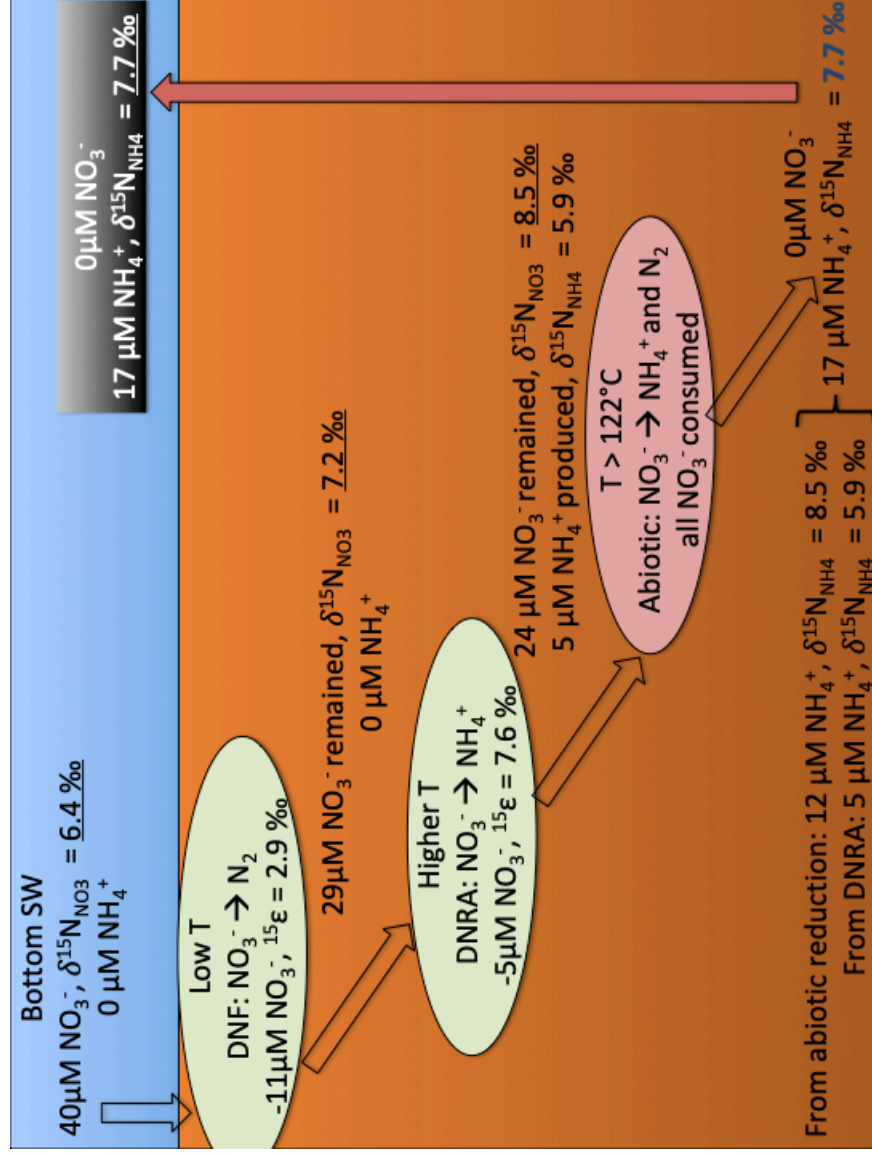
Figure 3. Hypothetical stepwise reduction of NO_3^- and production of NH_4^+ during the subduction of bottom seawater through oceanic crust from the low-temperature recharge zone to the high-temperature reaction zone. NO_3^- is first reduced by denitrification (DNF) and DNRA, and finally abiotic reduction at high temperatures resulting in the $\delta^{15}N_{NH4}$ value slightly higher than the $\delta^{15}N_{NO3}$ in the ambient seawater.
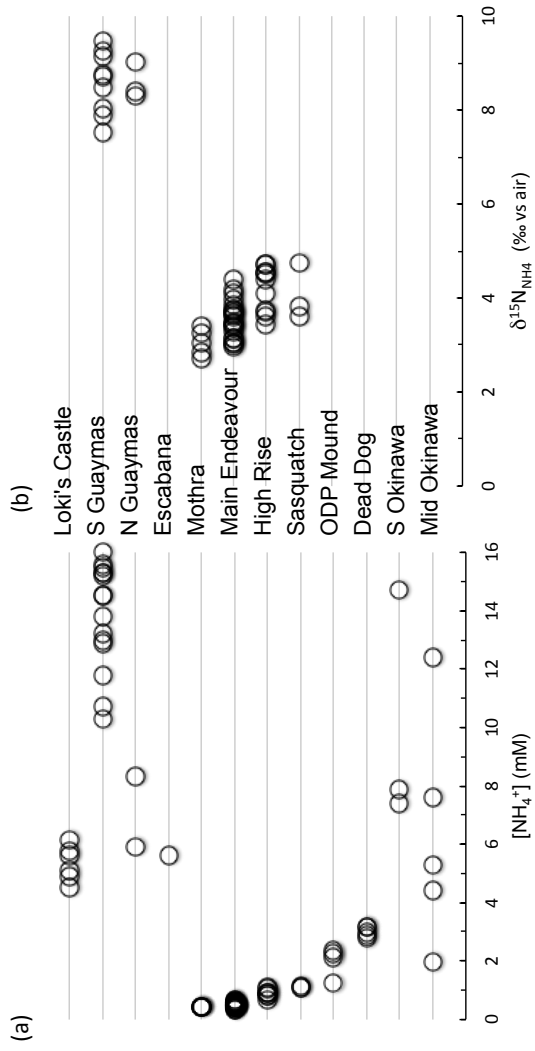
Figure 4. Concentrations (a) and N isotopic composition of vent NH_4^+ (b) in sedimented systems.
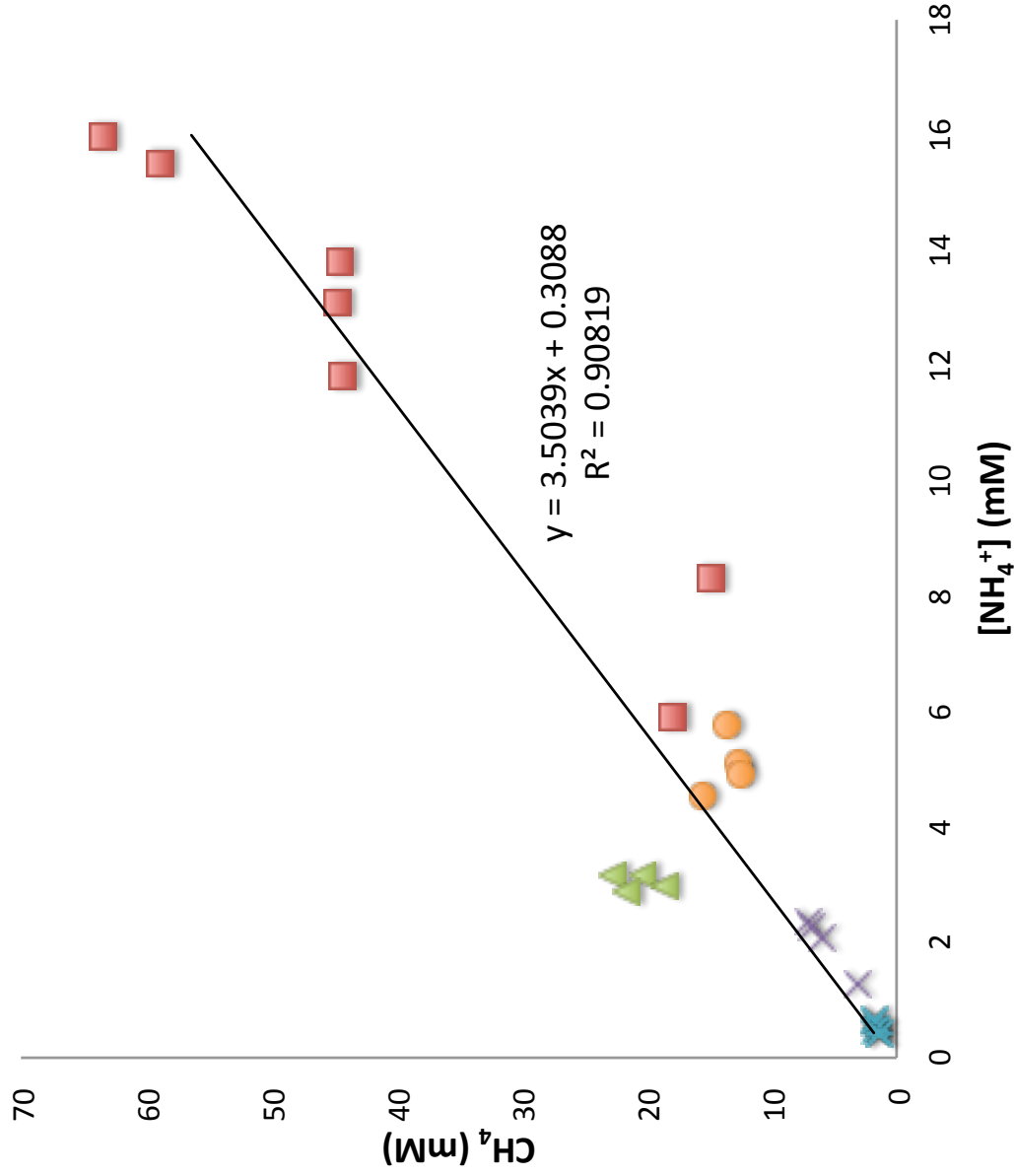
Figure 5. Relationship between [NH$_4^+$] and [CH$_4$] in sedimented systems. Data shown here are endmember concentrations from Guaymas Basin (red squares), Dead Dog (green triangles) and ODP Mound (purple crosses) of Middle Valley Field, Juan de Fuca Ridge, Loki's Castle (orange circles), and Main Endeavour Field, Juan de Fuca Ridge (blue crosses).
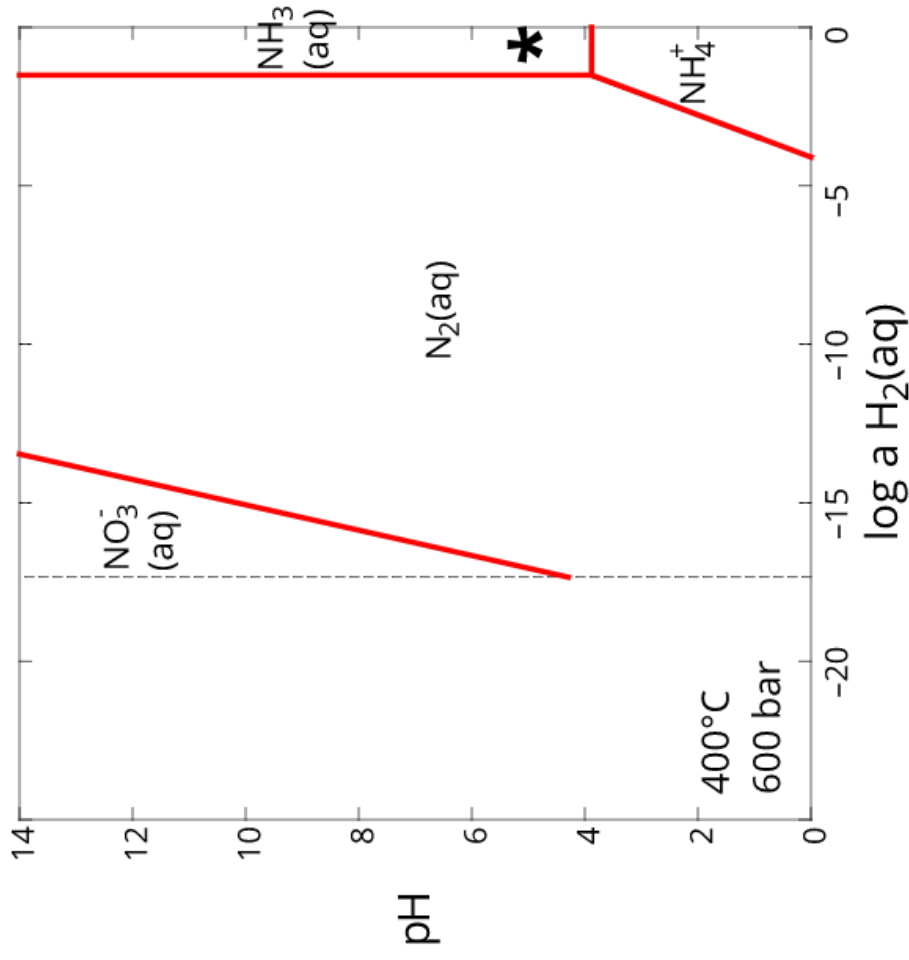
Figure 6. pH-activity diagram depicting N speciation at Piccard at 400°C (venting temperature) and 600 bar (equivalent to the depth of 1 km below the seafloor). The asterisk shows the conditions at *Beebe vent 5*. Note that our available database for speciation goes up to 400°C which does not cover the expect temperature of 535°C in the reaction zone.
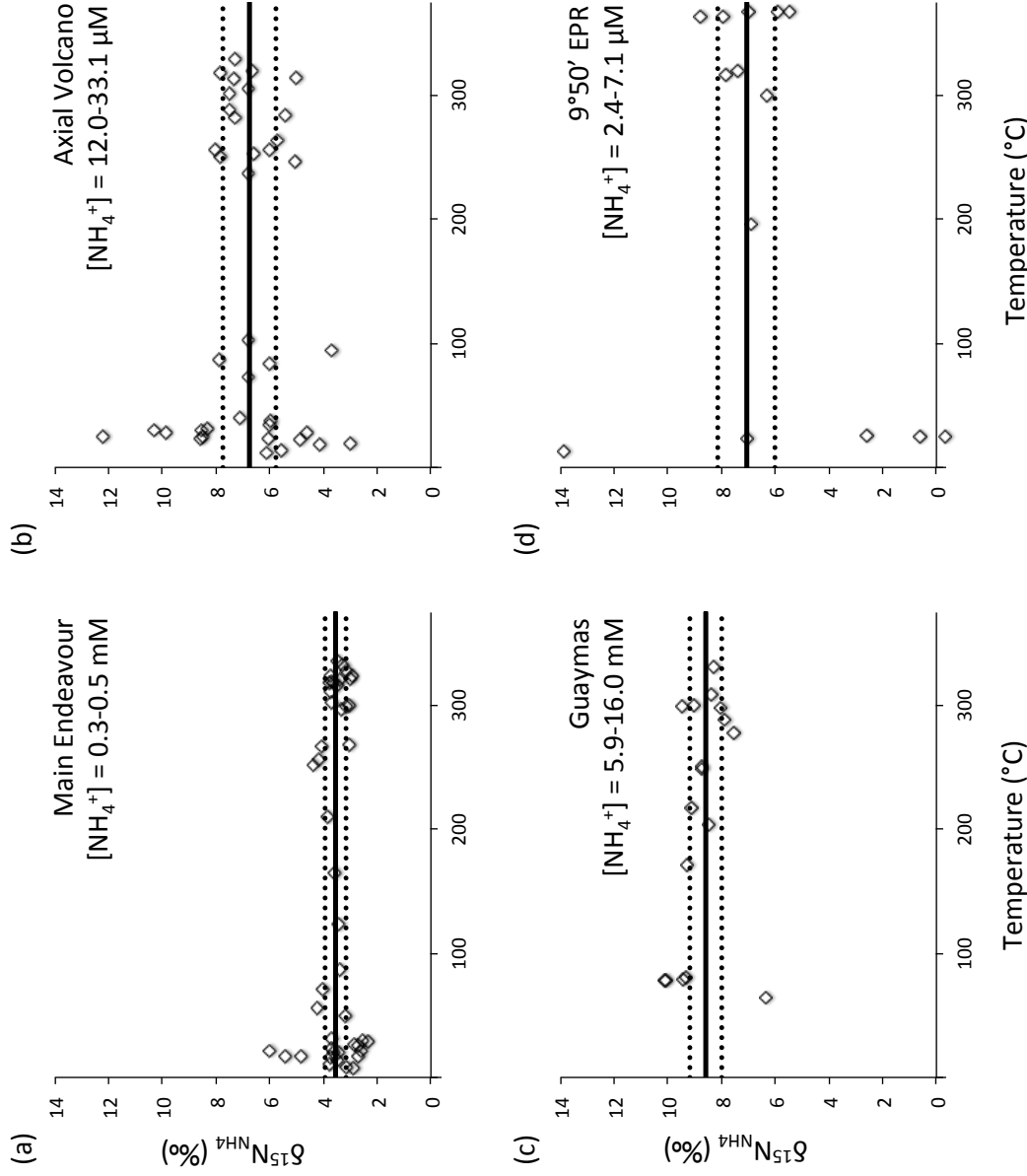
Figure 7. Variations in vent $\delta^{15}N_{NH4}$ (‰ vs air) with temperatures from selected vent fields from (a) Main Endeavour Field and (b) Axial Volcano of Juan de Fuca Ridge, (c) Guaymas Basin (both from Northern and Southern Troughs), and (d) 9°50' N East Pacific Rise. The solid and dashed lines represent the average value and standard deviations of the samples with T > 122°C respectively.

REFERENCES

Altabet, M. A., Pilskaln, C., Thunell, R., Pride, C., Sigman, D., Chavez, F., & Francois, R. (1999). The nitrogen isotope biogeochemistry of sinking particles from the margin of the Eastern North Pacific. *Deep Sea Research Part I: Oceanographic Research Papers*, *46*(4), 655-679.

Baker, B. J., Lesniewski, R. A., & Dick, G. J. (2012). Genome-enabled transcriptomics reveals archaeal populations that drive nitrification in a deep-sea hydrothermal plume. *The ISME journal*, *6*(12), 2269.

Baumberger, T., Früh-Green, G. L., Dini, A., Boschi, C., van Zuilen, K., Thorseth, I. H., & Pedersen, R. B. (2016b). Constraints on the sedimentary input into the Loki's Castle hydrothermal system (AMOR) from B isotope data. *Chemical Geology*, *443*, 111-120.

Baumberger, T., Früh-Green, G. L., Thorseth, I. H., Lilley, M. D., Hamelin, C., Bernasconi, S. M., ... & Pedersen, R. B. (2016a). Fluid composition of the sediment-influenced Loki's castle vent field at the ultra-slow spreading Arctic Mid-Ocean ridge. *Geochimica et Cosmochimica Acta*, *187*, 156-178.

Bazhenova, C. T., & Shilov, A. E. (1995). Nitrogen fixation in solution. *Coordination chemistry reviews*, *144*, 69-145.

Beaulieu, S. E., Baker, E. T., German, C. R., & Maffei, A. (2013). An authoritative global database for active submarine hydrothermal vent fields. *Geochemistry, Geophysics, Geosystems*, *14*(11), 4892-4905.

Bebout, G. E., Banerjee, N. R., Izawa, M. R. M., Kobayashi, K., Lazzeri, K., Ranieri, L. A., & Nakamura, E. (2018). Nitrogen concentrations and isotopic compositions of seafloor-altered terrestrial basaltic glass: implications for astrobiology. *Astrobiology*, *18*(3), 330-342.

Becker, K., & Davis, E. E. (2005). A review of CORK designs and operations during the Ocean Drilling Program. In *Proc. IODP| Volume* (Vol. 301, p. 2).

Bischoff, J. L., & Dickson, F. W. (1975). Seawater-basalt interaction at 200 C and 500 bars: implications for origin of sea-floor heavy-metal deposits and regulation of seawater chemistry. *Earth and Planetary Science Letters*, *25*(3), 385-397.

Bischoff, J. L., & Rosenbauer, R. J. (1989). Salinity variations in submarine hydrothermal systems by layered double-diffusive convection. *The Journal of Geology*, *97*(5), 613-623.

Bourbonnais, A., Juniper, S. K., Butterfield, D. A., Devol, A. H., Kuypers, M. M. M., Lavik, G., ... & Lehmann, M. F. (2012a). Activity and abundance of denitrifying bacteria in the

subsurface biosphere of diffuse hydrothermal vents of the Juan de Fuca Ridge. *Biogeosciences*, *9*, 4661-4678.

Bourbonnais, A., Lehmann, M. F., Butterfield, D. A., & Juniper, S. K. (2012b). Subseafloor nitrogen transformations in diffuse hydrothermal vent fluids of the Juan de Fuca Ridge evidenced by the isotopic composition of nitrate and ammonium. *Geochemistry, geophysics, geosystems*, *13*(2).

Brandes, J. A., Boctor, N. Z., Cody, G. D., Cooper, B. A., Hazen, R. M., & Yoder Jr, H. S. (1998). Abiotic nitrogen reduction on the early Earth. *Nature*, *395*(6700), 365.

Brandes, J. A., Hazen, R. M., & Yoder Jr, H. S. (2008). Inorganic nitrogen reduction and stability under simulated hydrothermal conditions. *Astrobiology*, *8*(6), 1113-1126.

Brown, L. L., & Drury, J. S. (1967). Nitrogen‐isotope effects in the reduction of nitrate, nitrite, and hydroxylamine to ammonia. I. In sodium hydroxide solution with Fe (II). *The Journal of Chemical Physics*, *46*(7), 2833-2837.

Brown, L. L., & Drury, J. S. (1969). Nitrogen Isotope Effects in the Reduction of Nitrate, Nitrite, and Hydroxylamine to Ammonia. II. The MgO and CuSO4 Systems. *The Journal of Chemical Physics*, *51*(9), 3771-3775.

Busigny, V., Cartigny, P., Philippot, P., & Javoy, M. (2003). Ammonium quantification in muscovite by infrared spectroscopy. *Chemical Geology*, *198*(1-2), 21-31.

Busigny, V., Laverne, C., & Bonifacie, M. (2005). Nitrogen content and isotopic composition of oceanic crust at a superfast spreading ridge: a profile in altered basalts from ODP Site 1256, Leg 206. *Geochemistry, Geophysics, Geosystems*, *6*(12).

Busigny, V., Laverne, C., & Bonifacie, M. (2005). Nitrogen content and isotopic composition of oceanic crust at a superfast spreading ridge: a profile in altered basalts from ODP Site 1256, Leg 206. *Geochemistry, Geophysics, Geosystems*, *6*(12).

Butterfield, D. A., McDuff, R. E., Franklin, J., & Wheat, C. G. (1994a). Geochemistry of hydrothermal vent fluids from Middle Valley, Juan de Fuca Ridge. In Mottl, M.J., Davis, E.E., Fisher, A.T., & Slack, J.F. (Eds.), *Proceedings of the Ocean Drilling Program, Scientific Results*.

Butterfield, D. A., McDuff, R. E., Mottl, M. J., Lilley, M. D., Lupton, J. E., & Massoth, G. J. (1994b). Gradients in the composition of hydrothermal fluids from the Endeavour segment vent field: Phase separation and brine loss. *Journal of Geophysical Research: Solid Earth*, *99*(B5), 9561-9583.

Byrne, N., Strous, M., Crépeau, V., Kartal, B., Birrien, J. L., Schmid, M., ... & Prieur, D. (2009). Presence and activity of anaerobic ammonium-oxidizing bacteria at deep-sea hydrothermal vents. *The ISME journal*, *3*(1), 117.

Campbell, A. C., Bowers, T. S., Measures, C. I., Falkner, K. K., Khadem, M., & Edmond, J. M. (1988). A time series of vent fluid compositions from 21° N, East Pacific Rise (1979, 1981, 1985), and the Guaymas Basin, Gulf of California (1982, 1985). *Journal of Geophysical Research: Solid Earth*, *93*(B5), 4537-4549.

Campbell, A. C., German, C. R., Palmer, M. R., Gamo, T., & Edmond, J. M. (1994). Chemistry of hydrothermal fluids from Escanaba Trough, Gorda Ridge. In Morton, J; L., Zierenberg, R. A., & Reiss, C. A. (Eds.) *Geological, Hydrothermal, and Biologic Studies at Escanaba Trough, Gorda Ridge, offshore Northern California* (pp. 201-222). U.S. Geological Survey.

Charlou, J. L., Donval, J. P., Fouquet, Y., Jean-Baptiste, P., & Holm, N. (2002). Geochemistry of high H2 and CH4 vent fluids issuing from ultramafic rocks at the Rainbow hydrothermal field (36 14′ N, MAR). *Chemical geology*, *191*(4), 345-359.

Cleaves, H. J. (2018). Nucleobases on the Primitive Earth: Their Sources and Stabilities. In *Prebiotic Chemistry and Chemical Evolution of Nucleic Acids* (pp. 1-19). Springer, Cham.

Corliss, J. B., Dymond, J., Gordon, L. I., Edmond, J. M., von Herzen, R. P., Ballard, R. D., ... & van Andel, T. H. (1979). Submarine thermal springs on the Galápagos rift. *Science, 203*(4385), 1073-1083.

Cruse, A. M., & Seewald, J. S. (2006). Geochemistry of low-molecular weight hydrocarbons in hydrothermal fluids from Middle Valley, northern Juan de Fuca Ridge. *Geochimica et cosmochimica acta*, *70*(8), 2073-2092.

Dick, G. J., & Tebo, B. M. (2010). Microbial diversity and biogeochemistry of the Guaymas Basin deep-sea hydrothermal plume. *Environmental Microbiology*, *12*(5), 1334-1347.

Ding, K., & Seyfried, W. E. (2007). In situ measurement of pH and dissolved H2 in mid-ocean ridge hydrothermal fluids at elevated temperatures and pressures. *Chemical reviews*, *107*(2), 601-622.

Ding, K., Seyfried Jr, W. E., Zhang, Z., Tivey, M. K., Von Damm, K. L., & Bradley, A. M. (2005). The in situ pH of hydrothermal fluids at mid-ocean ridges. *Earth and Planetary Science Letters*, *237*(1-2), 167-174.

Dörr, M., Käßbohrer, J., Grunert, R., Kreisel, G., Brand, W. A., Werner, R. A., ... & Weigand, W. (2003). A possible prebiotic formation of ammonia from dinitrogen on iron sulfide surfaces. *Angewandte Chemie International Edition*, *42*(13), 1540-1543.

Erzinger, J., and W. Bach (1996), Downhole variation of nitrogen in Hole 504B: Preliminary results, *Proc. Ocean Drill. Program Sci. Results*, *148*, 3–7.

Evans, G. N., Tivey, M. K., Seewald, J. S., & Wheat, C. G. (2017). Influences of the Tonga Subduction Zone on seafloor massive sulfide deposits along the Eastern Lau Spreading Center and Valu Fa Ridge. *Geochimica et Cosmochimica Acta*, *215*, 214-246.

Garcia, H. E., R. A. Locarnini, T. P. Boyer, J. I. Antonov, O.K. Baranova, M.M. Zweng, J.R. Reagan, D.R. Johnson, 2014. World Ocean Atlas 2013, Volume 4: Dissolved Inorganic Nutrients (phosphate, nitrate, silicate). S. Levitus, Ed., A. Mishonov Technical Ed.; NOAA Atlas NESDIS 76, 25 pp.

German, C. R., & Seyfried, W. E. (2014). Hydrothermal processes. In *Treatise on Geochemistry: Second Edition*. Elsevier Inc..

Hall, P. 0. J., & Aller, R. C. (1992). Rapid, small-volume, flow injection analysis for SCO2, and NH4+ in marine and freshwaters. *Limnology and Oceanography*, *37*(5), 1113-1119.

Hodgkinson, M. R., Webber, A. P., Roberts, S., Mills, R. A., Connelly, D. P., & Murton, B. J. (2015). Talc-dominated seafloor deposits reveal a new class of hydrothermal system. *Nature communications*, *6*, 10150.

Holmes, R. M., McClelland, J. W., Sigman, D. M., Fry, B., & Peterson, B. J. (1998). Measuring 15N–NH4+ in marine, estuarine and fresh waters: an adaptation of the ammonia diffusion method for samples with low ammonium concentrations. *Marine Chemistry*, *60*(3-4), 235-243.

Honma, H., & Itihara, Y. (1981). Distribution of ammonium in minerals of metamorphic and granitic rocks. *Geochimica et Cosmochimica Acta*, *45*(6), 983-988.

Johnson, H. P., Hutnak, M., Dziak, R. P., Fox, C. G., Urcuyo, I., Cowen, J. P., ... & Fisher, C. (2000). Earthquake-induced changes in a hydrothermal system on the Juan de Fuca mid-ocean ridge. *Nature*, *407*(6801), 174.

Kienast, S. S., Calvert, S. E., & Pedersen, T. F. (2002). Nitrogen isotope and productivity variations along the northeast Pacific margin over the last 120 kyr: Surface and subsurface paleoceanography. *Paleoceanography and Paleoclimatology*, *17*(4).

Klein, F., Humphris, S. E., Guo, W., Schubotz, F., Schwarzenbach, E. M., & Orsi, W. D. (2015). Fluid mixing and the deep biosphere of a fossil Lost City-type hydrothermal system at the Iberia Margin. *Proceedings of the National Academy of Sciences*, *112*(39), 12036-12041.

Knapp, A. N., Sigman, D. M., & Lipschultz, F. (2005). N isotopic composition of dissolved organic nitrogen and nitrate at the Bermuda Atlantic Time-series Study site. *Global Biogeochemical Cycles*, *19*(1).

Lam, P., Cowen, J. P., & Jones, R. D. (2004). Autotrophic ammonia oxidation in a deep-sea hydrothermal plume. *FEMS microbiology ecology*, *47*(2), 191-206.

Lam, P., Cowen, J. P., Popp, B. N., & Jones, R. D. (2008). Microbial ammonia oxidation and enhanced nitrogen cycling in the Endeavour hydrothermal plume. *Geochimica et Cosmochimica Acta*, *72*(9), 2268-2286.

Lepper, C. P., Williams, M. A., Penny, D., Edwards, P. J., & Jameson, G. B. (2018). Effects of Pressure and pH on the Hydrolysis of Cytosine: Implications for Nucleotide Stability around Deep-Sea Black Smokers. *ChemBioChem*, *19*(6), 540-544.

Lewis, C. A., Crayle, J., Zhou, S., Swanstrom, R., & Wolfenden, R. (2016). Cytosine deamination and the precipitous decline of spontaneous mutation during Earth's history. *Proceedings of the National Academy of Sciences*, *113*(29), 8194-8199.

Li, L., Bebout, G. E., & Idleman, B. D. (2007). Nitrogen concentration and $\delta^{15}N$ of altered oceanic crust obtained on ODP Legs 129 and 185: insights into alteration-related nitrogen enrichment and the nitrogen subduction budget. *Geochimica et Cosmochimica Acta*, *71*(9), 2344-2360.

Lilley, M. D., Butterfield, D. A., Lupton, J. E., & Olson, E. J. (2003). Magmatic events can produce rapid changes in hydrothermal vent chemistry. *Nature*, *422*(6934), 878.

Lilley, M. D., Butterfield, D. A., Olson, E. J., Lupton, J. E., Macko, S. A., & McDuff, R. E. (1993). Anomalous CH4 and NH4+ concentrations at an unsedimented mid-ocean-ridge hydrothermal system. *Nature*, *364*(6432), 45.

Lin, H. T., Cowen, J. P., Olson, E. J., Amend, J. P., & Lilley, M. D. (2012). Inorganic chemistry, gas compositions and dissolved organic carbon in fluids from sedimented young basaltic crust on the Juan de Fuca Ridge flanks. *Geochimica et Cosmochimica Acta*, *85*, 213-227.

Longnecker, K., Sievert, S. M., Sylva, S. P., Seewald, J. S., & Kujawinski, E. B. (2018). Dissolved organic carbon compounds in deep-sea hydrothermal vent fluids from the East Pacific Rise at 9° 50′ N. *Organic Geochemistry*, *125*, 41-49.

Lonsdale, P. F., Bischoff, J. L., Burns, V. M., Kastner, M., & Sweeney, R. E. (1980). A high-temperature hydrothermal deposit on the seabed at a Gulf of California spreading center. *Earth and Planetary Science Letters*, *49*(1), 8-20.

Madigan, M. T., Martinko, J. M., Stahl, D. A., & Calrk, D. P. (2010). *Brock biology of microorganisms* (13th ed.). Benjamin Cummings.

Martinez, F., & Taylor, B. (2002). Mantle wedge control on back-arc crustal accretion. *Nature*, *416*(6879), 417.

McDermott, J. M. (2015). *Geochemistry of deep-sea hydrothermal vent fluids from the Mid-Cayman Rise, Caribbean Sea* (Doctoral dissertation, Massachusetts Institute of Technology).

McDermott, J. M., Sylva, S. P., Ono, S., German, C. R., & Seewald, J. S. (2018). Geochemistry of fluids from Earth's deepest ridge-crest hot-springs: Piccard hydrothermal field, Mid-Cayman Rise. *Geochimica et Cosmochimica Acta*, *228*, 95-118.

McNichol, J., Stryhanyuk, H., Sylva, S. P., Thomas, F., Musat, N., Seewald, J. S., & Sievert, S. M. (2018). Primary productivity below the seafloor at deep-sea hot springs. *Proceedings of the National Academy of Sciences*, 201804351.

McNichol, J., Sylva, S. P., Thomas, F., Taylor, C. D., Sievert, S. M., & Seewald, J. S. (2016). Assessing microbial processes in deep-sea hydrothermal systems by incubation at in situ temperature and pressure. *Deep Sea Research Part I: Oceanographic Research Papers*, *115*, 221-232.

Mikhail, S., & Sverjensky, D. A. (2014). Nitrogen speciation in upper mantle fluids and the origin of Earth's nitrogen-rich atmosphere. *Nature Geoscience*, *7*(11), 816.

Miyazaki, J., Kawagucci, S., Makabe, A., Takahashi, A., Kitada, K., Torimoto, J., ... & Horai, S. (2017a). Deepest and hottest hydrothermal activity in the Okinawa Trough: the Yokosuka site at Yaeyama Knoll. *Royal Society open science*, *4*(12), 171570.

Mottl, M. J., & Holland, H. D. (1978). Chemical exchange during hydrothermal alteration of basalt by seawater—I. Experimental results for major and minor components of seawater. *Geochimica et Cosmochimica Acta*, *42*(8), 1103-1115.

Mottl, M. J., Seewald, J. S., Wheat, C. G., Tivey, M. K., Michael, P. J., Proskurowski, G., ... & Chan, L. H. (2011). Chemistry of hot springs along the Eastern Lau Spreading Center. *Geochimica et Cosmochimica Acta*, *75*(4), 1013-1038.

Mulholland, M. R., & Lomas, M. W. (2008). Nitrogen uptake and assimilation. In Capone, D. G., Bronk, D. A., Mulholland, M. R., & Carpenter, E. J. (Eds.) *Nitrogen in the marine environment*, 303-384. Elsevier.

Nunoura, T., Oida, H., Nakaseama, M., Kosaka, A., Ohkubo, S. B., Kikuchi, T., ... & Hirayama, H. (2010). Archaeal diversity and distribution along thermal and geochemical gradients in hydrothermal sediments at the Yonaguni Knoll IV hydrothermal field in the Southern Okinawa Trough. *Applied and environmental microbiology*, *76*(4), 1198-1211.

Pedersen, R. B., Rapp, H. T., Thorseth, I. H., Lilley, M. D., Barriga, F. J., Baumberger, T., ... & Jorgensen, S. L. (2010). Discovery of a black smoker vent field and vent fauna at the Arctic Mid-Ocean Ridge. *Nature Communications*, *1*, 126.

Pérez-Rodríguez, I., Ricci, J., Voordeckers, J. W., Starovoytov, V., & Vetriani, C. (2010). Nautilia nitratireducens sp. nov., a thermophilic, anaerobic, chemosynthetic, nitrate-ammonifying bacterium isolated from a deep-sea hydrothermal vent. *International journal of systematic and evolutionary microbiology*, *60*(5), 1182-1186.

Pérez-Rodríguez, I., Sievert, S. M., Fogel, M. L., & Foustoukos, D. I. (2017). Biogeochemical N signatures from rate-yield trade-offs during in vitro chemosynthetic NO_3^- reduction by deep-sea vent ε-Proteobacteria and Aquificae growing at different temperatures. *Geochimica et Cosmochimica Acta*, *211*, 214-227.

Pester, N. J., Reeves, E. P., Rough, M. E., Ding, K., Seewald, J. S., & Seyfried Jr, W. E. (2012). Subseafloor phase equilibria in high-temperature hydrothermal fluids of the Lucky Strike Seamount (Mid-Atlantic Ridge, 37 17′ N). *Geochimica et Cosmochimica Acta*, *90*, 303-322.

Reeves, E. P., McDermott, J. M., & Seewald, J. S. (2014). The origin of methanethiol in midocean ridge hydrothermal fluids. *Proceedings of the National Academy of Sciences*, 201400643.

Robinson, R. S., Kienast, M., Luiza Albuquerque, A., Altabet, M., Contreras, S., De Pol Holz, R., ... & Ivanochko, T. (2012). A review of nitrogen isotopic alteration in marine sediments. *Paleoceanography*, *27*(4).

Rosencrantz, E., Ross, M. I., & Sclater, J. G. (1988). Age and spreading history of the Cayman Trough as determined from depth, heat flow, and magnetic anomalies. *Journal of Geophysical Research: Solid Earth*, *93*(B3), 2141-2157.

Russ, L., Kartal, B., Op Den Camp, H. J., Sollai, M., Le Bruchec, J., Caprais, J. C., ... & Jetten, M. S. (2013). Presence and diversity of anammox bacteria in cold hydrocarbon-rich seeps and hydrothermal vent sediments of the Guaymas Basin. *Frontiers in microbiology*, *4*, 219.

Ryan, W.B.F., S.M. Carbotte, J.O. Coplan, S. O'Hara, A. Melkonian, R. Arko, R.A. Weissel, V. Ferrini, A. Goodwillie, F. Nitsche, J. Bonczkowski, and R. Zemsky (2009), Global Multi-Resolution Topography synthesis, *Geochem. Geophys. Geosyst.*, 10, Q03014, doi:10.1029/2008GC002332.

 Schoonen, M. A., & Xu, Y. (2001). Nitrogen reduction under hydrothermal vent conditions: Implications for the prebiotic synthesis of CHON compounds. *Astrobiology*, *1*(2), 133-142.

Seewald, J. (2017) Chemical composition of hydrothermal fluids collected on RV/Roger Revelle RR1507 in the Eastern Lau Spreading Center and Valu Fa Ridge, April-May 2015 (Functional microbial dynamics of vent deposits project). Biological and Chemical Oceanography Data Management Office (BCO-DMO). Dataset version 2017-01-13. http://lod.bco-dmo.org/id/dataset/674750 [accessed Oct 1, 2018]

Seewald, J. S., Doherty, K. W., Hammar, T. R., & Liberatore, S. P. (2002). A new gas-tight isobaric sampler for hydrothermal fluids. *Deep Sea Research Part I: Oceanographic Research Papers*, *49*(1), 189-196.

Seewald, J. S., Seyfried Jr, W. E., & Shanks III, W. C. (1994). Variations in the chemical and stable isotope composition of carbon and sulfur species during organic-rich sediment alteration: an experimental and theoretical study of hydrothermal activity at Guaymas Basin, Gulf of California. *Geochimica et Cosmochimica Acta*, *58*(22), 5065-5082.

Seewald, J., Cruse, A., & Saccocia, P. (2003). Aqueous volatiles in hydrothermal fluids from the Main Endeavour Field, northern Juan de Fuca Ridge: temporal variability following earthquake activity. *Earth and Planetary Science Letters*, *216*(4), 575-590.

Seyfried Jr, W. E., & Bischoff, J. L. (1981). Experimental seawater-basalt interaction at 300 C, 500 bars, chemical exchange, secondary mineral formation and implications for the transport of heavy metals. *Geochimica et Cosmochimica Acta*, *45*(2), 135-147.

Seyfried Jr, W. E., Seewald, J. S., Berndt, M. E., Ding, K., & Foustoukos, D. I. (2003). Chemistry of hydrothermal vent fluids from the Main Endeavour Field, northern Juan de Fuca Ridge: Geochemical controls in the aftermath of June 1999 seismic events. *Journal of Geophysical Research: Solid Earth*, *108*(B9).

Seyfried, W. E., Pester, N. J., Tutolo, B. M., & Ding, K. (2015). The Lost City hydrothermal system: Constraints imposed by vent fluid chemistry and reaction path models on subseafloor heat and mass transfer processes. *Geochimica et Cosmochimica Acta*, *163*, 59-79.

Shipboard Scientific Party (2004) Juan de Fuca hydrogeology: the hydrogeologic architecture of basaltic oceanic crust: compart- mentalization, anisotropy, microbiology, and crustal-scale properties on the eastern flank of Juan de Fuca Ridge, eastern Pacific Ocean. IODP Prel. Rep. 301.

Sievert, S. M., & Vetriani, C. (2012). Chemoautotrophy at deep-sea vents: past, present, and future. *Oceanography*, *25*(1), 218-233.

Sigman, D. M., Altabet, M. A., Michener, R., McCorkle, D. C., Fry, B., & Holmes, R. M. (1997). Natural abundance-level measurement of the nitrogen isotopic composition of oceanic nitrate: an adaptation of the ammonia diffusion method. *Marine Chemistry*, *57*(3-4), 227-242.

Slobodkina, G. B., Mardanov, A. V., Ravin, N. V., Frolova, A. A., Chernyh, N. A., Bonch-Osmolovskaya, E. A., & Slobodkin, A. I. (2017). Respiratory ammonification of nitrate coupled to anaerobic oxidation of elemental sulfur in deep-sea autotrophic thermophilic bacteria. *Frontiers in microbiology*, *8*, 87.

Solorzano, L. (1969). Determination of ammonia in natural waters by the phenolhypochlorite method. *Limnology and oceanography*, *14*(5), 799-801.

Soule, A. S., Seewald, J. S., Wankel, S. D., Michel, A. P., … & Karson, J. (2018). Exploration of the Northern Guaymas Basin. *Oceanography, 31*(1 Supplement), 39-41.

Sylvan, J. B., Wankel, S. D., LaRowe, D. E., Charoenpong, C. N., Huber, J. A., Moyer, C. L., & Edwards, K. J. (2017). Evidence for microbial mediation of subseafloor nitrogen redox processes at Loihi Seamount, Hawaii. *Geochimica et Cosmochimica Acta*, *198*, 131-150.

Takai, K., Nakamura, K., Toki, T., Tsunogai, U., Miyazaki, M., Miyazaki, J., ... & Horikoshi, K. (2008). Cell proliferation at 122 C and isotopically heavy CH4 production by a hyperthermophilic methanogen under high-pressure cultivation. *Proceedings of the National Academy of Sciences*, *105*(31), 10949-10954.

Takai, K., Nunoura, T., Ishibashi, J. I., Lupton, J., Suzuki, R., Hamasaki, H., ... & Hirayama, H. (2008). Variability in the microbial communities and hydrothermal fluid chemistry at the newly discovered Mariner hydrothermal field, southern Lau Basin. *Journal of Geophysical Research: Biogeosciences*, *113*(G2).

Taylor, B., Zellmer, K., Martinez, F., & Goodliffe, A. (1996). Sea-floor spreading in the Lau back-arc basin. *Earth and Planetary Science Letters*, *144*(1-2), 35-40.

Tivey, M. K., Stakes, D. S., Cook, T. L., Hannington, M. D., & Petersen, S. (1999). A model for growth of steep-sided vent structures on the Endeavour Segment of the Juan de Fuca Ridge: Results of a petrologic and geochemical study. *Journal of Geophysical Research: Solid Earth*, *104*(B10), 22859-22883.

Vedder, W. (1965). Ammonium in muscovite. *Geochimica et Cosmochimica Acta*, *29*, 221-228.

Von Damm, K. L. (2000). Chemistry of hydrothermal vent fluids from 9–10 N, East Pacific Rise:"Time zero," the immediate posteruptive period. *Journal of Geophysical Research: Solid Earth*, *105*(B5), 11203-11222.

Von Damm, K. L., & Bischoff, J. L. (1987). Chemistry of hydrothermal solutions from the southern Juan de Fuca Ridge. *Journal of Geophysical Research: Solid Earth*, *92*(B11), 11334-11346.

Von Damm, K. L., Edmond, J. M., Grant, B., Measures, C. I., Walden, B., & Weiss, R. F. (1985a). Chemistry of submarine hydrothermal solutions at 21° N, East Pacific Rise. *Geochimica et Cosmochimica Acta*, *49*(11), 2197-2220.

Von Damm, K. L., Parker, C. M., Lilley, M. D., Clague, D. A., Zierenberg, R. A., Olson, E. J., & McClain, J. S. (2006). Chemistry of vent fluids and its implications for subsurface conditions at Sea Cliff hydrothermal field, Gorda Ridge. *Geochemistry, Geophysics, Geosystems*, *7*(5).

Von Damm, K. V., Edmond, J. T., Measures, C. I., & Grant, B. (1985b). Chemistry of submarine hydrothermal solutions at Guaymas Basin, Gulf of California. *Geochimica et Cosmochimica Acta*, *49*(11), 2221-2237.

Wang, D. T., Reeves, E. P., McDermott, J. M., Seewald, J. S., & Ono, S. (2018). Clumped isotopologue constraints on the origin of methane at seafloor hot springs. *Geochimica et Cosmochimica Acta*, *223*, 141-158.

Wankel, S. D., Bourbonnais, A., & Charoenpong, C. N. (2017). Microbial processes at submarine hydrothermal vents. In J. Kallmeyer (Ed.), *Life at Vents and Seeps* (pp. 179-222). de Gruyter, Berlin/Boston.

Wong, C. S., Yu, Z., Waser, N. A. D., Whitney, F. A., & Johnson, W. K. (2002). Seasonal changes in the distribution of dissolved organic nitrogen in coastal and open-ocean waters in the North East Pacific: sources and sinks. *Deep Sea Research Part II: Topical Studies in Oceanography*, *49*(24-25), 5759-5773.

THIS PAGE INTENTIONALLY LEFT BLANK

CHAPTER 4

Subsurface modifications of NH$_4^+$ at low-temperature, diffuse vents at 9°50'N East Pacific Rise

4.1. ABSTRACT

Diffuse hydrothermal vents occur as the result of mixing between high-temperature vent fluids and ambient seawater, yielding low-temperature flows that allow microbial communities to thrive. Here we report the measurements of concentrations of different inorganic nitrogen pools and their nitrogen (N) and oxygen (O) isotope compositions taken from two diffuse vents at 9°50'N East Pacific Rise (EPR), *Crab Spa* and *Teddy Bear*. In comparison to the high-temperature, focused vents nearby, these diffuse vents exhibited depletion of nitrate (NO$_3^-$) and enrichment of ammonium (NH$_4^+$) attributable to microbial activities therein. Denitrification, dissimilatory nitrate reduction to ammonium (DNRA), and ammonia consumption are proposed to be the key N transformations at these sites. In addition to these natural sample measurements, we also report isotopic measurements from previously reported incubation experiments representing diffuse, low-temperature conditions (McNichol et al., 2016; 2018), in which varying environmental conditions (i.e., temperatures and electron donor) were used to investigate the microbial N transformation processes. The N isotopic composition of NH$_4^+$ (δ^{15}N$_{NH4}$) both from the natural and incubation samples displayed an unexpectedly large degree of variation ranging more than 16‰ and 22‰, respectively. Simulations of the incubation experiments using a multi-process kinetic isotope effect integrated Michaelis-Menten model highlight a complex interplay between different N transformation reactions and notably ammonium consumption.

4.2. INTRODUCTION

Submarine hydrothermal vents have been reported from all ocean basins (Beaulieu et al., 2015). The high-temperature, focused venting typified by 'black-smoker' vents is thought to make up a small fraction of the available heat flux from mid-ocean ridges (e.g., Nielson et al., 2006) suggesting that low-temperature, diffuse flow venting may be the dominant player in terms of the heat flux. While the impact of hydrothermal circulation on the chemical composition and cycling of many elements has been extensively studied, the nature of nitrogen cycling in these vent systems is still relatively unknown.

Early reports on deep-sea vent geochemistry were generally sparse in terms of N speciation and concentrations, limiting interpretation of N cycling at vents (Shock, 1992; Karl, 1995; Van Dover, 2000). In addition, concentration information alone is often insufficient in describing the network of N cycling, comprised of multiple microbially catalyzed redox transformations and abiotic processes. Hence, more recent attempts to interrogate N cycling have incorporated microbiological/molecular biological (e.g., Wang et al., 2009; Bourbonnais et al., 2012a, Nakagawa et al., 2015) and stable isotope (e.g., Bourbonnais et al., 2012b; Sylvan et al., 2017) approaches to provide additional constraints. To date, however, very few N cycling studies have used natural abundance stable isotopes in low-temperature, diffuse vent systems for constraining N cycling processes (Bourbonnais et al., 2012b; Sylvan et al., 2017).

In this study, we aim to expand the application of natural abundance stable isotope composition for constraining those processes regulating fluxes of NH_4^+ in low-temperature hydrothermal systems. Specifically, we investigated diffuse venting sites along the East Pacific Rise (between 9°N and 10°N) by analyzing concentration and isotopic composition data from

collection of both natural fluid samples as well as samples from a set of incubation experiments conducted on fluid samples from a well studied diffuse vent site, *Crab Spa*. Previously published results of the incubation experiments focus on rates of chemoautotrophy and carbon fixation as well as corresponding patterns in microbial community composition (McNichol et al., 2016; 2018). Expanding on these initial studies, we specifically examine the natural abundance stable isotope dynamics captured in subsamples of these experimental incubation fluids, with the goal of gaining a better understanding on the expression of isotope fractionation during microbially mediated transformations under geochemically distinct regimes. To scrutinize these new isotope data we also applied a closed system, Michaelis-Menten isotope model to simulate microbial reactions and provide insight into the microbially mediated N transformations occurring during the incubations and, in turn, shed light on microbial processes occurring under different temperature and electron donor/acceptor regimes in nature.

4.3. GEOLOGIC SETTING AND SAMPLING DESCRIPTIONS

The 9°50' East Pacific Rise (EPR) vent field is located on the northern, fast-spreading section of the East Pacific Rise with a reported opening rate of ~11 cm/yr (Carbotte and Macdonald, 1992). This particular segment has been extensively studied notably through the RIDGE and the Ridge2000 NSF-sponsored programs (Fornari et al., 2012). Like much of the EPR, this section is volcanically active and there have been at least two documented volcanic eruptions since 1990 roughly 14 years apart: 1991-92 and 2005-06 (Rubin et al., 2012 and references therein).

All vents reported in this study are located along the axial summit trough (AST) between 9°50' N and 9°51' N (Figure 1) with an average depth ~2500 m. The exact locations and depths

of these vents are shown in Table 1. While the focus of this paper is on the low-temperature vent fluids (from *Crab Spa* and *Teddy Bear*), the high-temperature counterparts within close proximity of these diffuse vents (from *Tica*, *Bio 9*, *Bio vent* and *P vent*) are also provided for baseline comparison. Fluid samples were taken during two separate campaigns in Jan 2014 (AT26-10) and Apr-May 2017 (AT37-12). Samples were taken with either 150-mL titanium isobaric gas-tight (IGT) samplers in 2014 (Seewald et al., 2002) or 750-mL titanium 'major' samplers in 2017 (Von Damm et al., 1985). All cruises were onboard the *R/V Atlantis* and samplers were deployed by *HOV Alvin* (in 2017) or *ROV Jason* (in 2014).

Two types of fluid samples were used in this study: (1) natural samples, and (2) samples from incubations of *Crab Spa* fluids conducted during the 2014 cruise. The former comprise unamended samples that were filtered and frozen after being drawn out of the samplers, while the latter were natural fluids amended with either NO_3^- or both NO_3^- and H_2 followed by incubation inside the IGT samplers for ~24 hours. Details of these incubations have been described previously (McNichol et al. 2016; 2018). The three incubation treatments that are investigated for stable isotope dynamics in this study are (1) NO_3^- addition and incubation at 24°C, (2) NO_3^- and H_2 addition and incubation at 24°C, and (3) NO_3^- and H_2 addition and incubation at 50°C. Amendments made at the start of the incubation aimed to raise the NO_3^- and H_2 concentrations to 100uM and 150uM, respectively.

4.4. METHODS

The methods described below are used to measure concentrations of chemical species of interest and also the N and O isotopic composition of different N pools for both natural samples and incubation samples.

4.4.1 Fluid chemistry

The pH values of the fluid samples were measured at room temperature (25°C) immediately after fluids were drawn out of the samplers using a Ag/AgCl electrode which was calibrated daily. Major anions and cations were analyzed by ion chromatography (IC) using a Dionex DX-500 IC System. Samples were gravimetrically diluted with DI water before concentration analyses for Cl^- and Mg^{2+}. Anions (for Cl^- analyses) were chromatographically separated using a Dionex IonPac AS15 column and carbonate removal cartridge (Dionex CRD200) run isocratically with eluent consisting of 50% DI water and 50% 75mM NaOH flowing at 1.2 mL/min. Cations (for Mg^{2+} analyses) were chromatographically separated using Dionex IonPac CS12A column run isocratically with eluent made up of 77% DI water and 23% 100mM H_2SO_4 flowing at 1.0 mL/min. Both anion and cation analyses were run in suppressed conductivity mode for increased sensitivity (suppressor current of 300 mA and 125 mA for anions and cations, respectively). Analytical uncertainty (2σ) was better than ±3%.

Total ammonium ($\Sigma NH_4 = NH_3 + NH_4^+$) concentrations were measured using flow injection analysis as previously described (Hall and Aller, 1992). This method relies on increasing the pH of the sample through the addition of the basic carrier solution which will deprotonate dissolved NH_4^+ in the sample forming NH_3. The product NH_3 then diffuses across a Teflon exchange membrane into an acidic carrier fluid resulting in re-protonation of NH_3 to NH_4^+ before being carried into the conductivity meter. The concentration is then calculated from the change in the measured conductivity.

Concentrations of nitrate (NO_3^-) plus nitrite (NO_2^-) (hereafter referred to as NO_x) were analyzed by reacting the sample with hot vanadium reagent to convert NO_x to nitric oxide gas (NO), which was detected chemiluminescently (Garside, 1982) using a NoxBox instrument

(Teledyne, San Diego CA, USA). NO_2^- was measured spectrophotometrically using sulfanilamide and N-(1-naphthyl)ethylene-diamine reagents (Strickland and Parsons, 1972). Nitrate concentrations were calculated from the difference between $[NO_x]$ and $[NO_2^-]$. Samples with measurable hydrogen sulfide (H_2S) were purged with either N_2 or Ar gas to avoid potential inference.

4.4.2. Isotope analyses

The N and O isotopic composition are reported using standard delta (δ) notation:

$$\delta^{15}N \quad (\text{‰ vs air}) = \left[\left(\frac{^{15}N:{}^{14}N_{sample}}{^{15}N:{}^{14}N_{air}} \right) - 1 \right] \times 1000$$

$$\delta^{18}O \quad (\text{‰ vs VSMOW}) = \left[\left(\frac{^{18}O:{}^{16}O_{sample}}{^{18}O:{}^{16}O_{VSMOW}} \right) - 1 \right] \times 1000$$

Isotopic measurements were made for nitrate, nitrite, nitrate plus nitrite, and ammonium N isotopic compositions (hereafter denoted as $\delta^{15}N_{NO3}$, $\delta^{15}N_{NO2}$, $\delta^{15}N_{NOx}$, and $\delta^{15}N_{NH4}$, respectively). All isotopic analyses involved conversion of the species of interest into nitrous oxide gas (N_2O), which was analyzed for isotopic ratios by an IsoPrime 100 isotope ratio mass spectrometer (IRMS). The $\delta^{15}N_{NOx}$ was measured using the denitrifier method (Casciotti 2002; Sigman 2001), in which sample NO_3^- (and any NO_2^-) is quantitatively converted to N_2O using a lab-grown denitrifying bacterium, *Psuedomonas aureofaciens*, before being extracted and purified on a purge and trap system similar to that previously described in McIlvin and Casciotti (2011). Where samples contained no NO_2^- or where NO_2^- was we deliberately removed from samples by sulfamic acid addition (Granger et al., 2009), isotopic values are reported instead as $\delta^{15}N_{NO3}$. Values of $\delta^{15}N_{NOx}$ or $\delta^{15}N_{NO3}$ were normalized using international isotopic reference

standards: USGS-32 ($\delta^{15}N$ = +180.0‰), USGS-34 ($\delta^{15}N$ = -1.8‰ and $\delta^{18}O$ = -27.9‰) and

USGS-35 ($\delta^{15}N$ = +2.7‰ and $\delta^{18}O$ = +57.5‰). Analytical precision for $\delta^{15}N$ and $\delta^{18}O$ of NO_3^-

were ±0.3‰ and ±0.5‰, respectively.

To measure $\delta^{15}N_{NO2}$, we used the azide method, which chemically converts NO_2^- to N_2O

(McIlvin and Altabet, 2005), normalizing to internal isotope standards WILIS-10 ($\delta^{15}N$ = -

1.7‰), WILIS-11 ($\delta^{15}N$ = +57.1‰), and WILIS-20 ($\delta^{15}N$ = -7.8‰). Analytical precision for

measurement of $\delta^{15}N_{NO2}$ was ±0.3‰.

Ammonium $\delta^{15}N$ analyses were carried out by passive diffusion of ammonia through

Teflon membranes and capture on acidified filters (Holmes et al., 1998; Sigman et al., 1997)

coupled with persulfate digestion to NO_3^- (Knapp et al., 2005) followed by conversion to N_2O by

denitrifier method and analysis by IRMS. The diffusion/oxidation/denitrifier protocol is similar

to that described previously (Bourbonnais et al., 2012a) with modifications detailed in Chapter 3.

Isotopic composition of the NH_4^+ pool was normalized using international isotopic reference

standards IAEA-N1 ($\delta^{15}N$ = 0.5‰), USGS-25 ($\delta^{15}N$ = -29.4‰) and USGS-26 ($\delta^{15}N$ = +52.9‰).

Precision for $\delta^{15}N_{NH4}$ measurement was ±0.5‰.

4.5. RESULTS

4.5.1. *Crab Spa* and *Teddy Bear* fluid chemistry

Vent fluids taken from *Crab Spa* had an average temperature of 24°C and pH of 5.75

(based on samples from all years). The maximum measured NH_4^+ concentration was 11.6 µM.

The nearby site of *Teddy Bear*, on the other hand, exhibited a lower average temperature (13°C),

a higher pH (5.97), and a lower maximum NH_4^+ concentration (6.6 µM). Compared with nearby

high-temperature vent fluids (Table 2), both *Crab Spa* and *Teddy Bear* have remarkably higher

pH, reflecting subsurface mixing between the high-temperature, acidic vent fluids and cold, alkaline bottom seawater as previously noted for other diffuse, low-temperature venting in the study area (Von Damm and Lilley, 2004). In addition, this mixing is evident in concentrations of conservative, major elements such as Cl^- and Mg^{2+} (McNichol et al., 2016).

Crab Spa samples from all three sampling campaigns exhibit high Mg-content (>50mM), with the exception of two samples taken in 2017: A4893-White2 and A4893-Green1. The former was taken just before removal of a patch of giant *Riftia pachyptila* tubeworms from around the *Crab Spa* orifice to allow for easy access to the site, while the latter was taken immediately afterwards. The N isotopic composition ($\delta^{15}N_{NH4}$) of these samples (+0.6‰ and -0.3‰) was also notably distinct from others taken two days later (+7.1‰ and +2.6‰). Sample $\delta^{15}N_{NH4}$ values from *Teddy Bear* are notably higher (+13.9‰ and +16.5‰). Most fluids from both *Crab Spa* and *Teddy Bear* also have $\delta^{15}N_{NH4}$ values distinct from those in the high-temperature vent fluids (Figure 7). In addition, NO_3^- from these low temperature diffuse vent fluids (from both sites) exhibited N and O isotopic compositions (averaged $\delta^{15}N_{NO3}$ = +8.6‰ and $\delta^{18}O_{NO3}$ = +10.5‰) that were significantly different from those of ambient seawater nitrate ($\delta^{15}N_{NO3}$ = +5.3‰ and $\delta^{18}O_{NO3}$ = +3.4‰).

4.5.2. Incubation results

Changes in geochemical composition (including O_2, H_2S, H_2, NO_3^- and NH_4^+), cell counts, and microbial community composition from the incubations described in this study have been reported elsewhere (McNichol et al., 2016; 2018). In terms of changes in N species, McNichol et al. (2016) formerly reported measurement of combined $NO_3^-+NO_2^-$ pools as well as NH_4^+. Here, we measured NO_2^- from the same samples and were consequently able to determine

NO_3^- and NO_2^- concentrations separately, aiding our interpretation of the dynamics of N metabolisms happening during the incubations.

Three experiments receiving amendments of nitrate only and incubated at 24°C (Figure 2) were performed (1A, 1B, and 1C). During the incubation period of 21-32 hours, drawdown of NO_3^- was observed, although never to completion (minimum of 30µM), often with a concomitant increase in NO_2^- (up to ~42µM). In two of the three experiments (1A and 1B), NH_4^+ concentrations showed an initial increase (up to 23µM) followed by a drop near the end of the incubation; no apparent change in NH_4^+ concentrations was observed in the third experiment (1C).

Three additional experiments receiving addition of both NO_3^- and H_2 and incubated at 24°C (Figure 3) were also conducted (2A, 2B, and 2C). Added NO_3^- was quickly consumed and was either completely or nearly exhausted by the end of all incubations. Some accumulation of NO_2^- (up 61µM) was apparent with a slight decrease near the end. Concentrations of NH_4^+ increased steadily (up 27µM) in all experiments.

Two experiments receiving addition of both NO_3^- and H_2 and incubated at 50°C (Figure 4) were carried out (3A and 3B). Here, consumption of NO_3^- was fastest compared with the other two experimental treatments. Within ~10 hours, NO_3^- was almost completely consumed. Buildup of NO_2^- (up 53µM) was observed followed by a notable decrease. Compared with the other treatments, production of NH_4^+ was more prominent with the largest NH_4^+ yield (up 89µM), relative to the amount of added NO_3^-.

Nitrogen isotopic composition of the various N species varied substantially. In general, most $\delta^{15}N_{NOx}$ showed an increase with incubation time associated with the rapid consumption of

NO_3^-. After initiation, the $\delta^{15}N_{NOx}$ values increased from near 0‰ (the added NO_3^- had $\delta^{15}N_{NO3} = +0.1‰$) up to values as high as +20.7‰. The few discrete $\delta^{15}N$ measurements of intermediate NO_2^- ranged from -9.6‰ to +14.0‰. Notably, $\delta^{15}N_{NH4}$ values at the end of incubations exhibited great variability even within the same experiment treatment with values ranging from -11.8‰ to +10.7‰.

4.6. DISCUSSION

4.6.1. Fluid mixing at *Crab Spa* and *Teddy Bear*

Hydrothermal fluids from low-temperature, diffuse vents around 9°50'N EPR have been suggested to reflect varying proportions of the high-temperature, Cl-poor endmember fluid as evidenced by the slight decrease in Cl-content compared to bottom seawater (Von Damm and Lilley, 2004). For the low-temperature *Crab Spa* fluids collected in 2014, McNichol et al. (2016) calculated a mixing between the *Tica* endmember and ambient seawater and found that the latter made up most of the total fluid mass. Similarly, the *Crab Spa* samples collected in 2017 consisted mostly of ambient seawater as well.

Conservative mixing between cold seawater and hot vent fluid as well as additional production/consumption processes result in low-temperature vent fluids containing both NO_3^- and NH_4^+ here at 9°50' EPR. This particular feature has also been observed in diffuse vents elsewhere including Axial Volcano (Butterfield et al., 2004; Bourbonnais et al., 2012b) and at Loihi Seamount (Sylvan et al., 2017).

For samples collected in 2014, despite the apparent compositional control by conservative endmember mixing, notable departures from conservative mixing were also observed, especially for known redox active species, including lower electron donors (H_2 and

H$_2$S), lower electron acceptors (O$_2$ and NO$_3^-$), and ten-fold higher NH$_4^+$ concentrations (McNichol et al., 2016). At *Crab Spa*, *in situ* O$_2$ concentrations of 3.6 uM (McNichol et al., 2016) poise the system for favorable biological utilization of NO$_3^-$ as the most favorable electron acceptor (the next most available most energy-yielding after O$_2$). Indeed we observe depletion of NO$_3^-$ with concurrent increases in NH$_4^+$ concentration in samples from the 2017 cruise as well (Figure 5). This NO$_3^-$ depletion and NH$_4^+$ enrichment were apparent both when compared with the high-temperature fluids and the predicted composition from conservative mixing between the high-temperature fluids with the ambient seawater (Figure 5).

The less characterized *Teddy Bear* vent site reflects a higher contribution from the seawater endmember during subsurface mixing with its hot fluid source as indicated by its lower venting temperature and higher Cl-content compared with *Crab Spa*. Although farther from *Tica*, we still treat this as the representative high-temperature endmember source as it is the nearest known high-temperature vent. Similar to Crab Spa, Teddy Bear exhibits depletion in NO$_3^-$ and enrichment in NH$_4^+$ (Figure 5).

4.6.2. Constraining subsurface microbial N cycling with isotopes

Diffuse hydrothermal fluids bearing lower than expected NO$_3^-$ concentrations when compared with the expected compositions calculated from the conservative mixing can be attributed to NO$_3^-$ consumption (either microbially-mediated or abiotic). This consumption of NO$_3^-$ is also evidenced in the departure of the measured $\delta^{15}N_{NO3}$ and $\delta^{18}O_{NO3}$ from that of NO$_3^-$ in the ambient seawater (Figure 6). Indeed, isotope fractionation by biological reduction of nitrate during denitrification leads to increases in both $\delta^{15}N_{NO3}$ and $\delta^{18}O_{NO3}$ of the remaining nitrate pool, expected to follow a $^{18}\varepsilon/^{15}\varepsilon = 1$ enrichment relationship (e.g., Casciotti et al., 2002;

Granger et al., 2008; Granger and Wankel, 2016; Peters et al., 2018). Here in these low-temperature vent fluids, however, we posit that this unity relationship ($^{18}\varepsilon/^{15}\varepsilon = 1$) may not be expected for at least two reasons. Firstly, a major assemblage of the microbial community at *Crab Spa* has been reported to belong to ε-proteobacteria (McNichol et al., 2016), which are known to use a periplasmic nitrate reductase (NAP) during NO_3^- reduction to NO_2^-, an enzymatic pathway thought to be distinct from those catalyzed by the cytoplasmic assimilatory (NAS), membrane-bound respiratory (NAR), or eukaryotic assimilatory nitrate reductases (e.g., Moreno-Vivián et al., 1999). In contrast to the canonical $^{18}\varepsilon/^{15}\varepsilon = 1$ relationship exhibited by the heterotrophic respiratory denitrifying nitrate reductase (NAR), Granger *et al.,* (2008) first demonstrated that NO_3^- reduction by NAP imparts $^{18}\varepsilon/^{15}\varepsilon = 0.6$. Indeed, similar trends have also been reported for other aquatic systems where NO_3^- consumption is ostensibly dominated by chemoautotrophic sulfur oxidizing bacteria (Wenk et al. 2014; Frey et al. 2014). Secondly, high temperature abiotic reduction of NO_3^- also exhibits a similar $^{18}\varepsilon/^{15}\varepsilon = 0.6$ dual fractionation pattern (Chapter 2). Thus, regardless of the partitioning between microbial reduction (via NAP) and abiotic reduction, the remaining NO_3^- pool may be reasonably expected to evolve along a coupled N/O isotope trajectory corresponding more closely to a slope of ~0.6 (when $\delta^{18}O_{NO3}$ is plotted against $\delta^{15}N_{NO3}$ as in Figure 6). Surprisingly, however, while low temperature Crab Spa fluids showed a movement in the expected direction (higher in both $\delta^{15}N_{NO3}$ and $\delta^{18}O_{NO3}$), the observed relationship relative to bottom seawater did not fall between 0.6 and 1, exhibiting a slope instead of ~2.

Such departures from expected dual isotope fractionation pattern are not unheard of in nature. For example, a reduced N fractionation relative to O fractionation in nitrate has been reported in open ocean oxygen deficient zones (e.g., Brandes et al., 1998; Sigman et al., 2005).

Several explanations for this phenomenon have been offered including contribution of N_2 fixation resulting in addition of N with lower $\delta^{15}N_{NO3}$ to the NO_3^- pool (Brandes et al., 1998; Sigman et al., 2005) and/or redox cycling between NO_3^- and NO_2^- - notably the unexpected reoxidation of NO_2^- to NO_3^- under reducing conditions (Casciotti and McIlvin, 2007; Casciotti, 2016). A number of modeling studies (e.g., Casciotti et al., 2013; Granger and Wankel, 2016) have also now suggested the potential role of NO_2^- oxidation in causing such deviation from the expected $^{18}\varepsilon/^{15}\varepsilon$ relationship. Sigman et al. (2005) introduced the term $\Delta(15,18)$ to describe such an anomaly, expressing it as:

$$\Delta(15,18) = (\delta^{15}N_{meas.} - \delta^{15}N_{source}) - (^{15}\varepsilon/^{18}\varepsilon)(\delta^{18}O_{meas.} - \delta^{18}O_{source})$$

where $\delta^{15}N$ or $\delta^{18}O$ refer to the measured or source pool NO_3^- isotopic composition and $(^{15}\varepsilon/^{18}\varepsilon)$ is the ratio of N versus O isotope enrichment during denitrification (i.e., 1).

Defining the source NO_3^- isotopic values of +5.3‰ for $\delta^{15}N$ and +3.4‰ for $\delta^{18}O$ based on measurement of bottom seawater (Table 2), *Crab Spa* fluids exhibit values of $\Delta(15,18)$ up to -5.9‰. Interestingly, Bourbonnais et al. (2012b) also reported such patterns in the NO_3^- dual isotope composition in diffuse vent fluids from Juan de Fuca Ridge with $\Delta(15,18)$ values ranging from slightly less than 0‰ to -8.5‰, proposing several mechanisms that might give rise to such negative $\Delta(15,18)$ values. These included the non-mutually exclusive contribution of low $\delta^{15}N_{NO3}$ from N_2 fixation (followed by remineralization and nitrification), the rapid and extensive reoxidation of NO_2^- to NO_3^-, and the influence of incomplete NH_3 oxidation during nitrification. Notably, the $\delta^{15}N$ of NO_3^- generation from NH_3 oxidation is dependent on $\delta^{15}N_{NH4}$ values, which we also found to be variable at *Crab Spa* (averaging -0.1‰ and +3.7‰ for low-Cl and high-Cl

samples, respectively). Adopting a $^{15}\epsilon$ value for NH_4^+ consumption (regardless of whether by assimilation or nitrification) of 1.9‰ (mean value for Cobb Segment and Axial Volcano of Juan de Fuca Ridge as reported in Bourbonnais et al., 2012a), yields values for $\delta^{15}N_{NO3}$ from nitrification of -2.0‰ and +1.8‰, respectively, for the low-Cl and high-Cl *Crab Spa* samples. While this may not be apparent in the reported $\delta^{15}N_{NO3}$ values for *Crab Spa*, we speculate that this nitrification-derived NO_3^- contributes the total NO_3^- pool and may explain the large negative $\Delta(15,18)$ values.

Nitrate in low temperature fluids from *Teddy Bear* is isotopically distinct from both ambient seawater as well as *Crab Spa.* In addition, the elevated $\delta^{15}N_{NH4}$ clearly indicates significant influence by NH_4^+ consumption. While it is difficult to estimate how much of this consumption can be attributed to NH_4^+ oxidation vs. assimilation, based on the low $\delta^{18}O$ value in the co-occurring NO_3^-, we posit that the NH_4^+ oxidation is likely the most dominant. Oxidation of NH_4^+ to NO_2^- and ultimately NO_3^- involves the incorporation of O atoms from O_2 and H_2O. The two oxygen atoms incorporated during the production of NO_2^- derive one O atom from O_2 and the other from H_2O (Andersson and Hooper, 1983). In addition, O atom incorporation has been shown to occur with a notable kinetic isotope fractionation resulting in a $\delta^{18}O_{NO2}$ values that are lower than the combination of the respective source pools (Casciotti et al., 2010). For conditions typifying the deep sea, this results in $\delta^{18}O_{NO2}$ produced from ammonia oxidation expected to range between -3‰ and 5‰ (Casciotti and Buchwald, 2012). The second step of nitrification involves the incorporation of another O atom from H_2O into NO_2^- to produce NO_3^-. While there are no available data on the $\delta^{18}O_{O2}$, the values for $\delta^{18}O_{H2O}$ in vent fluids from the study area were reported in Shanks et al. (1995) to be close to that of bottom seawater (~0‰).

Thus, the high contribution of nitrification represented in the $\delta^{18}O$ of the product NO_3^-, is consistent with the influence of NH_4^+ oxidation on elevation of $\delta^{15}N_{NH4}$ values. We note, however, that the relative influence of NH_4^+ assimilation by the resident microbial community cannot be completely ruled out.

4.6.3. Isotope dynamics in response to shifting activity of microbial metabolic pathways during incubation experiments

In addition to the interpretation of natural fluid samples, which harbor a high degree of heterogeneity, there is much to be learned from experimental manipulations under tightly regulated conditions. The results of the incubation experiments conducted by McNichol et al. (2016; 2018) at *in situ* temperatures and pressures, clearly demonstrated the effect of geochemical and physical controls on both the rates of microbial N transformations and corresponding changes in the composition of the microbial community inhabiting low-temperature, diffuse flow systems. McNichol et al. (2016) posited that transformations rates including those involved in N cycling (e.g., denitrification and DNRA) are limited by the supply of available electron acceptors, electron donors and temperature. For instance, incubations amended with NO_3^- (as an electron acceptor) and H_2 (as an electron donor) showed higher rates of NO_3^- reduction compared to incubations amended with NO_3^- alone. Additionally, incubations at higher temperature also exhibited higher NO_3^- reduction rates as well as a shift favoring DNRA over denitrification as the primary microbial pathway responsible for NO_3^- reduction.

Considering the evolution of different inorganic N species (NO_3^-, NO_2^- and NH_4^+) over the course of the incubations (now combining measurements reported in McNichol et al 2016 of NH_4^+ and ($NO_3^-+NO_2^-$) with the NO_2^- vs NO_3^- speciation measurements made here), significant

differences in the magnitude of the decrease in NO_3^- concentration among the three treatments

are observed (Table 3). Experiments amended with NO_3^- only at 24°C showed the smallest

decrease in NO_3^- levels by the end of the incubation period. The inclusion of H_2 to the

incubations resulted in more extensive NO_3^- drawdown, with the experiment conducted at 50°C

exhibiting complete NO_3^- removal in ~12 hours. As the first intermediate of NO_3^- reduction

(whether by denitrification or DNRA), NO_2^- concentrations initially increased followed by a

decline as NO_2^- was presumably converted to either N_2 or NH_4^+, by denitrification or DNRA,

respectively. Although changes in the dissolved N_2 pool were not measured, concentrations of

NH_4^+ steadily increased throughout all experiments, with the exception of one incubation (1A),

in which no change in NH_4^+ concentration was noted which might indicate the balance between

the production and consumption of NH_4^+.

Changes in N stable isotope composition were generally consistent with changes in

concentrations. For example, $\delta^{15}N_{NO3}$ values are expected to increase during biological NO_3^-

consumption as a function of kinetic isotope fractionation associated with enzymatic NO_3^-

reduction (Granger et al., 2008, Granger et al 2010; Kritee et al., 2012, Karsh et al., 2012).

Interestingly, a high degree of variability in $\delta^{15}N_{NH4}$ values was observed over all three

experimental treatments. For example, the experiments receiving only NO_3^- at 24°C (1A, 1B and

1C) yielded a range of $\delta^{15}N_{NH4}$ values of up to ~20‰ despite the fact that trends in the

concentrations and isotopic composition of NO_3^- and NO_2^- exhibited a general similarity within

these experiments (Figures 3-5).

In order to explore plausible explanations for such stark differences in the $\delta^{15}N_{NH4}$ values

at the end of the incubations, we used a simple, multi-process Michaelis-Menten (MM) model

with integrated kinetic isotope effects to simulate the changes in both concentrations and isotopic

composition of different N pools over the course of each experimental incubation. The model

(Figure 8) includes three biologically catalyzed reductive N transformations: 1) NO_3^- reduction

to NO_2^- by nitrate reductase (NAR), 2) reduction of NO_2^- to N_2 representing denitrification

(NIR), and 3) reduction of NO_2^- to NH_4^+ representing the final 6 electron transfer step of

dissimilatory reduction of nitrate to ammonium (NRF). Rates of each process are defined by MM

parameters V_{max} and K_m with each process imparting a kinetic isotopic fractionation ($^{15}\varepsilon$). Model

simulations were conducted using a finite-difference approach in which reaction progress was

incremented in small discrete steps to minimize error propagation. Thus, the degree of change in

the isotopic composition of each substrate/product pool is inherently controlled by the isotope

fractionation of the three steps as well as the dynamics of the substrate/product pool sizes. We

adopted $^{15}\varepsilon$ values for NO_3^- reduction to NO_2^- ($^{15}\varepsilon_{NAR}$), NO_2^- reduction to N_2 ($^{15}\varepsilon_{NIR}$) and NO_2^-

reduction to NH_4^+ ($^{15}\varepsilon_{NRF}$) of 1.3‰, 1.3‰, and 7.6‰, respectively, holding these constant during

the simulation. The value of for $^{15}\varepsilon_{NAR}$ used in this model was the average reported value for

closed-system community nitrate reduction calculated from *Crab Spa* samples taken in 2017.

This value ($^{15}\varepsilon_{NAR} = 1.3‰$) is similar to the averaged value for vents along Juan de Fuca Ridge

(1.1‰, Bourbonnais et al., 2012b). Since there is no available value for $^{15}\varepsilon_{NIR}$ from vent

microbes, we assumed the use of similar value to $^{15}\varepsilon_{NAR}$. Meanwhile, the value for the $^{15}\varepsilon_{NRF}$ was

the average values from incubation experiments on vent bacterial isolates capable of DNRA

(Pérez-Rodríguez et al., 2017).

Model simulations included the initial composition of both amended NO_3^- ($\delta^{15}N_{NO3} =$

0‰) and NH_4^+ initially present in the fluid prior to the incubation (10uM; $\delta^{15}N_{NH4} = 0‰$). The

evolving concentrations of NO_3^-, NO_2^- and NH_4^+ were controlled by the maximum reaction rate

(V_{max}) and the half-saturation constant (K_m). Here we used the V_{max} values calculated for NAR

and NRF and reported by McNichol et al. (2016) based on these experiments, as well as the values for NIR that were derived from %DNRA, also reported by McNichol et al. (2016). K_m values were numerically fit to the measured concentration data (Table 4).

Model fits to the concentration data (Figures 9-11) were generally good with the exception of an inability to reproduce the notable drawdown of NH_4^+ in the later stages of the incubation, as the model lacks a sink for NH_4^+. Ultimately, the combination of NH_4^+ producing process (i.e., DNRA) and NH_4^+ consuming process (i.e., NH_4^+ assimilation or NH_4^+ oxidation) exerts control over any changes in the NH_4^+ concentrations. In fact, NH_4^+ assimilation was likely active throughout the incubations as indicated by the NH_4^+ drawdown during the latter stages of the incubation that was also accompanied by increases in microbial cell counts (McNichol et al., 2016).

Similarly, the predicted changes in both $\delta^{15}N_{NOx}$ and $\delta^{15}N_{NO2}$ are also consistent with the measured values. Notably, however, modeled values of $\delta^{15}N_{NH4}$ at the end of each experiment mostly fall below measured values of $\delta^{15}N_{NH4}$ (Figure 12). As with the NH_4^+ concentrations, this observation is consistent with the potential influence of NH_4^+ consumption, which would act to increase $\delta^{15}N_{NH4}$ values (Bourbonnais et al., 2012b). Although O_2 concentrations were generally $< 5\mu M$ throughout these experiments (McNichol et al., 2016), we also cannot exclude ammonia oxidation as recent reports have suggested its operation in very low O_2 environments down to 10-200 nM O_2 (Bristow et al., 2017).

Although this simple KIE-integrated MM model captures the general trends in the change in N species concentrations and isotopic compositions, its application is limited and may not fully capture a number a of important aspects. Firstly, the assumed constancy in the isotope effect of each process may not hold true under all conditions. For example, drawing upon

examples from the microbial reduction of sulfate (SO_4^{2-}) which has been assessed using

experimental and modeling approaches (e.g., Sim et al., 2011; Bradley et al., 2016), variations in

isotope effects can be influenced by sulfate concentrations, the supply level and type of electron

donor, and factors influencing microbial growth rate. Nitrate reduction also shows similar

variability in N isotope fractionation under different carbon substrates serving as electron donors

(Wunderlich et al., 2012) and culture conditions including growth phase and the

presence/absence of O_2 (Krittee et al., 2012). In the context of the incubations presented here, the

reduction of substrate NO_3^- was clearly linked to utilization of electron donors H_2 and H_2S.

While each experiment began with similar level of NO_3^- addition, the presence of H_2 in 2 of the 3

experimental treatments as well as the steady drawn down of NO_3^-, and the complete drawdown

of H_2 and H_2S over the course of the incubation (McNichol et al., 2016) could easily have

influenced the magnitude of isotope fractionation. In addition, cell abundances over the course of

the incubations were not constant. Notably, experiments at 50°C showed a 10-fold increase in

cell counts over the incubation (McNichol et al., 2016). This increase in cell abundances was

also accompanied by notable changes in microbial community composition (McNichol et al.,

2018). Hence, the oversimplification of constant isotope effects as adopted in our model may

also inadvertently neglect important shifts in the expression of isotope effects.

     Secondly, the three-reaction framework used here may also represent an

oversimplification. As discussed, we did not include the process of NH_4^+ consumption, as this

leads to an underdetermined set of equations with non-unique solutions that cannot be directly

addressed with the data available. Clearly, the consumption of NH_4^+, at least towards the end of

the incubations, appears to have affected both concentration and $\delta^{15}N_{NH4}$ values. Furthermore,

many different microbial groups may carry out the reactions represented here, including some

that may be able to mediate more than one reaction. Hence, the influence of substrate availability on each microbial group may not be shared across the whole community. For example, the production of intermediate NO_2^- may or may not be available to all members of the microbial community depending on differences in efflux levels of intracellular pools. Reduction of NO_3^- by denitrifying bacteria likely offers them greater access to NO_2^- for reduction to N_2, as compared to organisms catalyzing DNRA, and vice versa. These types of interactions could be difficult to model without a better understanding of microbial metabolic dynamics and their relative enzymatic activity driving N cycling under these conditions.

Finally, it is important to recognize that our model is based upon the incubations contained within a closed system. Hence, there was no resupply of substrate and the isotope fractionation inherently followed a closed-system Rayleigh model. In contrast, N cycling dynamics in field settings at low-temperature, diffuse vents are more appropriately represented by open system dynamics.

4.7. CONCLUSION

The dynamics of ammonium in low-temperature, submarine hydrothermal systems are controlled by the combination of both mixing processes as well as key modifications stemming from complex microbial transformation processes. Here at 9°50'N EPR, the variable $\delta^{15}N_{NH4}$ values in both the field samples and under controlled experimental incubations distinctly illustrates the strong influence of microbial activities and the complex interplay between different N transformation reactions. While the application of the KIE-integrated MM model substantiated much of the observed dynamics of microbial NO_3^- reduction (and NH_4^+ production), modification of NH_4^+ is also heavily (and perhaps unpredictably) influenced by

NH_4^+ consumption processes. Moving forward, it will be critical to apply multiple isotopic, geochemical and molecular approaches in tandem when tackling the multifaceted nature of nitrogen cycling at diffuse vents and the dynamic environmental conditions they comprise.

<u>Acknowledgements</u>
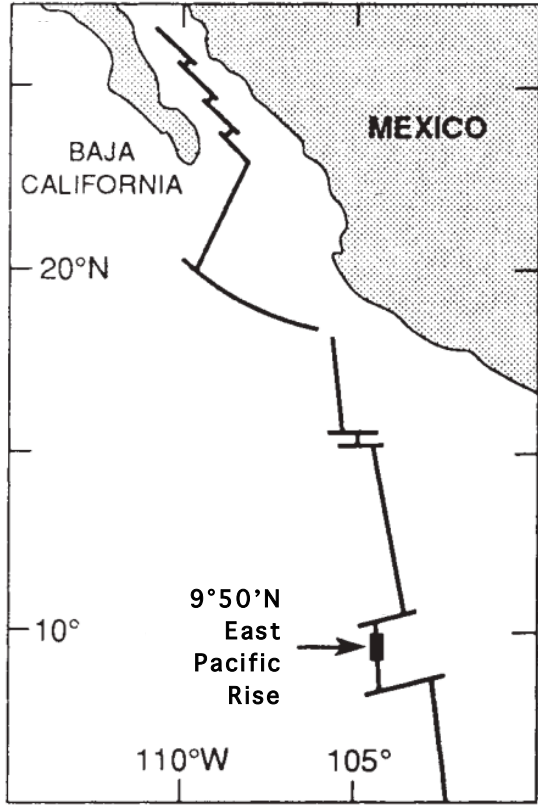
Figure 1. 9°50'N East Pacific Rise hydrothermal vent field is located along the spreading ridge south of a transform fault. This map is a modification from Von Damm et al. (1995).

Table 1. Geographical locations and selected physical parameters of the vent sites in this study

Site	Lat (°N)	Long (°W)	Depth (m)	Max T (°C)	Min pH (at 25°C)
P vent	9°50.28'	104°17.47'	2506	350	3.37
Bio 9	9°50.30'	104°17.30'	2503	368	3.44
Crab Spa*	9°50.39'	104°17.48'	2503	26	5.75**
Alvinella mound (Tica)	9°50.39'	104°17.49'	2511	300	4.56**
Teddy Bear*	9°50.50'	104°17.51'	2514	13	5.80**
Bio vent	9°50.95'	104°17.61'	2499	320	4.06

Note:　* Low-temperature, diffuse vents
　　　　**Minimum pH values taken from samples where [Mg] > 10 mM

Table 2. Fluid chemistry and isotopic composition of samples taken at low-temperature and high-temperature vent sites in 2017.

Vent site	Sample	max T	pH at 25°C	[Mg^{2+}] (mm)	[Cl$^-$] (mm)	[NH$_4^+$] (µM)	$\delta^{15}N_{NH4}$ (‰ vs air)	[NO$_3^-$] (µM)	$\delta^{15}N_{NO3}$ (‰ vs air)	$\delta^{18}O_{NO3}$ (‰ vs VSMOW)
BOTTOM SEAWATER			~8	53.5	538	0	-	40	5.3	3.4
LOW-T FLUIDS										
Crab Spa	A4893-Green1	25	5.81	39.3	430	9.5	0.6	4.0	8.6	9.7
	A4893-White2	25	5.81	36.3	393	9.6	-0.3	2.8	8.4	10.7
	A4896-Yellow1	24	5.80	50.7	534	6.8	7.1	-	12.3	16.3
	A4902-Yellow2	26	5.93	49.8	526	6.1	2.6	7.6	5.1	5.2
Teddy Bear	A4898-Green1	13	6.10	51.0	544	6.6	13.9	-	12.6	-5.1
	A4898-Green2	13	6.07	48.4	509	4.8	16.5	-	-	-
	A4903-Red2	12	5.75	51.1	541	2.9	-	-	-	-
HIGH-T FLUIDS										
Tica (Alvinella Cupcake)	A4895-Green1	190	5.39	35.5	443	3.8	-	-	-	-
	A4895-Green1	190	5.39	36.0	443	2.4	-	-	-	-
	A4898-Yellow1	196	4.56	23.0	341	2.3	-	-	-	-
	A4898-Yellow2	196	4.75	27.0	394	3.2	6.9	-	-	-
Tica (Alvinella Mound)	A4896-Black1	300	5.05	41.5	487	4.8	6.3	-	-	-
	A4896-Black1	300	5.05	41.8	491	2.2	-	-	-	-
	A4896-Black2	300	5.91	42.5	492	2.1	-	-	-	-
	A4896-Black2	300	5.91	51.3	549	1.9	-	-	-	-
	Endmember		*<4.56*	*0.0*	*236*	*7.1*	**-**	**-**	**-**	**-**
Biovent	A4901-Red1	316	4.35	3.8	394	3.2	7.9	-	-	-
	A4901-Black1	320	4.57	3.5	397	4.6	7.4	-	-	-
	A4901-Black2	320	4.06	3.9	396	4.4	-	-	-	-
	Endmember		*4.06*	*0.0*	*385*	*4.4*	**-**	**-**	**-**	**-**
P-vent	A4896-Red1	350	3.37	4.8	318	3.4	-	-	-	-
	A4896-Red2	350	3.70	4.2	324	4.9	-	-	-	-
	Endmember		*3.37*	*0.0*	*302*	*4.5*	**-**	**-**	**-**	**-**
Bio9	A4898-Red1	364	3.59	5.8	256	5.3	7.9	-	-	-
	A4898-Red2	364	3.63	6.0	266	5.8	8.8	-	-	-
	A4895-Blue1	368	4.05	5.2	287	5.3	5.9	-	-	-
	A4895-Blue1	368	4.05	5.2	285	3.8	5.5	-	-	-
	A4895-Blue2	368	3.44	4.3	285	5.1	7.0	-	-	-
	Endmember		*3.44*	*0.0*	*247*	*5.6*	**-**	**-**	**-**	**-**

Table 3. Fluid chemistry and isotopic composition for 2014 incubation samples.

| Treatment	Experiment	Sampler ID	Time (hr)	[NOx] (µM)	$\delta^{15}N_{NOx}$ (‰ vs air)	[NO$_3^-$] (µM)	[NO$_2^-$] (µM)	$\delta^{15}N_{NO2}$ (‰ vs air)	[NH$_4^+$] (µM)	$\delta^{15}N_{NH4}$ (‰ vs air)
+NO$_3^-$ @24°C	1A	759-UW2A	0.0	4.5	-	3.2	1.3	-	-	-
			1.9	58.5	-	47.4	11.2	-	9.1	-
			11.2	91.7	0.60	58.9	32.8	-	8.6	-
			19.3	84.4	1.58	50.2	34.1	-9.59	8.9	-
			29.7	70.8	2.58	33.5	37.3	-5.05	8.7	-
			30.9	52.7	-	29.9	32.5	-3.26	-	5.47
	1B	760-8A	0.0	8.0	-	-	-	-	9.4	-
			1.5	83.4	-	-	-	-	8.5	-
			8.9	69.8	-	-	-	-	12.3	-
			16.9	58.4	-	-	-	-	14.8	-
			25.0	45.2	-	-	-	-	13.9	-
			25.4	-	-	-	-	-	-	-11.84
	1C	760-7A	0.0	5.6	-	3.2	0.0	-	8.9	-
			1.8	108.2	-	103.2	5.0	-	8.5	-
			9.8	81.1	-	45.8	35.3	-8.70	20.6	-
			17.9	73.2	-	31.6	41.6	-6.84	23.0	-
			25.8	63.6	-	29.7	33.9	-4.65	18.3	-
			26.0	62.3	-	36.6	25.7	-2.39	-	-4.49
+NO$_3^-$/H$_2$ @24°C	2A	761-7A	0.0	5.0	-	2.9	2.1	-	9.5	-
			2.8	153.4	-0.14	152.2	1.2	-	7.8	-
			10.9	106.2	1.36	71.1	35.0	-	15.8	-
			18.0	73.8	1.79	15.1	58.7	-	25.0	-
			26.2	64.7	2.01	14.5	50.2	-	25.0	-
			27.2	-	3.26	-	39.5	-	-	-9.34
	2B	761-UW4A	0.0	4.2	-	2.4	1.8	-	10.9	-
			2.1	142.6	-0.66	140.5	2.1	-	10.0	-
			11.0	101.7	4.95	61.3	40.4	-4.74	17.4	-
			18.2	69.9	1.78	9.3	60.6	4.09	24.9	-
			26.1	59.3	1.50	5.9	53.5	1.51	27.0	-
			26.6	-	1.29	-	51.0	1.95	-	1.50
	2C	761-3A	0.0	6.1	-	5.0	1.1	-	9.7	-
			3.1	110.6	-0.17	109.1	1.5	-	11.9	-
			11.5	72.6	2.18	23.4	49.2	2.31	18.5	-
			19.6	51.2	2.96	10.1	41.1	5.39	25.5	-
			27.2	28.2	4.21	4.2	24.0	0.38	24.7	-
			27.5	-	3.67	-	15.7	3.42	-	10.86
+NO$_3^-$/H$_2$ @50°C	3A	761-UW2B	0.0	13.1	-	7.5	0.0	-	8.7	-
			4.0	168.1	0.41	166.9	1.3	-	7.5	-
			12.8	22.5	11.74	3.4	19.0	10.42	83.2	-
			21.3	12.1	-	2.0	10.1	12.59	89.1	0.18
			21.5	-	16.48	-	6.6	13.97	-	0.06
			21.5	-	13.64	-	8.0	-	-	-
	3B	761-8B	0.0	9.5	-	7.5	2.0	-	11.0	-
			2.9	154.4	-0.52	153.0	1.4	-	12.3	-
			11.5	56.1	-	7.5	48.6	7.28	72.7	-
			20.2	38.9	7.26	-	-	-	63.2	-
			25.7	-	-	-	37.2	6.24	-	-
			26.7	-	9.20	-	31.2	10.11	-	6.91
			26.7	-	8.91	-	31.3	-	-	-

Figure 2. Experimental incubation with addition of NO_3^- only at 24°C. (a) NO_3^- plus NO_2^- concentrations, (b) NO_3^- concentrations, (c) NO_2^- concentrations, (d) NH_4^+ concentrations, (e) N isotopic composition in the NO_3^- plus NO_2^- pool, (f) N isotopic composition in NO_2^- pool, and (g) N isotopic composition in NH_4^+ pool.
Legend: Diamond = Exp 1A, square = Exp 1B, and triangle = Exp 1C
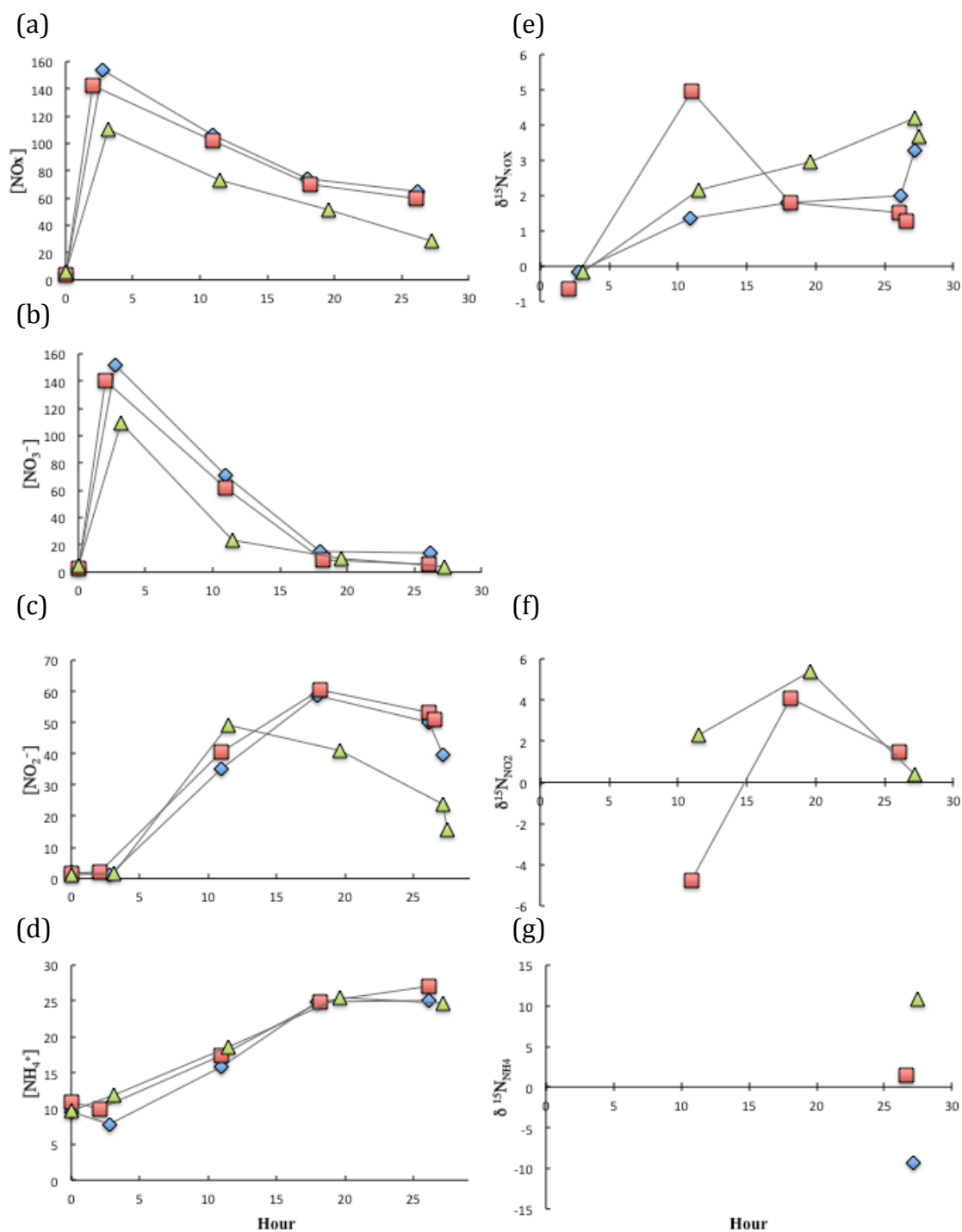
Figure 3. Experimental incubation with addition of NO_3^- and H_2 at 24°C. (a) NO_3^- plus NO_2^- concentrations, (b) NO_3^- concentrations, (c) NO_2^- concentrations, (d) NH_4^+ concentrations, (e) N isotopic composition in the NO_3^- plus NO_2^- pool, (f) N isotopic composition in NO_2^- pool, and (g) N isotopic composition in NH_4^+ pool.
Legend: Diamond = Exp 2A, square = Exp 2B, and triangle = Exp 2C
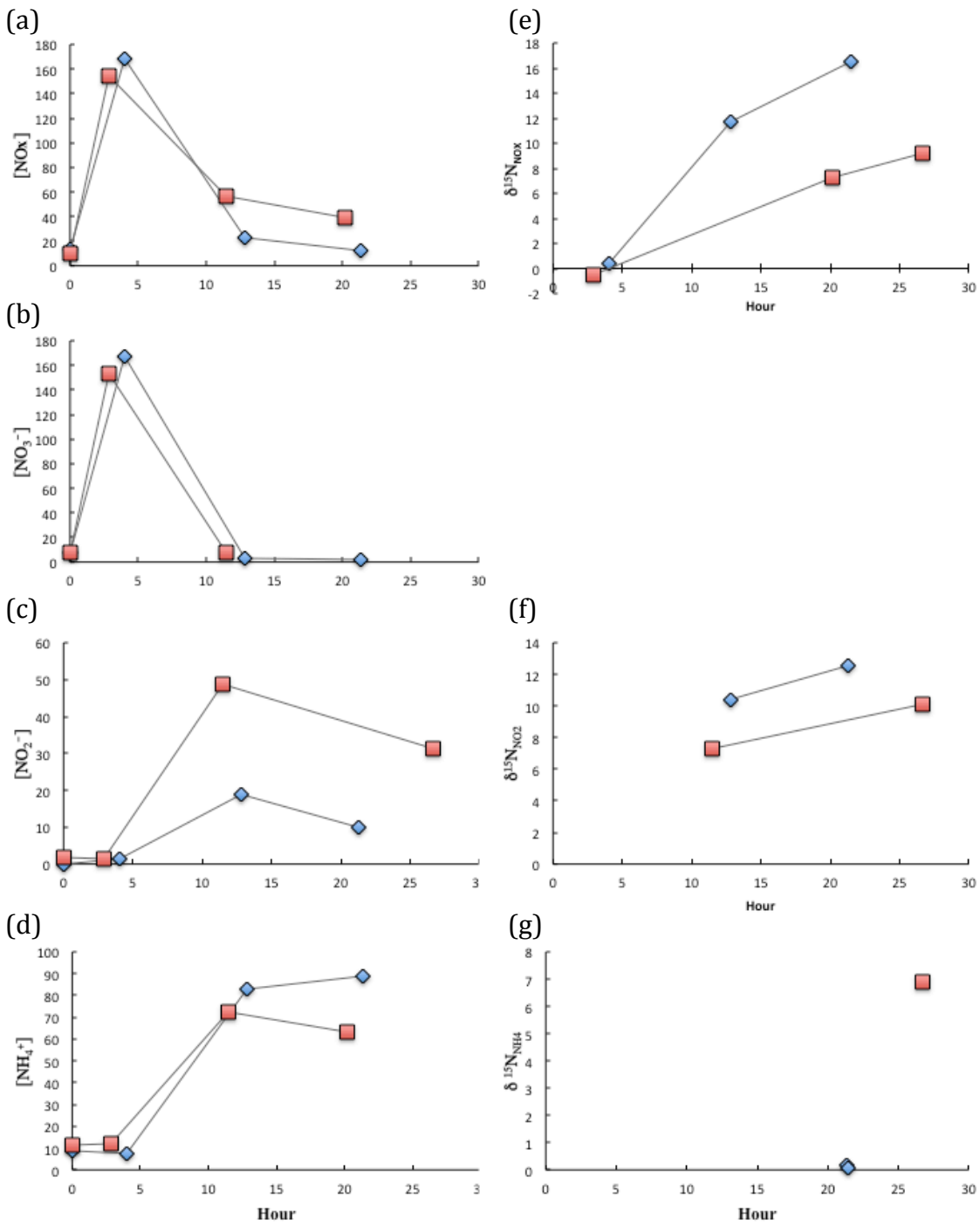
Figure 4. Experimental incubation with addition of NO_3^- and H_2 at 50°C. (a) NO_3^- plus NO_2^- concentrations, (b) NO_3^- concentrations, (c) NO_2^- concentrations, (d) NH_4^+ concentrations, (e) N isotopic composition in the NO_3^- plus NO_2^- pool, (f) N isotopic composition in NO_2^- pool, and (g) N isotopic composition in NH_4^+ pool.
Legend: Square = Exp 3A and diamond = Exp 3B
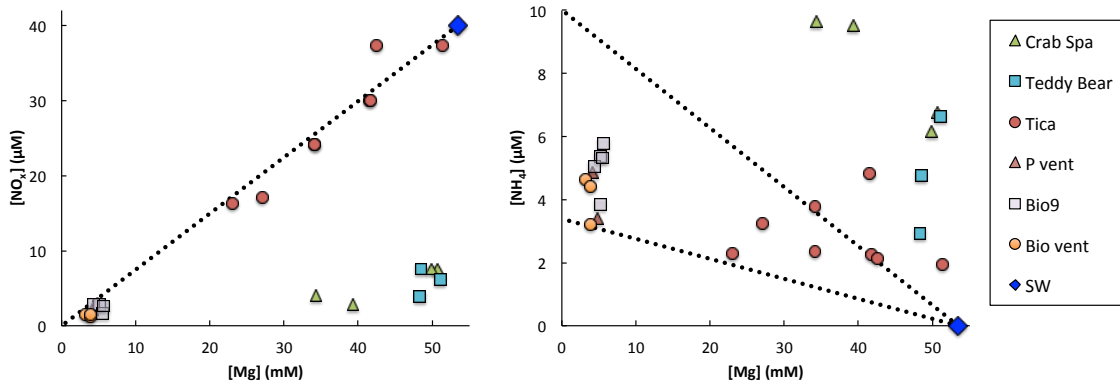
Figure 5. Nitrate plus nitrite (NO_x) and ammonium (NH_4^+) concentrations from the 2017 cruise. (a) NO_x vs Mg. Line from bottom seawater (SW) to the origin shows mixing of a zero-nitrate vent fluid with seawater. (b) NH_4^+ vs Mg. Hot fluids have 3.6-10.0 μM endmember NH_4^+.
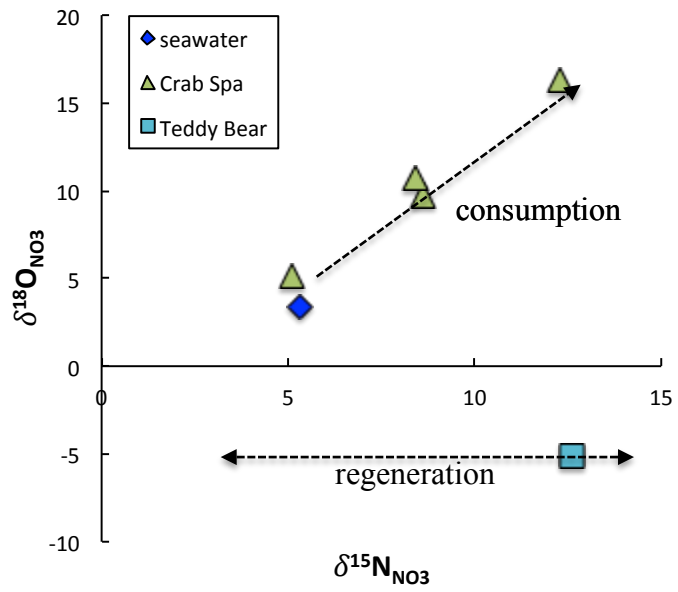
**Figure 6.** N and O isotopic composition of NO_3^- from the ambient seawater, *Crab Spa* and *Teddy Bear* collected in 2017.
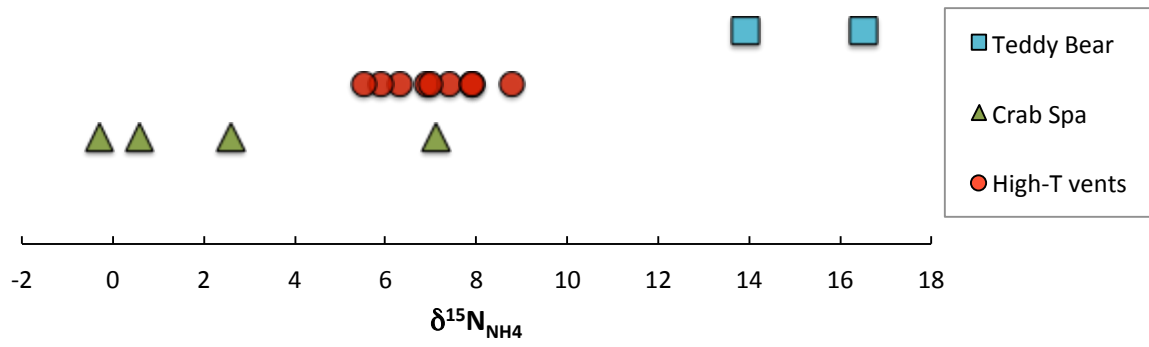
Figure 7. N isotopic composition of NH_4^+ from the high-temperature vent fluids, *Crab Spa,* and *Teddy Bear* collected in 2017.
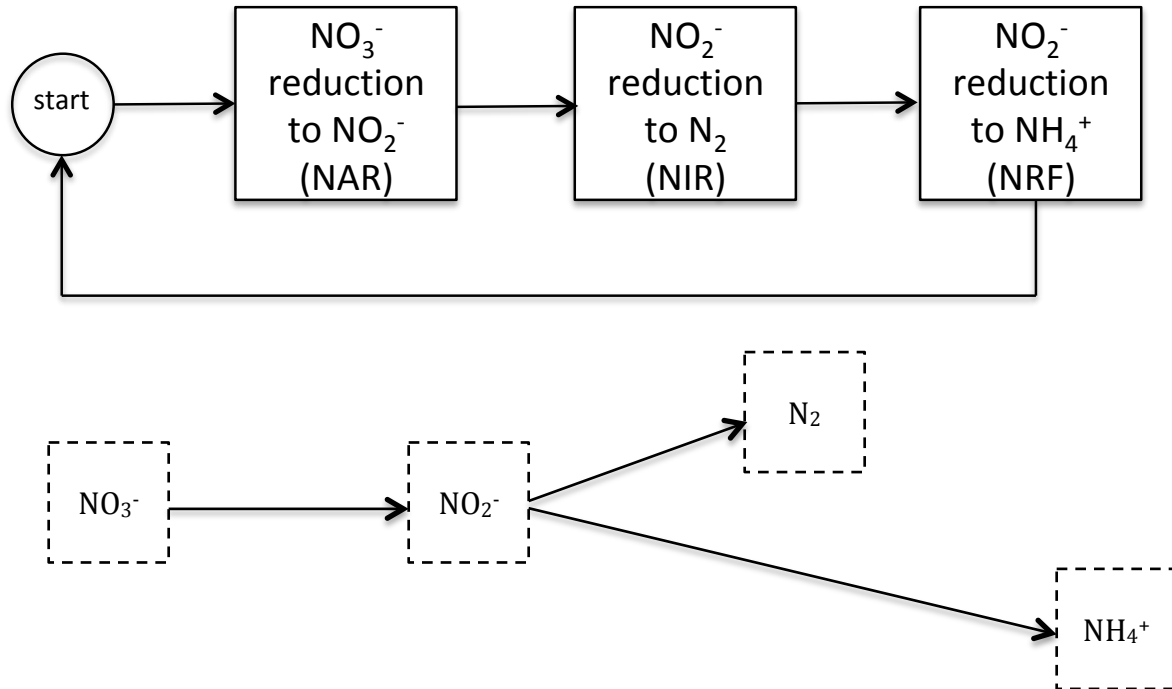
Figure 8. The simple workflow of the Michaelis-Menten model used in this study (top) and the substrate/product for each transformation (bottom). Each loop in the workflow represents one incremental step (6 minutes) during the incubation.

**Table 4.** Michaelis-Menten model parameterization.

| Treatment	Experiment	Sampler ID	Start NO$_3^-$ (μM)	NAR Vmax (μM/6min)	Km (nM)	NIR Vmax (μM/6min)	Km (nM)	NRF Vmax (μM/6min)	Km (nM)
+NO3 @24°C	1A	759-UW2A	108	4.45	1500	7.07	1000	1.89	300
	1B	760-8A	83	3.72	1000	5.76	600	0.77	400
	1C	760-7A	92	2.7	500	2.7	500	0	0
+NO3/H2 @24°C	2A	761-7A	153	12.55	1500	9.71	1500	2.06	1500
	2B	761-UW4A	143	10.79	1000	7.64	1600	1.84	1500
	2C	761-3A	111	8.66	1000	8.67	800	1.93	900
+NO3/H2 @50°C	3A	761-UW2B	168	39.81	2000	11.33	1000	13.96	1000
	3B	761-8B	154	27.33	2500	11.36	5500	12.86	600
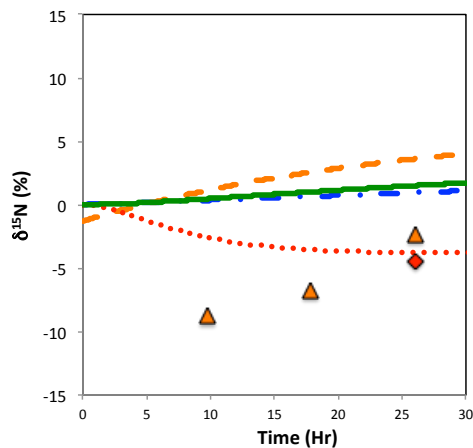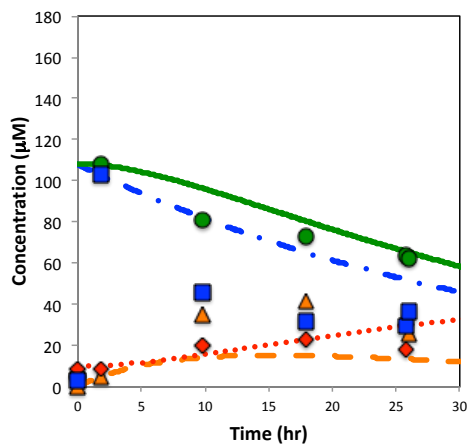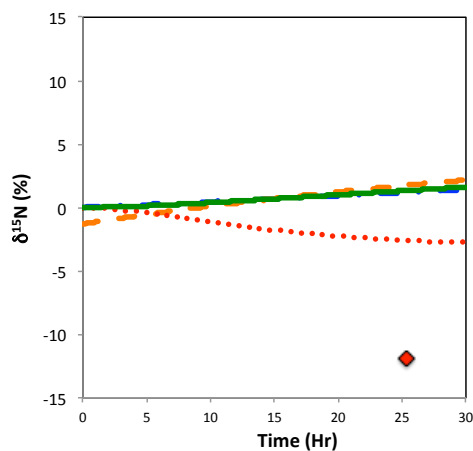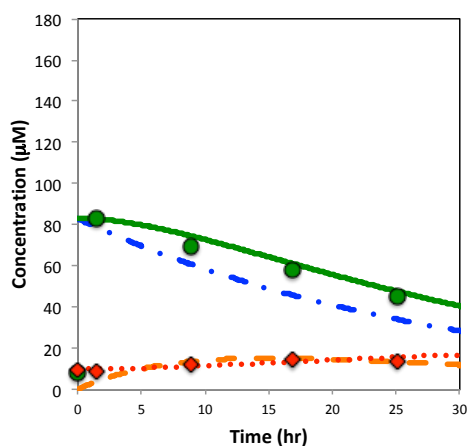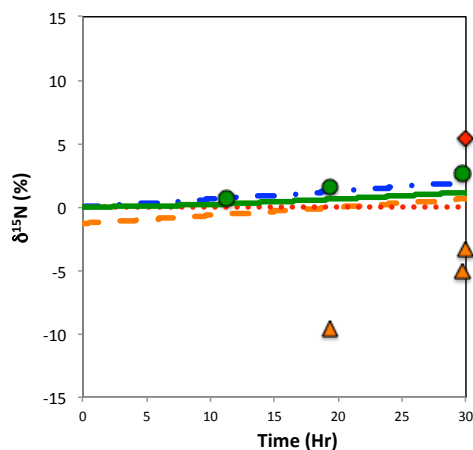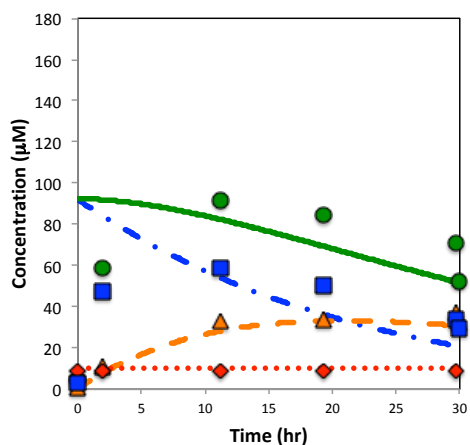
Figure 9. Model results for incubations with addition of NO_3^- only at 24°C.
Note: Modeled data are the lines and the measured data are the markers. Solid lines and circles (green) = NOx, dash dot lines and squares (blue) = NO_3^-, dash lines and triangles (orange) = NO_2^-, and round dot lines and diamonds (red) = NH_4^+
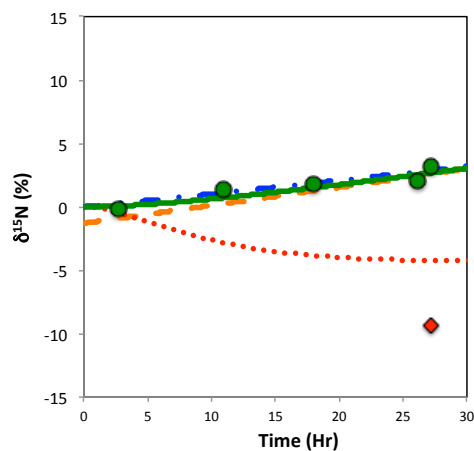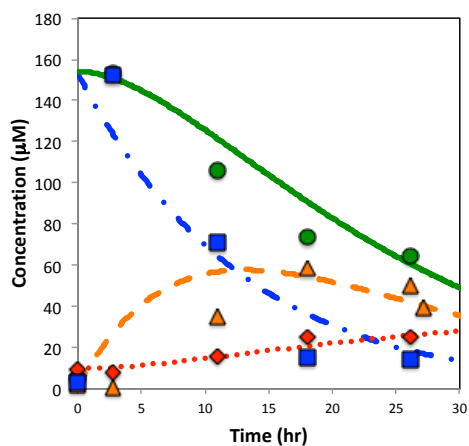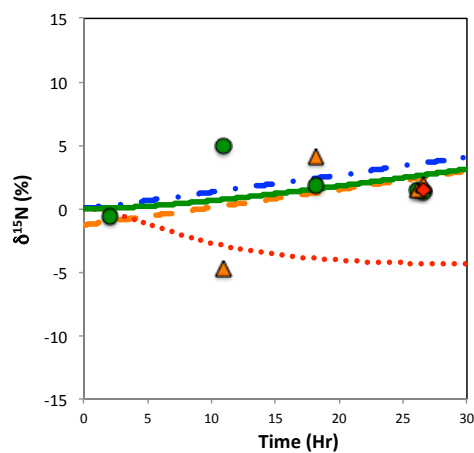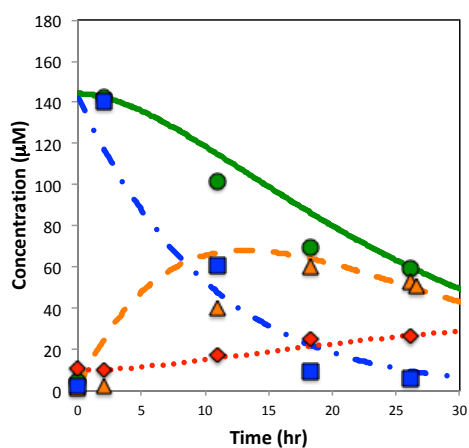
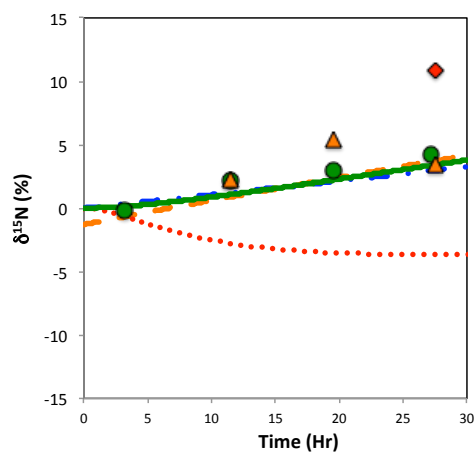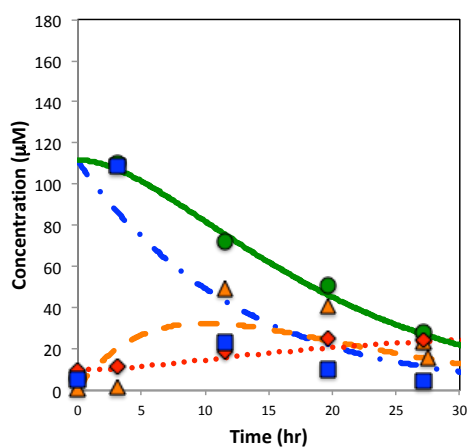**Figure 10.** Model results for incubations with addition of NO_3^- and H_2 at 24°C.
Note: Modeled data are the lines and the measured data are the markers. Solid lines and circles (green) = NOx, dash dot lines and squares (blue) = NO_3^-, dash lines and triangles (orange) = NO_2^-, and round dot lines and diamonds (red) = NH_4^+
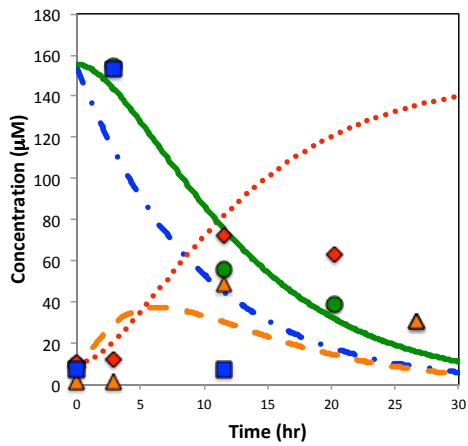
Figure 11. Model results for incubations with addition of NO_3^- and H_2 at 50°C.
Note: Modeled data are the lines and the measured data are the markers. Solid lines and circles (green) = NOx, dash dot lines and squares (blue) = NO_3^-, dash lines and triangles (orange) = NO_2^-, and round dot lines and diamonds (red) = NH_4^+
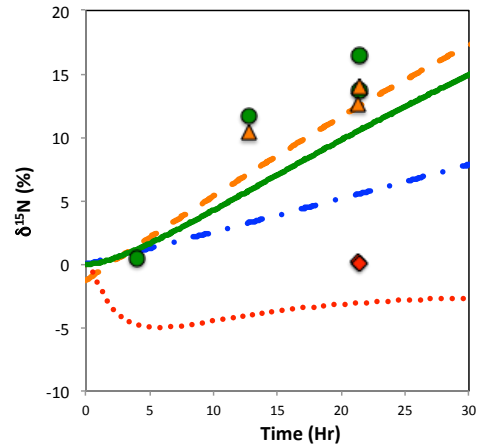
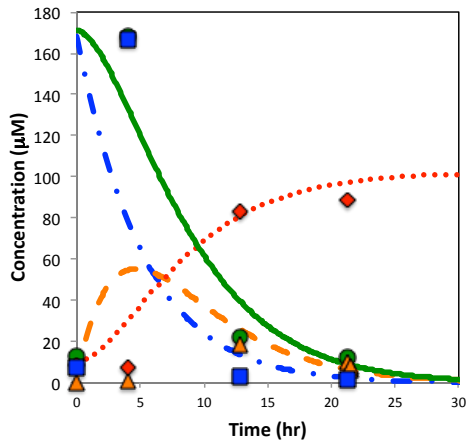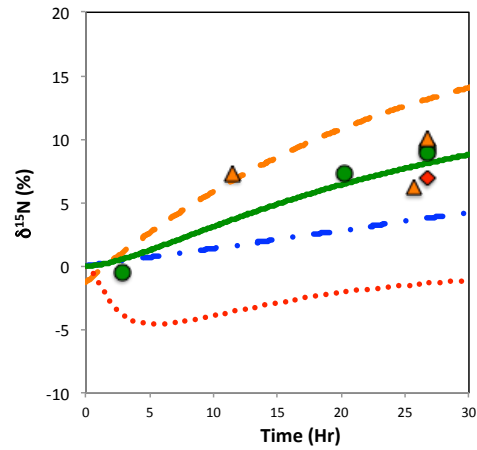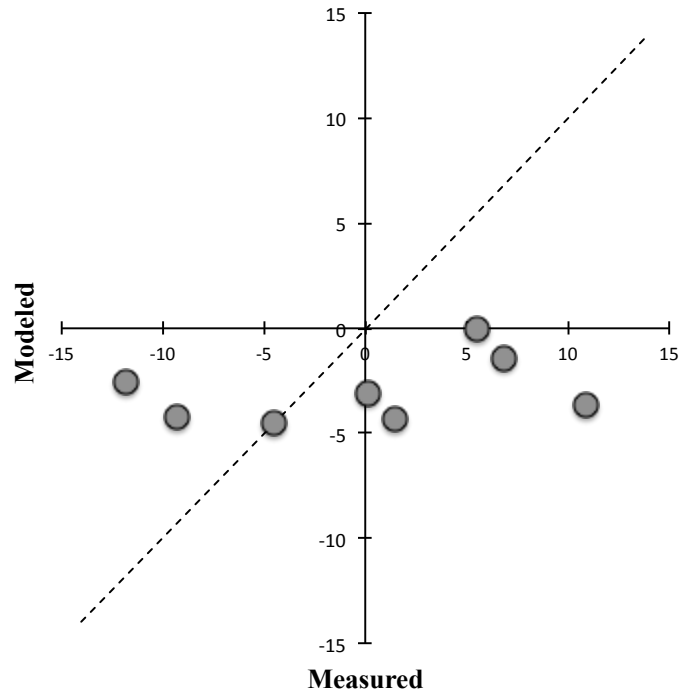**Figure 12.** Comparison between the measured and modeled values for $\delta^{15}N_{NH4}$. The dashed line is the 1:1 relationship (i.e., modeled value = measured value)

REFERENCES

Andersson, K. K., & Hooper, A. B. (1983). O_2 and H_2O are each the source of one O in NO_2^- produced from NH_3 by *Nitrosomonas*: ^{15}N-NMR evidence. *FEBS letters*, *164*(2), 236-240.

Beaulieu, S. E., Baker, E. T., & German, C. R. (2015). Where are the undiscovered hydrothermal vents on oceanic spreading ridges?. *Deep Sea Research Part II: Topical Studies in Oceanography*, *121*, 202-212.

Bourbonnais, A., Juniper, S. K., Butterfield, D. A., Devol, A. H., Kuypers, M. M. M., Lavik, G., ... & Lehmann, M. F. (2012a). Activity and abundance of denitrifying bacteria in the subsurface biosphere of diffuse hydrothermal vents of the Juan de Fuca Ridge. *Biogeosciences discussions*, *9*, 4661-4678.

Bourbonnais, A., Lehmann, M. F., Butterfield, D. A., & Juniper, S. K. (2012b). Subseafloor nitrogen transformations in diffuse hydrothermal vent fluids of the Juan de Fuca Ridge evidenced by the isotopic composition of nitrate and ammonium. *Geochemistry, geophysics, geosystems*, *13*(2).

Brandes, J. A., Devol, A. H., Yoshinari, T., Jayakumar, D. A., & Naqvi, S. W. A. (1998). Isotopic composition of nitrate in the central Arabian Sea and eastern tropical North Pacific: A tracer for mixing and nitrogen cycles. *Limnology and Oceanography*, *43*(7), 1680-1689.

Butterfield, D. A., Roe, K. K., Lilley, M. D., Huber, J. A., Baross, J. A., Embley, R. W., & Massoth, G. J. (2004). Mixing, reaction and microbial activity in the sub-seafloor revealed by temporal and spatial variation in diffuse flow vents at Axial Volcano. *The Subseafloor Biosphere at Mid-Ocean Ridges*, *144*, 269-289.

Carbotte, S., & Macdonald, K. (1992). East Pacific Rise 8°–10°30′ N: Evolution of ridge segments and discontinuities from SeaMARC II and three-dimensional magnetic studies. *Journal of Geophysical Research: Solid Earth*, *97*(B5), 6959-6982.

Casciotti, K. L. (2016). Nitrogen and oxygen isotopic studies of the marine nitrogen cycle. *Annual review of marine science*, *8*, 379-407.

Casciotti, K. L., & McIlvin, M. R. (2007). Isotopic analyses of nitrate and nitrite from reference mixtures and application to Eastern Tropical North Pacific waters. *Marine Chemistry*, *107*(2), 184-201.

Casciotti, K. L., Sigman, D. M., Hastings, M. G., Böhlke, J. K., & Hilkert, A. (2002). Measurement of the oxygen isotopic composition of nitrate in seawater and freshwater using the denitrifier method. *Analytical Chemistry*, *74*(19), 4905-4912.

Fornari, D. J., Von Damm, K. L., Bryce, J. G., Cowen, J. P., Ferrini, V., Fundis, A., ... & Meana-Prado, M. F. (2012). The East Pacific Rise between 9° N and 10° N: Twenty-five years of integrated, multidisciplinary oceanic spreading center studies. *Oceanography*, *25*(1), 18-43.

Frey, C., Hietanen, S., Jürgens, K., Labrenz, M., & Voss, M. (2014). N and O isotope fractionation in nitrate during chemolithoautotrophic denitrification by Sulfurimonas gotlandica. *Environmental science & technology*, *48*(22), 13229-13237.

Garside, C. (1982). A chemiluminescent technique for the determination of nanomolar concentrations of nitrate and nitrite in seawater. *Marine Chemistry*, *11*(2), 159-167.

Granger, J., & Sigman, D. M. (2009). Removal of nitrite with sulfamic acid for nitrate N and O isotope analysis with the denitrifier method. *Rapid Communications in Mass Spectrometry*, *23*(23), 3753-3762.

Granger, J., Sigman, D. M., Rohde, M. M., Maldonado, M. T., & Tortell, P. D. (2010). N and O isotope effects during nitrate assimilation by unicellular prokaryotic and eukaryotic plankton cultures. *Geochimica et Cosmochimica Acta*, *74*(3), 1030-1040.

Granger, J., Sigman, D. M., Lehmann, M. F., & Tortell, P. D. (2008). Nitrogen and oxygen isotope fractionation during dissimilatory nitrate reduction by denitrifying bacteria. *Limnology and Oceanography*, *53*(6), 2533-2545.

Granger, J., & Wankel, S. D. (2016). Isotopic overprinting of nitrification on denitrification as a ubiquitous and unifying feature of environmental nitrogen cycling. *Proceedings of the National Academy of Sciences*, *113*(42), E6391-E6400.

Hall, P. 0. J., & Aller, R. C. (1992). Rapid, small-volume, flow injection analysis for ΣCO_2, and NH_4^+ in marine and freshwaters. *Limnology and Oceanography*, *37*(5), 1113-1119.

Holmes, R. M., McClelland, J. W., Sigman, D. M., Fry, B., & Peterson, B. J. (1998). Measuring 15N–NH4+ in marine, estuarine and fresh waters: an adaptation of the ammonia diffusion method for samples with low ammonium concentrations. *Marine Chemistry*, *60*(3-4), 235-243.

Karl, D. M. (1995). Ecology of free-living, hydrothermal vent microbial community. In Karl, D. M. (Ed.), *The microbiology of deep-sea hydrothermal vents* (pp. 35-124). CRC Press.

Karsh, K. L., Granger, J., Kritee, K., & Sigman, D. M. (2012). Eukaryotic assimilatory nitrate reductase fractionates N and O isotopes with a ratio near unity. *Environmental science & technology*, *46*(11), 5727-5735.

Knapp, A. N., Sigman, D. M., & Lipschultz, F. (2005). N isotopic composition of dissolved organic nitrogen and nitrate at the Bermuda Atlantic Time-series Study site. *Global Biogeochemical Cycles*, *19*(1).

Kritee, K., Sigman, D. M., Granger, J., Ward, B. B., Jayakumar, A., & Deutsch, C. (2012). Reduced isotope fractionation by denitrification under conditions relevant to the ocean. *Geochimica et Cosmochimica Acta*, *92*, 243-259.

McIlvin MR, Altabet MA. 2005. Chemical conversion of nitrate and nitrite to nitrous oxide for nitrogen and oxygen isotopic analysis in freshwater and seawater. *Anal. Chem.* 77:5589–95

McIlvin, M. R., & Casciotti, K. L. (2011). Technical updates to the bacterial method for nitrate isotopic analyses. *Analytical Chemistry*, *83*(5), 1850-1856.

McNichol, J., Stryhanyuk, H., Sylva, S. P., Thomas, F., Musat, N., Seewald, J. S., & Sievert, S. M. (2018). Primary productivity below the seafloor at deep-sea hot springs. *Proceedings of the National Academy of Sciences*, 201804351.

McNichol, J., Sylva, S. P., Thomas, F., Taylor, C. D., Sievert, S. M., & Seewald, J. S. (2016). Assessing microbial processes in deep-sea hydrothermal systems by incubation at in situ temperature and pressure. *Deep Sea Research Part I: Oceanographic Research Papers*, *115*, 221-232.

Moreno-Vivián, C., Cabello, P., Martínez-Luque, M., Blasco, R., & Castillo, F. (1999). Prokaryotic nitrate reduction: molecular properties and functional distinction among bacterial nitrate reductases. *Journal of bacteriology*, *181*(21), 6573-6584.

Nakagawa, S., Takai, K., Inagaki, F., Chiba, H., Ishibashi, J. I., Kataoka, S., ... & Sako, Y. (2005). Variability in microbial community and venting chemistry in a sediment-hosted backarc hydrothermal system: impacts of subseafloor phase-separation. *FEMS microbiology ecology*, *54*(1), 141-155.

Nielsen, S. G., Rehkämper, M., Teagle, D. A., Butterfield, D. A., Alt, J. C., & Halliday, A. N. (2006). Hydrothermal fluid fluxes calculated from the isotopic mass balance of thallium in the ocean crust. *Earth and Planetary Science Letters*, *251*(1), 120-133.

Peters, B., Horak, R., Devol, A., Fuchsman, C., Forbes, M., Mordy, C. W., & Casciotti, K. L. (2018). Estimating fixed nitrogen loss and associated isotope effects using concentration and isotope measurements of NO3–, NO2–, and N2 from the Eastern Tropical South Pacific oxygen deficient zone. *Deep Sea Research Part II: Topical Studies in Oceanography*.

Rubin, K. H., Soule, S. A., Chadwick Jr, W. W., Fornari, D. J., Clague, D. A., Embley, R. W., ... & Dziak, R. P. (2012). Volcanic eruptions in the deep sea. *Oceanography*, *25*(1), 142-157.

Seewald, J. S., Doherty, K. W., Hammar, T. R., & Liberatore, S. P. (2002). A new gas-tight isobaric sampler for hydrothermal fluids. *Deep Sea Research Part I: Oceanographic Research Papers*, *49*(1), 189-196.

Shanks, W. C., Boehlke, J. K., Seal, R. R., & Humphris, S. E. (1995). Stable isotopes in mid-ocean ridge hydrothermal systems: Interactions between fluids, minerals, and organisms. *Geophysical Monograph-American Geophysical Union*, *91*, 194-194.

Shock, E. L. (1992). Chemical environments of submarine hydrothermal systems. In Holm, N. G. (Ed.), *Origins of Life and Evolution of the Biosphere* (pp. 67-107). Springer, Netherlands.

Sigman, D. M., Altabet, M. A., Michener, R., McCorkle, D. C., Fry, B., & Holmes, R. M. (1997). Natural abundance-level measurement of the nitrogen isotopic composition of oceanic nitrate: an adaptation of the ammonia diffusion method. *Marine Chemistry*, *57*(3-4), 227-242.

Sigman, D. M., Casciotti, K. L., Andreani, M., Barford, C., Galanter, M. B. J. K., & Böhlke, J. K. (2001). A bacterial method for the nitrogen isotopic analysis of nitrate in seawater and freshwater. *Analytical chemistry*, *73*(17), 4145-4153.

Sigman, D. M., Granger, J., DiFiore, P. J., Lehmann, M. M., Ho, R., Cane, G., & van Geen, A. (2005). Coupled nitrogen and oxygen isotope measurements of nitrate along the eastern North Pacific margin. *Global Biogeochemical Cycles*, *19*(4).

Strickland, J. D., & Parsons, T. R. (1972). A practical handbook of seawater analysis.

Sylvan, J. B., Wankel, S. D., LaRowe, D. E., Charoenpong, C. N., Huber, J. A., Moyer, C. L., & Edwards, K. J. (2017). Evidence for microbial mediation of subseafloor nitrogen redox processes at Loihi Seamount, Hawaii. *Geochimica et Cosmochimica Acta*, *198*, 131-150.

Van Dover, C. (2000). Chemical and physical properties of vents fluids. In Van Dover, C. (Ed.), *The ecology of deep-sea hydrothermal vents* (pp. 76-98). Princeton University Press.

Von Damm, K. L., Edmond, J. M., Grant, B., Measures, C. I., Walden, B., & Weiss, R. F. (1985). Chemistry of submarine hydrothermal solutions at 21° N, East Pacific Rise. *Geochimica et Cosmochimica Acta*, *49*(11), 2197-2220.

Von Damm, K. L., & Lilley, M. D. (2004). Diffuse flow hydrothermal fluids from 9 50′ N East Pacific Rise: origin, evolution and biogeochemical controls. *The Subseafloor Biosphere at Mid‑Ocean Ridges*, *144*, 245-268.

Wang, F., Zhou, H., Meng, J., Peng, X., Jiang, L., Sun, P., ... & Wu, L. (2009). GeoChip-based analysis of metabolic diversity of microbial communities at the Juan de Fuca Ridge hydrothermal vent. *Proceedings of the National Academy of Sciences*, *106*(12), 4840-4845.

Wenk, C. B., Zopfi, J., Blees, J., Veronesi, M., Niemann, H., & Lehmann, M. F. (2014). Community N and O isotope fractionation by sulfide-dependent denitrification and anammox in a stratified lacustrine water column. *Geochimica et cosmochimica acta, 125*, 551-563.

Wunderlich, A., Meckenstock, R., & Einsiedl, F. (2012). Effect of different carbon substrates on nitrate stable isotope fractionation during microbial denitrification. *Environmental science & technology*, *46*(9), 4861-4868.

CHAPTER 5

MAJOR FINDINGS AND FUTURE RESEARCH DIRECTIONS

Abiotic reduction of NO_3^- with magnetite

The abiotic reduction of NO_3^- to NH_4^+ under high-temperature, high-pressure conditions presented in **CHAPTER 2** challenges the formerly proposed notion of quantitative conversion (Brandes et al., 1998). Here, in this study, two reaction product patterns were recognized. At high pH, all NO_3^- was converted to NH_4^+. On the other hand, N_2 was detected as another product in addition to NH_4^+ when reactions proceeded at low pH. The reaction partitioning between the two products not only controls the concentrations of NH_4^+ but also its $\delta^{15}N_{NH4}$. Indeed, the abiotic pathway for the reduction of NO_3^- to N_2 represents a fixed N loss term (i.e., the removal of bioavailable forms of N that support primary productivity in the ocean). Such N loss terms (also including denitrification and anammox in oxygen deficient zones, ODZs) are important in controlling the bioavailable N inventory of the ocean. How much of this abiotic reduction of NO_3^- to N_2 at vents contributes to modern global N loss? A back-of-an-envelope calculation shows this term to be roughly 1% of total N loss terms. While small, it is important to note that the volume of the ODZs throughout the geologic past has likely not always been the same. Hence, this hydrothermal removal of NO_3^- could represent a more substantial contributor to the total oceanic N inventory during periods when water-column fixed N removal was lower.

A noteworthy result of the experiment in pH-buffered, NaCl matrix was that the $\delta^{15}N_{N2}$ immediately after the substrate NO_3^- was depleted was similar to $\delta^{15}N_{NH4,}$ indicating a lack of any fractionation despite a branching of two final products (N_2 and NH_4^+). However,

measurements made on fluids collected after the experiment ran for two more months revealed a shift in $\delta^{15}N_{N2}$ that is consistent with what might be expected when N_2 is in isotopic equilibrium with NH_4^+, that is N_2 exhibiting higher $\delta^{15}N$ due to its higher bond strength. This particular possibility regarding the N isotope equilibration between N_2 and NH_4^+ (or perhaps NH_3 depending speciation of NH_3/NH_4^+ at *in situ* conditions) should be investigated further for a number of reasons. Firstly, both N_2 and NH_4^+ are the predominant N compounds in high-temperature vent fluids. Secondly, depending on the timescale over which vent fluids remain within the high-temperature zones during hydrothermal circulation, N isotope equilibrium between N_2 and NH_4^+ may affect the $\delta^{15}N_{NH4}$ in the vent fluids that ultimately emerge at the seafloor.

While NO_3^- reduction to NH_4^+ occurs rapidly at high temperatures and results in the complete consumption of any NO_3^- in the inflowing seawater within the hydrothermal circulation, incomplete reaction might still occur within low-temperature mixing zones where diffuse venting results from the mixing of high-temperature fluids and ambient seawater. In this case, the incomplete consumption of NO_3^- will impart isotope fractionation on the remaining NO_3^- pool. Here we found the coupled N and O isotope effects ($^{18}\varepsilon/^{15}\varepsilon$) to be 0.64, which is similar to the value of 0.62 reported from the respiratory denitrifier *Rhodobacter sphaeroides* (Granger et al., 2008). This particular denitrifier dissimilates NO_3^- exclusively using the periplasmic nitrate reductase, NAP (Gavira et al., 2002). Interestingly, a major proportion of microbial communities in submarine, low-temperature, diffuse vents is comprised of epsilon-proteobacteria (e.g., Alain et al., 2004; Bourbonnais et al., 2012; Huber et al., 2007; López‐García et al., 2002; Nakagawa et al., 2005), a group that is also known to use NAP for NO_3^- reduction (e.g., Vetriani et al., 2014). Therefore, it appears impossible to discern the relative

contribution of abiotic reduction from microbial reaction during NO_3^- reduction at diffuse vents using coupled N and O isotopes of NO_3^- alone.

This study used magnetite as a model for the source of reduced iron acting as the electron donor during NO_3^- reduction. Nevertheless, there are other minerals that might be relevant in the context of high-temperature reactions at vents including sulfide-bearing minerals such as pyrite (FeS_2), chalcopyrite ($CuFeS_2$) or pyrrhotite ($Fe_{1-x}S$) —all of which have been shown to reduce NO_3^- (Brandes et al., 1998; 2008; Summers 2005). It would be worth exploring dynamics of reduction of NO_3^- by these minerals commonly found in deep-sea vents, and notably whether they are similar to or different from the current study using magnetite.

Analysis of NH_4^+ and $\delta^{15}N_{NH4}$ in high-temperature vent fluids

CHAPTER 3 presents the analyses of NH_4^+ concentrations and $\delta^{15}N_{NH4}$ values from a range of deep-sea vents from around the global ocean. The dichotomy in NH_4^+ concentrations between sedimented and unsedimented systems has been acknowledged since early studies in the 1980's (Von Damm et al., 1985a; 1985b). Sedimented systems often exhibit mM-level NH_4^+ while their unsedimented counterparts generally exhibit concentrations as much as 3 orders of magnitude lower (i.e., µM level). For sedimented systems, this study links the variation in $\delta^{15}N_{NH4}$ values to its sedimentary organic matter source originally deriving from the organic matter sinking from the overlying surface water. Interestingly, in the eastern Pacific, there is a clear progression of measured $\delta^{15}N_{NH4}$ from higher values in vents underneath the oxygen deficient zones to the lower values in the vents underneath the oxygen-replete waters. This pattern reflects the influence of isotopic fractionation by water-column denitrification on the nutrient NO_3^- supplying the surface productivity and hence the sinking particulate pools, the

ultimate source of the NH_4^+ to these sedimented vent systems. It is important to recognize that in addition to the oceanic input, some deep-sea vents located near shore could receive terrigenous input of organic matter as a source of vent NH_4^+ as well.

Of many processes that might affect the NH_4^+ after it is produced, phase separation has been largely ignored in previous studies. During phase separation, NH_3 can be partitioned between the vapor and brine phases resulting in the lowering of NH_4^+ in the vent fluids compared to the source fluids. To assess the possible impact of phase separation on the observed NH_4^+ pool, *in situ* pH needs to be carefully considered as a primary regulator of speciation between NH_4^+ and NH_3.partitioning into vapor and brine phases, respectively.

Furthermore, two unsedimented systems with anomalously high NH_4^+ content were discussed. Despite the apparent lack of sediment cover, we postulated that *Sea Cliff* was a case that received a small influence of sedimentary input due to its proximity to other reported sediment-influenced hydrothermal sites along the Gorda Ridge. On the other hand, *Piccard* (Mid-Cayman Rise) was hypothesized to have additional NH_4^+ from the reduction of N_2, a process conventionally thought to be uncommon in nature due to the high activation energy required to overcome the breakage of triple-bonded N_2. Notably, *Piccard* is the deepest known vent site to date (at ~5km) and the formation of vent fluids here has been suggested to reach temperatures surpassing 500°C (McDermott et al., 2018). Such high-pressure and high-temperature conditions within *Piccard* reaction zone might prime the system for N_2 reduction to NH_4^+ to occur – analogous to the Haber-Bosch process of industrial N_2 fixation for NH_3 production.

While this study represents a large compilation of NH_4^+ measurements, we are still far from providing sufficient coverage as most data are from mid-ocean ridges. Other hydrothermal

systems such as those from back-arc and off-axis venting are underrepresented in the current compilation. We could not obtain any $\delta^{15}N_{NH4}$ values from back-arc basin venting at Lau Basin due to insufficient sample volume required for such exceptionally low NH_4^+ concentrations. Other sites of prime interest include Lost City where vent fluids are highly alkaline. Here we reported the NH_4^+ concentrations without any $\delta^{15}N_{NH4}$ measurements.

Impact of low-temperature microbial transformations on vent NH_4^+

Two low-temperature, diffuse sites, *Crab Spa* and *Teddy Bear* at 9°50'N East Pacific Rise, were investigated in **CHAPTER 4.** When compared to high-temperature vents nearby, these diffuse vents clearly exhibited depletion of NO_3^- and enrichment of NH_4^+ attributable to microbial activity as evidenced by non-conservative isotopic behavior in both the NO_3^- and NH_4^+ pools. In addition to these natural sample measurements, we also report isotopic measurements of previously conducted incubation experiments (McNichol et al., 2016; 2018), in which different environmental conditions (i.e., temperatures and electron donor) were subject to fluid samples taken from *Crab Spa*. The N isotopic composition of NH_4^+ ($\delta^{15}N_{NH4}$) both from the natural and incubation samples displayed an unexpectedly large degree of variation (with replicate experiments ranging more than 16‰ and 22‰, respectively). Simulations of the incubation experiments using a simple kinetic isotope effect integrated Michaelis-Menten model highlight a complex interplay between different N reduction reactions as well as, notably, ammonium consumption, which appears to heavily impact vent NH_4^+ and $\delta^{15}N_{NH4}$ in low temperature systems.

Prebiotic chemistry and hydrothermal systems on other planetary bodies

The ability to constrain the occurrence of abiotic reactions occurring at submarine hydrothermal vents at present day is key to understand Earth's evolution and the origin of life that might have emerged at vents in the distant geologic past. Nitrogen, as we know it, is a crucial biochemical ingredient for life and ammonia is one of the key ingredients for production of N-containing molecules such as proteins and DNA/RNA. Understanding what environmental conditions are required for different abiotic reactions to proceed will be critical in hypothesizing what have occurred billions of years ago. Unlike microbially-mediated N transformations, our current knowledge of abiotic N cycling is much more limited, demanding more studies be carried out.

Our current understanding of Earth's submarine hydrothermal vents can potentially be applied to similar systems found elsewhere on other planetary bodies. Within the solar system, several moons of Jupiter and Saturn have been confirmed to have liquid water (e.g., Kivelson et al., 2000; Vance et a., 2014). Amongst these moons, Europa (e.g., Greenberg et al., 1999; Thomson and Delaney, 2001; Collins et al., 2000; Goodman et al., 2004) and Enceladus (e.g., Waite et al., 2017; Hsu et al., 2015) are thought to host hydrothermal vents underneath their ice-covered oceans, as evidenced by NASA's Cassini mission capturing images of a plume of water and gas erupting from beneath the icy surface of Enceladus (Dougherty et al., 2006; Waite et al., 2006; Hansen et al., 2006). More importantly within these plumes, Cassini Saturn Orbiter's Ion and Neutral Mass Spectrometer (INMS, Waite et al., 2004) measured N compounds including N_2, NH_3 and HCN (Waite et al., 2009). Hsu et al. (2015) reported an analysis of silicon-rich, nanometer-sized dust particles emitted from the plume suggesting that the hydrothermal vents on

Enceladus might be of high-temperature ($\geq 90°C$), moderate salinity (~4%), and alkaline seawater (pH 8.5–10.5).

Saturn's giant moon, Titan, is yet another system that shows relevance to hydrothermal systems on Earth. Glein (2015) suggested that the thick N_2-CH_4 atmosphere of Titan might stem from hydrothermal activity. Indeed, several other works also proposed that the early CH_4/NH_3 atmosphere on Titan may be a result of subsequent photochemical conversion of NH_3 to N_2 (e.g., Johnson et al., 2016). These ocean worlds in the outer solar system represent exciting avenues for future research. In the future, with more advanced instrumentation, we should be able to gather more information from these moon and better constrain the abundance and isotopic composition of chemical species including those containing N. To this end, I posit that it will be instrumental to further our knowledge of N dynamics in hydrothermal systems on Earth as the currently available information is still limited and does not cover all relevant geological settings. Systems such as *Lost City* are still poorly understood especially with respect to N dynamics; it will be instrumental to better understand this unique system for its use as an analog to hydrothermal systems elsewhere in our solar system.

REFERENCES

Alain, K., Zbinden, M., Le Bris, N., Lesongeur, F., Quérellou, J., Gaill, F., & Cambon-Bonavita, M. A. (2004). Early steps in microbial colonization processes at deep-sea hydrothermal vents. *Environmental microbiology*, *6*(3), 227-241.

Bourbonnais, A., Juniper, S. K., Butterfield, D. A., Devol, A. H., Kuypers, M. M. M., Lavik, G., ... & Lehmann, M. F. (2012). Activity and abundance of denitrifying bacteria in the subsurface biosphere of diffuse hydrothermal vents of the Juan de Fuca Ridge. *Biogeosciences discussions*, *9*, 4661-4678.

Brandes, J. A., Boctor, N. Z., Cody, G. D., Cooper, B. A., Hazen, R. M., & Yoder Jr, H. S. (1998). Abiotic nitrogen reduction on the early Earth. *Nature*, *395*(6700), 365.

Brandes, J. A., Hazen, R. M., & Yoder Jr, H. S. (2008). Inorganic nitrogen reduction and stability under simulated hydrothermal conditions. *Astrobiology*, *8*(6), 1113-1126.

Dougherty, M. K., Khurana, K. K., Neubauer, F. M., Russell, C. T., Saur, J., Leisner, J. S., & Burton, M. E. (2006). Identification of a dynamic atmosphere at Enceladus with the Cassini magnetometer. *Science*, *311*(5766), 1406-1409.

Gavira, M., Roldán, M. D., Castillo, F., & Moreno-Vivián, C. (2002). Regulation of nap gene expression and periplasmic nitrate reductase activity in the phototrophic bacterium Rhodobacter sphaeroides DSM158. *Journal of bacteriology*, *184*(6), 1693-1702.

Glein, C. R. (2015). Noble gases, nitrogen, and methane from the deep interior to the atmosphere of Titan. *Icarus*, *250*, 570-586.

Goodman, J. C., Collins, G. C., Marshall, J., & Pierrehumbert, R. T. (2004). Hydrothermal plume dynamics on Europa: Implications for chaos formation. *Journal of Geophysical Research: Planets*, *109*(E3).

Granger, J., Sigman, D. M., Lehmann, M. F., & Tortell, P. D. (2008). Nitrogen and oxygen isotope fractionation during dissimilatory nitrate reduction by denitrifying bacteria. *Limnology and Oceanography*, *53*(6), 2533-2545.

Greenberg, R., Hoppa, G. V., Tufts, B. R., Geissler, P., Riley, J., & Kadel, S. (1999). Chaos on Europa. *Icarus*, *141*(2), 263-286.

Hansen, C. J., Esposito, L., Stewart, A. I. F., Colwell, J., Hendrix, A., Pryor, W., ... & West, R. (2006). Enceladus' water vapor plume. *Science*, *311*(5766), 1422-1425.

Hsu, H. W., Postberg, F., Sekine, Y., Shibuya, T., Kempf, S., Horányi, M., ... & Kuwatani, T. (2015). Ongoing hydrothermal activities within Enceladus. *Nature*, *519*(7542), 207.

Huber, J. A., Welch, D. B. M., Morrison, H. G., Huse, S. M., Neal, P. R., Butterfield, D. A., & Sogin, M. L. (2007). Microbial population structures in the deep marine biosphere. *science*, *318*(5847), 97-100.

Johnson, R. E., Tucker, O. J., & Volkov, A. N. (2016). Evolution of an early Titan atmosphere. *Icarus*, *271*, 202-206.

Kivelson, M. G., Khurana, K. K., Russell, C. T., Volwerk, M., Walker, R. J., & Zimmer, C. (2000). Galileo magnetometer measurements: A stronger case for a subsurface ocean at Europa. *Science*, *289*(5483), 1340-1343.

López-García, P., Duperron, S., Philippot, P., Foriel, J., Susini, J., & Moreira, D. (2003). Bacterial diversity in hydrothermal sediment and epsilonproteobacterial dominance in experimental microcolonizers at the Mid-Atlantic Ridge. *Environmental Microbiology*, *5*(10), 961-976.

McDermott, J. M., Sylva, S. P., Ono, S., German, C. R., & Seewald, J. S. (2018). Geochemistry of fluids from Earth's deepest ridge-crest hot-springs: Piccard hydrothermal field, Mid-Cayman Rise. *Geochimica et Cosmochimica Acta*, *228*, 95-118.

McNichol, J., Stryhanyuk, H., Sylva, S. P., Thomas, F., Musat, N., Seewald, J. S., & Sievert, S. M. (2018). Primary productivity below the seafloor at deep-sea hot springs. *Proceedings of the National Academy of Sciences*, 201804351.

McNichol, J., Sylva, S. P., Thomas, F., Taylor, C. D., Sievert, S. M., & Seewald, J. S. (2016). Assessing microbial processes in deep-sea hydrothermal systems by incubation at in situ temperature and pressure. *Deep Sea Research Part I: Oceanographic Research Papers*, *115*, 221-232.

Nakagawa, S., Takai, K., Inagaki, F., Hirayama, H., Nunoura, T., Horikoshi, K., & Sako, Y. (2005). Distribution, phylogenetic diversity and physiological characteristics of epsilon-Proteobacteria in a deep-sea hydrothermal field. *Environmental Microbiology*, *7*(10), 1619-1632.

Nakagawa, S., Takai, K., Inagaki, F., Hirayama, H., Nunoura, T., Horikoshi, K., & Sako, Y. (2005). Distribution, phylogenetic diversity and physiological characteristics of epsilon‑Proteobacteria in a deep‑sea hydrothermal field. *Environmental Microbiology*, *7*(10), 1619-1632.

Summers, D. P. (2005). Ammonia formation by the reduction of nitrite/nitrate by FeS: ammonia formation under acidic conditions. *Origins of Life and Evolution of Biospheres*, *35*(4), 299-312.

Suzuki, R., Ishibashi, J. I., Nakaseama, M., Konno, U., Tsunogai, U., Gena, K., & Chiba, H. (2008). Diverse Range of Mineralization Induced by Phase Separation of Hydrothermal Fluid: Case Study of the Yonaguni Knoll IV Hydrothermal Field in the Okinawa Trough Back‑Arc Basin. *Resource Geology*, *58*(3), 267-288.

Thomson, R. E., & Delaney, J. R. (2001). Evidence for a weakly stratified Europan ocean sustained by seafloor heat flux. *Journal of Geophysical Research: Planets*, *106*(E6), 12355-12365.

Tobie, G. (2015). Planetary science: Enceladus' hot springs. *Nature*, *519*(7542), 162.

Vetriani, C., Voordeckers, J. W., Crespo-Medina, M., O'brien, C. E., Giovannelli, D., & Lutz, R. A. (2014). Deep-sea hydrothermal vent Epsilonproteobacteria encode a conserved and widespread nitrate reduction pathway (Nap). *The ISME journal*, *8*(7), 1510.

Vance, S., Bouffard, M., Choukroun, M., & Sotin, C. (2014). Ganymede′s internal structure including thermodynamics of magnesium sulfate oceans in contact with ice. *Planetary and Space Science*, *96*, 62-70.

Von Damm, K. L., Edmond, J. M., Grant, B., Measures, C. I., Walden, B., & Weiss, R. F. (1985a). Chemistry of submarine hydrothermal solutions at 21° N, East Pacific Rise. *Geochimica et Cosmochimica Acta*, *49*(11), 2197-2220.

Von Damm, K. V., Edmond, J. T., Measures, C. I., & Grant, B. (1985b). Chemistry of submarine hydrothermal solutions at Guaymas Basin, Gulf of California. *Geochimica et Cosmochimica Acta*, *49*(11), 2221-2237.

Waite Jr, J. H., Lewis, W. S., Magee, B. A., Lunine, J. I., McKinnon, W. B., Glein, C. R., ... & Nguyen, M. J. (2009). Liquid water on Enceladus from observations of ammonia and 40 Ar in the plume. *Nature, 460*(7254), 487.

Waite, J. H., Combi, M. R., Ip, W. H., Cravens, T. E., McNutt, R. L., Kasprzak, W., ... & Magee, B. (2006). Cassini ion and neutral mass spectrometer: Enceladus plume composition and structure. *science*, *311*(5766), 1419-1422.

Waite, J. H., Glein, C. R., Perryman, R. S., Teolis, B. D., Magee, B. A., Miller, G., ... & Lunine, J. I. (2017). Cassini finds molecular hydrogen in the Enceladus plume: evidence for hydrothermal processes. *Science*, *356*(6334), 155-159.

Wankel, S. D., Bourbonnais, A., & Charoenpong, C. N. (2017). Microbial processes at submarine hydrothermal vents. In J. Kallmeyer (Ed.), *Life at Vents and Seeps* (pp. 179-222). de Gruyter, Berlin/Boston.